UNIVERSITY OF OKLAHOMA
GRADUATE COLLEGE

AN EXAMINATION OF MOISTURE AND PRECIPITATION IN TROPICAL EASTERLY WAVES

A DISSERTATION
SUBMITTED TO THE GRADUATE FACULTY
in partial fulfillment of the requirements for the
Degree of
DOCTOR OF PHILOSOPHY

by MARGARET ANNE HOLLIS
Norman, Oklahoma
2026

Downloaded from SHAREOK. Persistent Handle URL: https://hdl.handle.net/11244/342612

AN EXAMINATION OF MOISTURE AND PRECIPITATION IN TROPICAL EASTERLY WAVES

A DISSERTATION APPROVED FOR THE
SCHOOL OF METEOROLOGY

BY THE COMMITTEE CONSISTING OF

Dr. Elinor Martin (Chair)

Dr. Naoko Sakaeda

Dr. Pierre Kirstetter

Dr. Gerilyn Soreghan

©Copyright by MARGARET ANNE HOLLIS 2026

All Rights Reserved.

Acknowledgments

There are a lot of people who have supported me on the way to completing this dissertation, both academically and outside of the NWC. Without this network of support, making it here would have been a lot harder.

First, I have to thank my advisor, Dr. Elinor Martin, for convincing me to join a project looking at precipitation around tropical easterly waves. I did not anticipate how much I would enjoy working with the easterly wave tracks, and having the opportunity to continue TEW research into my dissertation has been an incredible journey. In addition to Elinor, I also want to thank the rest of the TEW team, Carrie, Justin, and Rachel, for being great collaborators and colleagues.

Next, I'd like to thank my family for their support, both through the grad school journey and all of the years leading here. While not every late night spent meticulously working through homework in high school was actually worth it, that determination to see things through has served me well. I will also be forever grateful for the phone calls for help with things like filing my taxes on my own for the first time and the many, many, many cat photos in the family group chat.

To my friends in the School of Meteorology, we sure had an interesting grad school experience, from Fundies followed immediately by the COVID-19 pandemic and then the various changes the School has undergone over the years. Your support has been invaluable through the years, and it has been one of the joys in my life to be there for the rest of you. We've commiserated about classes, gone to gymnastics meets, and collectively lost our minds a few times, but all of those things have made the grad school experience so much richer.

I've already mentioned a few of my colleagues, but I'd like to thank a few others,

especially those I met through the CPEX-AW and CPEX-CV field campaigns. These teams were large groups with diverse research backgrounds, but I'd specifically like to thank Rosi, Kelly, and Quinton for the various wave-related discussions we've had over the years. I've learned a lot about what productive collaboration looks like from working with the TEW and CPEX teams, and have also just outright learned a lot from so many on both teams. Science is so much more productive when we work together and leverage everyone's strengths and expertise.

Like most universities, the University of Oklahoma has lots of resources for students to support their academic success and their physical and mental health. I am incredibly grateful for those services, especially those at Goddard Health Center. Knowing I can take care of my physical and mental health without excessive financial strain has been critical for me to be able to make it through this PhD.

My time in Norman has included people beyond the meteorology community, and these people have made this flat, relatively treeless town feel a bit more like home for the last few years. The Norman Pokemon Go community and the choir at St. Thomas More University Parish have become valued parts of my life. Both communities have brought me a lot of joy even when I was losing my mind over my dissertation, and I will miss both as I move into the next chapter of my life.

In addition to local friends, I also have to thank my online communities, especially Nerdfighteria, for the joy and support they've provided through the years. Having a community that celebrates unironic enthusiasm, kindness, and working to make the world better is so incredibly valuable.

Finally, in addition to all of the people who have supported me in so many ways, I would like to acknowledge the funding that made my graduate studies possible, including grants from NASA and NSF, as well as the availability of TA positions within the School of Meteorology.

Table of Contents

Acknowledgments iv

List of Tables viii

List of Figures ix

Abstract xv

1 Introduction 1

2 Moisture and Tropical Easterly Waves 6
2.1 Introduction 6
2.2 Data and Methods 10
2.2.1 Data 10
2.2.2 TEW Track Point Grouping 13
2.2.3 Moisture Modes 15
2.2.4 Near-TEW Fields 18
2.3 Results 18
2.3.1 Moisture and Precipitation Comparisons 18
2.3.2 Moisture Mode Assessment 22
2.3.3 Longitudinal Variations in Structure 36
2.4 Discussion and Conclusions 44

3 Diurnal Cycle in TEW Strength and Precipitation 48
3.1 Introduction 48
3.2 Data and Methods 50
3.2.1 Data 50
3.2.2 Wave Subgroupings 52
3.3 Results 53
3.3.1 Diurnal Variation in TEW Counts 53
3.3.2 Wave-focused Diurnal Variations 54
3.3.3 Effects of TEWs on Local Diurnal Cycles 59
3.4 Discussion and Conclusions 66

4 Extremes in TEW-associated Precipitation 70

4.1 Introduction . . . 70
4.2 Data and Methods . . . 73
4.2.1 Data . . . 73
4.2.2 Defining Impactful TEWs . . . 74
4.3 Results . . . 75
4.3.1 Globally Rainiest TEWs . . . 75
4.3.2 Locally Rainiest TEWs . . . 83
4.3.3 Evolution of Rainiest TEWs . . . 88
4.4 Discussion and Conclusions . . . 93

5 Summary and Conclusions . . . 96

Appendix ATEW-Following Wave Phases . . . 104
A.1 Introduction . . . 104
A.2 Methods . . . 105
A.3 Results . . . 106
A.4 Discussion . . . 113

Appendix BAlternative Heating Calculations . . . 114

Appendix CSelected Figures for 850 hPa TEWs . . . 120

Reference List . . . 133

List of Tables

2.1 Table reporting correlations between various methods to calculate apparent heating, Q_1. Methods are abbreviated as follows: Temp. Tend. is an approximation using MERRA-2's temperature tendency variables; P-MERRA2 is an approximation using surface fluxes and MERRA-2 precipitation; P-IMERG is an approximation using surface fluxes and IMERG precipitation; DSE uses DSE tendencies and transport calculated from MERRA-2 wind and temperature data. 17

4.1 Correlation values for the CV-precipitation linear regression. 92

A.1 Mean CV averaged across 0-40° latitude for each level/hemisphere combination. 106

A.2 Standard deviation of CV averaged across 0-40° latitude for each level/hemisphere combination. 106

List of Figures

2.1 Maps of TEW track center frequency in grid boxes corresponding to MERRA-2 resolution for TEWs tracked at 700 hPa (top) and 850 hPa (bottom). Green boxes superimposed on both maps highlight selected areas compared in some sections of this study. 12

2.2 Scatterplots showing the number of TEW points in each longitude bin over each surface type for TEWs in the NH (top) and SH (bottom). The grey dashed line delineates 100 points. 14

2.3 Contoured plots showing the composite mean precipitation (shaded) and standardized anomalies of q (black solid and dashed lines) for the 500 km radius around TEWs in the NH (top row), SH (bottom row), tracked at 700 hPa (left column) and 850 hPa (right column). 20

2.4 Contoured plots showing the composite mean precipitation (shaded) and standardized anomalies of q (black solid and dashed lines) for the 500 km radius around 700 hPa TEWs in selected hemisphere/longitude bin combinations. 21

2.5 Heatmaps of area-average standardized anomalies of precipitation (x-axis) and column-integrated specific humidity (y-axis) for TEWs a) all NH b) NH land c) NH ocean d) all SH e) SH land f) SH ocean. In each panel, the linear best fit is shown in solid dark blue, while x=y is shown in dashed grey. The correlation is given in the lower left corner of each panel. 23

2.6 Scatterplot of the slope (left column) and correlation (right column) for the linear regression between standardized precipitation anomalies and column-integrated specific humidity for 700 hPa TEWs in the NH (top row) and SH (bottom row) t 24

2.7 As Fig. 2.5 but for area-average standardized anomalies of the column-integrated DSE flux divergence (x-axis) and column-integrated Q1 (y-axis). 28

2.8 As in Fig. 2.6 but for the linear regression between standardized anomalies of the column-integrated DSE flux divergence and column-integrated Q1. 29

2.9 As Fig. 2.5 but for area-average standardized anomalies of MSE (x-axis) and column-integrated moisture (y-axis). 32

2.10 As Fig. 2.6 but for for the linear regression between standardized MSE anomalies and column-integrated moisture. 33

2.11 Scatterplots showing the values of the N-mode parameter for TEWs in the NH (top) and SH (bottom). The horizontal grey dashed line denotes the threshold for small N-mode values, 0.1. Subgroups with fewer than 100 TEW points have been excluded. The rightmost points in each panel, which do not have a tick beneath them, are the global averages. 34

2.12 Plan view of MSE (shaded) and streamlines (black lines) for a 1000 km sided box around TEWs tracked at 700 hPa over the a) Caribbean (285-300°), b) West Africa (330-345°), c) North Indian Ocean (90-115°), d) southeastern Pacific (270-285°), e) South Atlantic (345-360°), and f) Maritime Continent/northern Australia (120-135°) 37

2.13 Meridional cross sections of u-wind for TEWs tracked at 700 hPa over a) the Caribbean (285-300°), b) West Africa (330-345°), c) North Indian Ocean (90-115°), d) southeastern Pacific (270-285°), e) South Atlantic (345-360°), and f) Maritime Continent/northern Australia (120-135°) . 39

2.14 Zonal cross sections of q standardized anomalies for TEWs tracked at 700 hPa over a) the Caribbean (285-300°), b) West Africa (330-345°), c) North Indian Ocean (90-115°), d) southeastern Pacific (270-285°), e) South Atlantic (345-360°), and f) Maritime Continent/northern Australia (120-135°) 41

2.15 As Fig. 2.14 but for temperature. 43

3.1 Maps of TEW track points in 2.5° grid boxes for TEWs tracked at 700 hPa during a) boreal summer (MJJASO) and b) austral summer (NDJFMA). 51

3.2 Local and UTC times of initial track points of TEWs, aggregated globally for each level, for TEWs tracked at a) 700 hPa and b) 850 hPa. . . 55

3.3 Line plots showing the diurnal cycle of TEW-associated rainfall, as a percent of the daily maximum, for each longitude bin, for TEWs in the top) NH and bottom) SH, and for TEWs over left) ocean and right) land. 56

3.4 Line plots showing the mean percent of daily max CV for TEWs in each longitude bin (colors) for TEWs in the top) NH and bottom) SH, and for TEWs over left) ocean and right) land. 58

3.5 Line plots showing the ratio of values from Fig. 3.3 to Fig. 3.4 for TEWs in the top) NH and bottom) SH, and for TEWs over left) ocean and right) land. 59

3.6 Maps showing a) the average diurnal range when 700 hPa TEWs are not present, b) the average diurnal range when 700 hPa TEWs are present, and c) the ratio of the diurnal ranges TEW:non-TEW 60

3.7 Maps showing a) the average diurnal range when TEWs are not present for MJJASO, b) the average diurnal range when TEWs are not present for NDJFMA, c) the average diurnal range when TEWs are present for MJJASO, d) the average diurnal range when TEWs are present for NDJFMA, e) the ratio of the diurnal ranges TEW:non-TEW for MJJASO and f) the ratio of diurnal ranges TEW:non-TEW for NDJFMA. 62

3.8 As Fig. 3.7 but for the daily maximum rain rate. 64

3.9 As Fig. 3.7 but for the daily minimum rain rate. 65

4.1 Maps of the locations of TEW points with the highest area total accumulations for 700 hPa TEWs a) over land and b) over oceans. 76

4.2 As Fig. 4.1 but for the globally driest TEWs. 78

4.3 Bar/line plots showing the total number of extremely rainy TEWs per month globally and in each hemisphere that occur a) over land and b) over oceans. In each panel, the global counts are shaded in light blue, while the NH is shown with a red line and the SH with a black line. . . 80

4.4 As Fig. 4.3 but for the globally driest TEWs. 82

4.5 Map of the TEW tracks with the highest track duration-normalized accumulated precipitation. 83

4.6 Scatter plots of the thresholds used for the locally-defined determination of rainiest TEWs for TEWs in the a) NH and b) SH. Longitude/surface groupings with less than 100 total points have been excluded. 85

4.7 Maps showing the rainiest TEW track points using locally-defined rainy thresholds for TEWs during a) MJJASO and b) NDJFMA. 86

4.8 As Fig. 4.7 but for the locally driest TEWs. 88

4.9 Line plots showing the average evolution of CV over the life of various categories of TEWs in the a) NH and b) SH, with CV shown as a function of the percent of the TEW's life elapsed. The mean CV is in solid color, while the 95% confidence interval for each group is shaded in the same color. Note that the x-axis is intended to be read right to left. 90

4.10 Heatmaps of TEW CV against area-accumulated precipitation for a) all NH TEWs, b) all NH rainy TEWs, c) NH rainy non-developing TEWs, d) NH pre-TC TEWs, e) driest NH TEWs, f) all SH TEWs, g) all SH rainy TEWs, h) SH rainy non-developing TEWs, i) SH pre-TC TEWs, and j) driest SH TEWs. 92

5.1 A schematic summarizing the results of this dissertation. Part a) summarizes the spectrum of moisture importance for TEWs when separated by the surface they are over and how rainy the TEW is. Part b) summarizes the relationship between TEWs, the diurnal range, and the moisture in the near-TEW environment. 103

A.1 Means (left panels) and standard deviations (right panels) of CV at 700 (top panels) and 850 hPa (bottom panels). 106

A.2 Phase space (left column) and maps (right column) for four selected TEW tracks from 2014. The first point in the phase space is marked with a dot. 108

A.3 Scatterplots of TEW-following CV phase space for TEWs at a) 700 hPa and b) 850 hPa, with CV standardized using tropics-wide averages. The y-axis is marked with a purple line. 110

A.4 As Fig. A.3 but with CV standardized using the climatology for the nearest grid point. 111

A.5 As Fig. A.3 but with CV standardized using the climatology of TEW CV, and with the addition of an additional purple line on the x-axis. . 112

B.1 Heatmaps of area-average standardized anomalies of the column-integrated DSE budget (x-axis) and column-integrated Q1 (y-axis) for TEWs a) all NH b) NH land c) NH ocean d) all SH e) SH land f) SH ocean, using Q1 calculated directly from the DSE tendency. In each panel, the linear fit is shown in solid dark blue while x=y is shown in dashed grey. The correlation is given in teh lower left corner of each panel. 115

B.2 As Fig. B.1 but using IMERG precipitation to calculate Q1. 116

B.3 As Fig. B.1 but using MERRA-2 precipitation to calculate Q1. 116

B.4 Scatterplot of the slope (left column) and correlation (right column) for the linear regression between column-integrated DSE budget and column-integrated Q1 for TEWs in the NH (top row) and SH (bottom row), with Q1 calculated directly from the DSE tendency. 117

B.5 As Fig. B.4 but using IMERG precipitation to calculate Q1. 118

B.6 As Fig. B.4 but using MERRA-2 precipitation to calculate Q1. 119

C.1 Scatterplots showing the number of TEW points in each longitude buin over each surface type for TEWs in the NH (top) and SH (bottom). The grey dashed line delineates 100 points. 121

C.2 Contoured plots showing the composite mean precipitation (shaded) and standardized anomalies of q (black solid and dashed lines) for the 500 km radius around 850 hPa TEWs in selected hemisphere/longitude bin combinations. 122

C.3 Heatmaps of area-average standardized anomalies of precipitation (x-axis) and column-integrated specific humidity (y-axis) for TEWs a) all NH b) NH land c) NH ocean d) all SH e) SH land f) SH ocean. In each panel, the linear fit is shown in solid dark blue while x=y is shown in dashed grey. The correlation is given in teh lower left corner of each panel. 123

C.4 Scatterplot of the slope (left column) and correlation (right column) for the linear regression between standardized precipitation anomalies and column-integrated specific humidity for 850 hPa TEWs in the NH (top row) and SH (bottom row) 124

C.5 As Fig. C.3 but for area-average standardized anomalies of the column-integrated DSE budget (x-axis) and column-integrated Q1 (y-axis). . . 125

C.6 As Fig. C.4 but for the linear regression between standardized anomalies of the column-integrated DSE budget and column-integrated Q1. . . . 126

C.7 As Fig. C.3 but for area-average standardized anomalies of MSE (x-axis) and column-integrated moisture (y-axis). 127

C.8 As Fig. C.4 but for the linear regression between standardized anomalies MSE and column-integrated moisture. 128

C.9 Scatterplots showing the values of the N-mode parameter for TEWs in the NH (top) and SH (bottom). The horizontal grey dashed line denotes the threshold for small N-mode values, 0.1. Subgroups with fewer than 100 TEW points have been excluded. The rightmost points in each panel, which do not have a tick beneath them, are the global averages. 129

C.10 Maps of TEW track points in 2.5° grid boxes for TEWs tracked at 700 hPa during a) boreal summer (MJJASO) and b) austral summer (NDJFMA). 130

C.11 Line plots showing the diurnal cycle of TEW-associated rainfall, as a percent of the daily maximum, for each longitude bin, for TEWs in the top) NH and bottom) SH, and for TEWs over left) ocean and right) land. 131

C.12 Line plots showing the mean percent of daily max CV for TEWs in each longitude bin (colors) for TEWs in the top) NH and bottom) SH, and for TEWs over left) ocean and right) land. 131

C.13 Line plots showing the ratio of values from Fig. C.11 to Fig. C.12 for TEWs in the top) NH and bottom) SH, and for TEWs over left) ocean and right) land. 132

Abstract

Tropical easterly waves (TEWs) are important components of synoptic-scale variability in the tropical atmosphere, affecting precipitation across the tropics and sometimes serving as precursor disturbances for tropical cyclones (TCs). While their behavior can be partially explained by temperature variations and shear-related instabilities, recent work has turned to the role of moisture in TEW maintenance and propagation.

One such framework for understanding the importance of moisture to tropical systems is the moisture mode, a category of systems where moisture is the main driver of thermodynamic variations. Some recent studies have determined that TEWs in some oceanic basins are moisture modes, but not all tropical basins have been studied, and TEWs over land have had very little attention. Using a global database of TEW tracks, we find that TEWs in many regions, especially over oceans, are moisture mode-like, but that temperature variations still play roles in the thermodynamics of TEWs over land, near coastlines, and in oceanic regions with lower SSTs. The differences in the relative importance of moisture translate to differences in near-TEW environmental structure, with less moisture mode-like TEWs also having weaker cyclonic circulations.

The diurnal cycle of precipitation near TEWs approximately mirrors that of tropical precipitation, with precipitation peaking over the ocean in the early morning and over land in the late afternoon to early evening. TEW strength, however, does not have a strong diurnal cycle, especially for TEWs over ocean. Despite this lack of diurnal coupling between TEW strength and precipitation, we find that over the life of TEWs, the two are related, with the rainiest TEWs on average being stronger than the average TEW, while the driest TEWs are typically weaker. Pre-TC TEWs are also more likely to be stronger and rainier than the average TEW.

Even though TEW-associated precipitation follows a similar phasing to the typical diurnal cycle of the tropics, the presence of TEWs enhances the diurnal range, mainly by increasing the daily maximum rain rate. TEW-associated diurnal ranges are greatest in the areas where TEWs most frequently occur, but their relative enhancement is strongest at the periphery of some peak TEW activity regions, suggesting TEWs interact with other tropical convective features like the ITCZ.

TEWs are most active during the summertime, but occur year-round. The TEWs with the least and most precipitation also follow this general pattern, though the frequency of the driest TEWs increases earlier in the warm season and stays elevated longer than that of the rainiest TEWs. The rainiest TEWs occur most frequently in climatologically rainy locations, but some highly precipitating TEWs occur over regions with less rainfall, highlighting the need to study TEWs not only in areas of peak activity but across the entire tropics.

Better understanding the relationship between TEWs, precipitation, and moisture helps us to better understand tropical convection and hydroclimate. These connections have implications for forecasting TEW-related impacts, including TC genesis and rainfall extremes, both wet and dry. Better understanding the relationship between TEWs, moisture, and precipitation may also be valuable in building theories of how TEWs will behave in a warmer climate.

Chapter 1

Introduction

Tropical easterly waves (TEWs) are a westward-propagating synoptic-scale mode of variability in the tropical atmosphere. TEWs are typically convectively coupled, and while some convective metrics like outgoing longwave radiation (OLR) show TEW-associated power at 2-7 days for wavenumbers -6 to -20, they do not correspond with theoretical dry wave modes (Wheeler and Kiladis, 1999). Their wavenumber/frequency space corresponds with a phase speed of 6-10 m s^{-1}, which is characteristic of observed TEWs (e.g., Carlson, 1969; Reed and Recker, 1971; Cifelli et al., 2010). However, the periodicity of TEWs varies by region and season, affecting the spectral power of TEWs in some regions (e.g., Berry et al., 2012).

As convectively coupled waves, TEWs make significant contributions to precipitation across the tropics, especially summertime precipitation. Hollis et al. (2024b) showed that TEWs contribute 10% of the total annual precipitation across much of the tropics, and up to 30% of the total annual precipitation at some locations. For summertime precipitation, TEWs over Central America contribute up to 50% of summertime precipitation (Dominguez et al., 2020). While not specifically described as TEWs, TEW-like features over northern Australia are similarly associated with 30-50% of summertime precipitation (Berry et al., 2012).

TEWs have been identified through various methods, including manual analysis (e.g., Carlson, 1969), spectral analysis (e.g., Kiladis et al., 2006), and objective point-wise tracking (e.g., Belanger et al., 2016; Brammer and Thorncroft, 2015; Hollis et al.,

2024a). Choices in dataset, identification method, and, for objective pointwise tracking, tracking algorithm, all result in identifying different numbers of TEWs or levels of activity for any given location. Despite these discrepancies, literature broadly agrees that TEWs are most active along approximately 10° latitude in each hemisphere, and that they are most active in each hemisphere's summer.

Many studies have offered perspectives on how TEWs form and propagate, many of which focus on the relationship between African easterly waves (AEWs; a subset of TEWs over West Africa and the North Atlantic) and their relationship with the African easterly jet (AEJ). These studies have linked AEWs to both the shear-related instability along the jet (e.g., Charney and Stern, 1962; Burpee, 1972) and the soil moisture gradient across the Sahel (Hsieh and Cook, 2005). Easterly jet-related instabilities have also been identified for TEWs in the Pacific Ocean (Holton, 1971) and near northern Australia (Dickinson and Molinari, 2000; Berry et al., 2012).

Recently, attention has shifted to the role of moisture in TEWs, particularly through moisture mode theory and moisture-vortex instability (MVI) (e.g., Adames et al., 2019; Mayta and Adames Corraliza, 2024; Mayta et al., 2025a; Núñez Ocasio and Rios-Berrios, 2023; Núñez Ocasio et al., 2024). For a pure moisture mode, variations in moisture govern a convectively-coupled wave's thermodynamics, as compared to temperature-driven variations in buoyancy in other convectively-coupled waves (Adames et al., 2019). Oceanic TEWs are often considered moisture modes (e.g., Mayta and Adames Corraliza, 2024), while TEWs over land are currently hypothesized to be mixed systems (Núñez Ocasio and Rios-Berrios, 2023), where both moisture and and temperature variations are important to the system. This hypothesis for land-based TEWs is currently primarily based on one case study in Núñez Ocasio and Rios-Berrios (2023) and there has been no systematic analysis of a large population of TEWs over land.

The typical criteria for moisture modes are that enhanced moisture and precipitation are in-phase, the environment near the system obeys weak temperature gradient balance, and that moisture is the leading contributor to moist static energy in the system. Across literature on TEWs as moisture modes, many studies use spatiotemporal filtering (Wheeler and Kiladis, 1999) to identify TEW activity in oceanic domains, and then extract the moisture mode criteria based on the results of this filtering. However, filter-based methods may not adequately capture TEW activity in all basins (e.g., Berry et al., 2012). Therefore, global objective TEW tracks provide a unique opportunity to assess the importance of moisture to TEWs across the tropics, over both ocean and understudied land regions.

The significant role of TEWs in tropical precipitation and the ongoing investigation of how closely TEWs in various regions resemble moisture modes motivates the following research questions:

Q1: Are TEWs moisture modes, and does this vary regionally across the tropics?

Differences in temperature gradients between land and ocean support broadening the current hypothesis from literature that land-based TEWs are less moisture mode-like than their oceanic counterparts. Local variations in the strength of both temperature and moisture gradients, over both land and ocean, likely affect this, and some tropical land with weaker temperature variation or ocean areas with stronger variation may prove exceptions to this general hypothesis.

Evaluating how closely TEWs resemble moisture modes furthers our understanding of the importance of moisture to TEWs, and the role moist processes play in the organization of tropical convection. The case study AEW in Núñez Ocasio and Rios-Berrios (2023) showed differences in its strength and when it underwent tropical cyclone (TC) genesis that the authors largely attributed to differences in moist processes near

the wave. This suggests that better understanding the role of moisture near TEWs could aid in our understanding of the convective activity near TEWs, including extreme precipitation, and processes contributing to TC genesis.

Q2: How does TEW precipitation and strength vary diurnally?

Regardless of whether all TEWs or only some behave as moisture modes, precipitation is often enhanced near these features (Hollis et al., 2024b). This enhancement has been observed both at the seasonal to annual level (e.g., Berry et al., 2012; Dominguez et al., 2020; Hollis et al., 2024b; Fahrin et al., 2024) and at the daily level (e.g., Wiggins et al., 2023). While Hollis et al. (2024b) recently quantified what percent of the total annual rainfall is associated with TEWs across the tropics, analysis at the scale of the diurnal cycle is largely limited to single locations or small regions (e.g., Wiggins et al., 2023).

Furthermore, the diurnal cycle of TEWs themselves has received relatively little attention. While we expect near-TEW precipitation to follow some diurnal cycle, likely related to the local diurnal cycle at the wave's location, the diurnal cycle of other characteristics, such as TEW strength, is unknown.

Assuming the presence of a diurnal cycle in precipitation, we might expect to also see a diurnal cycle in TEW rotational strength. Increases in low-level vorticity, indicative of TEW strengthening, may result in increased vertical motion and precipitation. Furthermore, Lewis-Merritt and Stachnik (2026) recently showed differences in moist static energy (MSE) near amplifying and decaying TEWs, with both enhanced MSE and change in MSE near amplifying waves. This behavior supports the hypothesis of positive relationship between TEW dynamical strength and moist thermodynamic processes, including those contributing to precipitation.

Q3: What is the climatology of the extremes in TEW-associated precipitation and

how are these extremes related to TEW strength?

Beyond the diurnal cycle, there may be further multi-day scale relationships between TEW strength and precipitation. In such a relationship, we would expect the rainiest waves to have greater CV, and the driest waves to be relatively weaker. However, depending on the strength of this relationship, there may be a large degree of variation in more "average" TEWs.

As the occurrence of TEWs is strongly seasonal (Hollis et al., 2024a), the occurrence of extremely rainy TEWs is likely also seasonally dependent, with more rainy TEWs occurring during the warm/wet season of a given location. However, we may still find some extremely rainy TEWs outside of the warm/wet season (e.g., Jury, 2014).

All of these questions help to quantify the role of moisture in TEWs and their relationship to tropical precipitation. While we broadly understand that moisture is important to TEWs and that TEWs are important to tropical precipitation, the depth of this understanding varies across tropical basins. Applying consistent frameworks to the global population of TEWs allows for more systematic comparison of the different regions and the interactions between moisture, TEWs, and precipitation.

Chapter 2

Moisture and Tropical Easterly Waves

2.1 Introduction

Tropical easterly waves (TEWs) are westward-propagating synoptic-scale waves in the tropical atmosphere that are typically convectively coupled (e.g., Carlson, 1969; Reed and Recker, 1971; Hopsch et al., 2010; Gomes et al., 2015). TEWs may occur year-round, but are most active during the summertime (Hollis et al., 2024a), where they play a key role in modulating precipitation, including contributing to extreme rainfall events (e.g., Dominguez et al., 2020; Fink and Reiner, 2003; Hollis et al., 2024b).

Multiple field campaigns have documented the structure of TEWs in the North Atlantic and eastern North Pacific. TEWs across these two basins share key characteristics, namely a low-level cyclonic circulation and association with enhanced precipitation, but do not have identical structures. African easterly waves (AEWs), TEWs originating over West Africa and which propagate over the North Atlantic, have been observed over numerous campaigns, from GATE in 1974 to NASA's Convective Processes Experiments–Cabo Verde (CPEX-CV) field campaign in 2022 (Nowottnick et al., 2024). These field campaigns in the North Atlantic have helped to characterize the relationship between AEWs, mesoscale convective systems (MCSs), land-ocean inter-

actions, and Saharan dust events (Nowottnick et al., 2024; Sakaeda et al., 2025). Using CPEX-CV data, Sakaeda et al. (2025) showed differences in MCS size and intensity as the MCS propagated across the West African coastline, where the MCS with a strong AEW nearby had more intense convection, even despite the presence of dry, dusty Saharan air near the AEW.

As they propagate across the North Atlantic, some AEWs develop into tropical cyclones (TCs), while others cross the Caribbean Sea and Central America into the Pacific Ocean (e.g., Pasch and Avila, 1994; Schreck et al., 2011; Mayta et al., 2025b). Like AEWs, TEWs in the eastern North Pacific are associated with enhanced convection and rainfall (e.g., Huaman et al., 2021). However, unlike AEWs near the West African coastline, whose nearby dry air is largely sourced from the Sahara Desert, Huaman et al. (2021) suggests that the dry air between convectively active TEW troughs in the eastern North Pacific is at least partially sourced from colder air over the East Pacific cold tongue.

Global reanalysis data provides further opportunities to study TEWs across the tropics, rather than only in field campaign study areas. In a study encompassing most of the world's tropical oceans, but also including all cyclonic features that occur in the tropical monsoon region regardless of direction of motion, Hurley and Boos (2015) showed cross-sections for summertime monsoon depressions in some regions. They showed that while these features were all cyclonic in nature, the specific structures of wind, potential temperature, and PV vary by region. For systems in the northern hemisphere (NH), their analysis showed much shallower circulations with greater low-level potential temperature anomalies for monsoon depressions over West Africa compared to other areas in the NH. In the other NH regions analyzed, monsoon depressions had vertical circulations spanning much of the atmospheric column, illustrated in both the wind and PV. In the southern hemisphere (SH), Hurley and Boos (2015) found that the

structures of monsoon depressions near Australia and the Indian ocean more closely resembled their NH counterparts, while depressions over Southern Africa and South America had different structures than other regions shown.

While the Hurley and Boos (2015) analysis gives example structures for multiple domains across the tropics, their regional domains are limited to areas approximately 30° by 30°. For large ocean basins like the Pacific Ocean, these limited domains may not be representative of the entire basin and may not capture the nuances of transitions between sub-domains in the larger basin. The limited number of domains also mean that large portions of the tropics were not included, including much of the tropical North Atlantic and the central North Pacific.

Recently, multiple studies have examined whether TEWs, also called TD-type waves and similar terms, meet criteria for moisture modes. Moisture modes differ from dry waves predicted in shallow water theory due to the importance of moisture and convection to their propagation (e.g., Adames et al., 2019). Moisture modes are characterized by four main criteria, as outlined in Mayta et al. (2022), Mayta and Adames Corraliza (2024), and others:

1. Enhanced precipitation and moisture are in-phase
2. Weak temperature gradient (WTG) approximation holds for the temperature budget
3. Moisture is the dominant driver to thermodynamic variations
4. A dimensionless parameter, N_{mode}, which quantifies contributions of moisture and temperature, must be at least an order of magnitude less than 1.

Recently, TEWs in the tropical North Atlantic and parts of the North Pacific have been shown to meet these criteria (e.g., Mayta and Adames Corraliza, 2024; Mayta

et al., 2025a). Over land, simulations of a single AEW over the African continent and near the West African coastline did not necessarily meet all criteria (Núñez Ocasio and Rios-Berrios, 2023), but displayed some moisture mode-like qualities. That some but not all TEWs are moisture modes is consistent with some categorizations of tropical waves, such as in Adames et al. (2019), which presented a continuum-like model for whether temperature or moisture variations govern the wave's motion. In such a model, TD-type waves lie in a "mixed" part of the spectrum, where both temperature and moisture variations are important. For oceanic TEWs, recent work like Mayta et al. (2025a) indicates that moisture is slightly more important, while the case study in Núñez Ocasio and Rios-Berrios (2023) suggests that temperature and moisture play comparable roles for TEWs over land.

Whether TEWs in other regions of the tropics may be moisture modes remains an open question. TEWs across most regions are typically convectively coupled, with enhanced precipitation occurring near most TEWs (Hollis et al., 2024b). While other scales of tropical variability have been shown to behave as moisture modes (Adames et al., 2019; Mayta et al., 2022), the relationship between precipitation, moisture, and heating is not as well understood for TEWs outside of the North Atlantic and eastern North Pacific. Furthermore, there has not been a large-scale systematic evaluation of the relative importance of moisture to land-based TEWs to ask how moisture mode-like land-based TEWs in a larger dataset are.

The global database of objectively identified TEWs from Hollis et al. (2024a) provides an opportunity to further study the relationship between TEWs, their precipitation, and moisture, as well as how these variables vary across the tropics. Because the database uses consistent, objective criteria to identify TEW tracks in global reanalysis data, using these tracks to compare composite TEW characteristics across regions reduces disparities in data and methods, which can pose a challenge when

comparing some regional studies. While examining composite TEW structures will not answer whether individual TEWs are moisture modes, this study will better characterize whether TEWs in various parts of the tropics are typically moisture-mode like and how the relationship between moisture and other key features vary across different regions.

Based on existing work, we broadly expect oceanic TEWs to be more moisture mode-like than those over land. As TEWs are often convectively coupled over both land and ocean, however, even TEWs over land will likely demonstrate some moisture mode-like qualities. Areas where TEWs are less highly precipitating, even over oceanic areas like the southeastern Pacific, are in turn likely less moisture mode-like.

2.2 Data and Methods

2.2.1 Data

This study utilizes the global database of TEWs described in Hollis et al. (2024a), which we have extended using the same methods to include 2022 and 2023. The TEWs in this database were objectively identified using TRACK (Hodges, 1995), and further filtered to TEWs using motion-based criteria. Within TRACK, cyclonic features met an initial curvature vorticity (CV) threshold of $1 \times 10^{-5} s^{-1}$ and persisted for at least two days. To filter TRACK output to TEWs, features were further required to propagate westward at least 15°. Additionally, Hollis et al. (2024a) removed the TC portions of TEW tracks to focus their study on TEWs. These criteria may have excluded some weaker or shorter-lived TEWs, but this database uses consistent methodology across the globe, enabling comparisons across regions.

The TEW database contains tracks from two levels, 850 and 700 hPa. TEWs at

each level were tracked independently. Differences in TEW structure affect the strength of CV at different heights, and therefore the trackability of TEWs at different heights. Hollis et al. (2024a) compared the differences in TEW occurrence for the two levels, and identified the times and locations where a TEW was trackable at both levels, but did not examine the structures of other variables in and around those TEWs.

While the TEW database provides consistently defined global wave tracks, the methods used in its creation do not necessarily exclude other types of tropical waves, so long as they have westward-propagating cyclonic circulations. The lifetime and distance restrictions remove most local, short-lived features, but with no other speed or structural restrictions, other westward-propagating waves, including Rossby and some gravity waves, may be included in the track database. Based on the locations of peak activity and other characteristics reported in Hollis et al. (2024a), most of the tracks in the database are TEWs, though the potential inclusion of other types of cyclonic features should be kept in mind. Additionally, this database only tracks wave troughs, which are typically the convectively active portion of the wave, and does not include information about the convectively suppressed ridges or the wavelength of the waves.

To maintain consistency with the TEW database, this study will use dynamic and thermodynamic fields from the Modern-Era Retrospective Analysis for Research and Applications, Version 2 (MERRA-2) (Gelaro et al., 2017) to analyze TEW structures. Additionally, we will use final-run calibrated precipitation from the Integrated Multi-satelliE Retrievals for the Global Precipitation Measurement (IMERG) (Huffman et al., 2019), version 7, for near-TEW precipitation. As done in Hollis et al. (2024b), we use three-hourly averaged rain rates and a 500 km radius for associating precipitation with TEWs. Hollis et al. (2024b) showed that this radius is effective at capturing most of the precipitation around most TEWs. Dynamically, this radius captures the quarter-

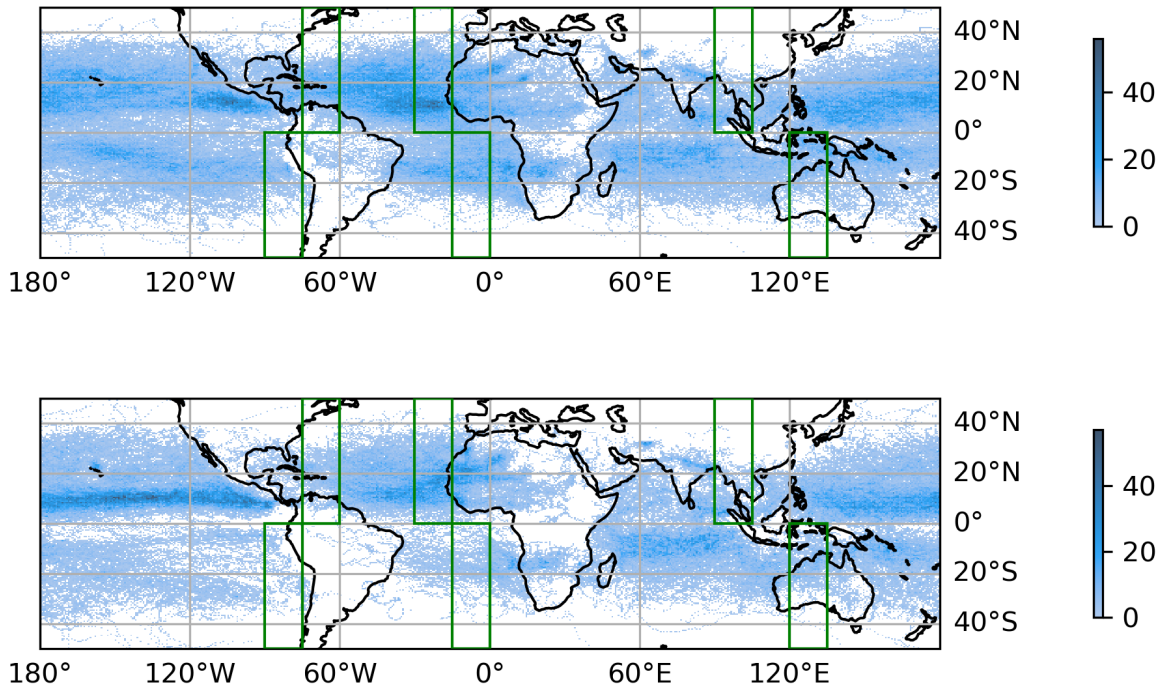


Figure 2.1: Maps of TEW track center frequency in grid boxes corresponding to MERRA-2 resolution for TEWs tracked at 700 hPa (top) and 850 hPa (bottom). Green boxes superimposed on both maps highlight selected areas compared in some sections of this study.

to half-wavelength centered on the cyclonic circulation at the wave trough, assuming an average TEW wavelength of 2000-4000 km (e.g., Brammer and Thorncroft, 2017; Serra et al., 2008; Gomes et al., 2019).

While the TEW tracks are available for 1981-2023, due to our use of IMERG precipitation for some fields, all analysis here will only use data from 2001-2023. Maps of the geographical distributions of the tracks for this period are shown in Fig. 2.1. While there are some differences between the TEWs tracked at each level (Hollis et al., 2024a,b), for the rest of this paper we will focus on TEWs tracked at 700 hPa, with results for 850 available in C.

2.2.2 TEW Track Point Grouping

While the TEW database provides TEW tracks globally, in order to compare TEW structures across different regions, it is necessary to divide the wave tracks and points into regions. However, we found that whole-ocean regions were too broad for some aspects of our analysis. Therefore, we grouped TEW track points into 15° wide longitude bins. In figures in this study, longitude bins are labeled by their westernmost boundaries. For example, the longitude bin labeled 60° covers the longitudes from 60°E to 75°E.

In addition to separating TEWs by longitude, we also separated the wave track points by whether they were over land or ocean. We used the land-sea mask available for IMERG, using a threshold of 50% to delineate the different surfaces, with values below 50% being considered land and values above 50% being considered ocean. The counts of TEW points over each surface type in each 15°longitude bin in each hemisphere for TEWs at 700 hPa are shown in Fig. 2.2. In most longitude bins, there are at least 100 points over ocean surfaces. For a number of longitude bins, especially over the Pacific Ocean (longitude bins 150-225°), there are less than 100 TEW points over land. Due to the relative lack of data, these longitudes are excluded from some of the longitudinally-based results in Section 2.32.3.2, and will be noted when they are excluded. For both hemispheres, many of the excluded groupings are land TEWs in the Pacific Ocean, which would be over islands. Even though these TEWs likely share characteristics with those whose CV centers are over oceans, with more than 5000 total points in these longitude bins, excluding the 100 or fewer TEW points over islands will not have drastic impacts on our findings. The only two excluded oceanic groupings are in the SH, the 15° and 300° longitude bins, which are largely continental between the equator and 25°S, the latitudes where most TEWs occur.

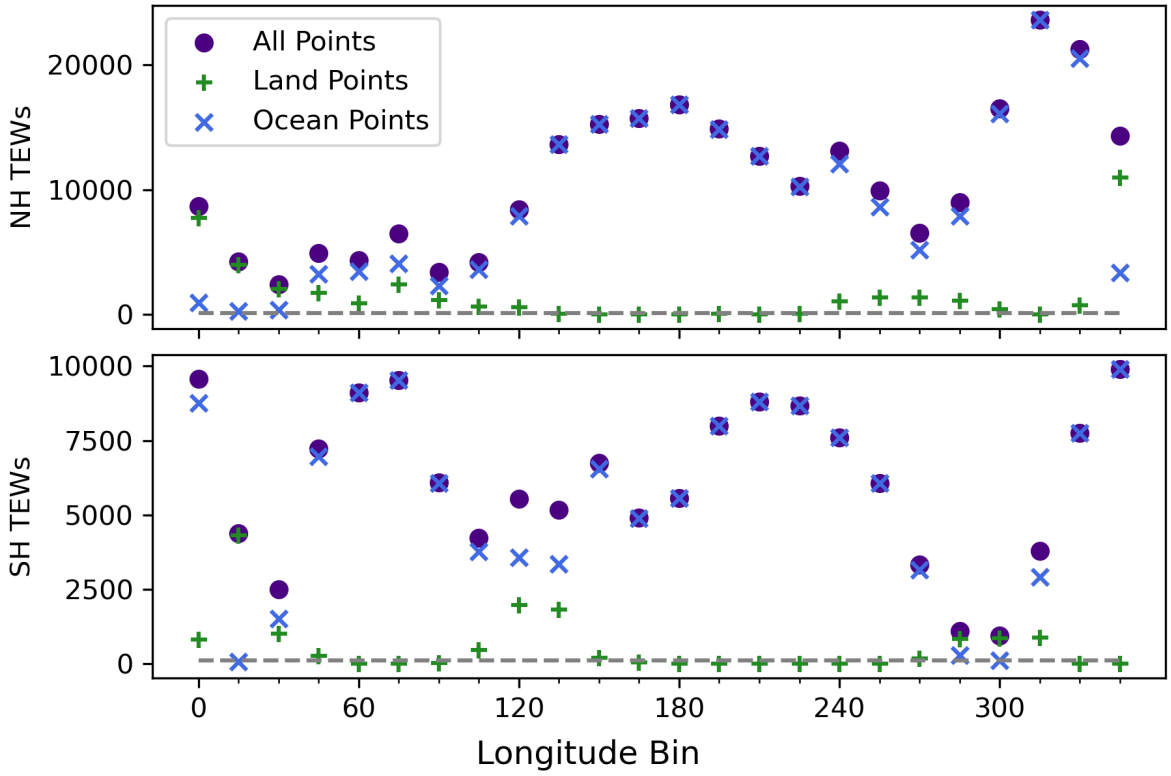


Figure 2.2: Scatterplots showing the number of TEW points in each longitude bin over each surface type for TEWs in the NH (top) and SH (bottom). The grey dashed line delineates 100 points.

2.2.3 Moisture Modes

The four moisture mode criteria described in Section 2.1 can be expressed mathematically with the following equations:

$$\langle q \rangle' \propto P' \tag{2.1}$$

$$\langle \nabla \cdot s\mathbf{v} \rangle' \simeq \langle Q_1 \rangle' \tag{2.2}$$

$$\langle m \rangle' \approx L_v \langle q \rangle' \tag{2.3}$$

$$N_{mode} \simeq \frac{c_p^2 \tau}{c^2 \tau_c} \ll 1 \tag{2.4}$$

where $\langle \cdot \rangle$ denotes a vertical integral from 100 to 1000 hPa and $'$ indicates an anomaly. Q_1 is the apparent heating rate, the calculation of which which we will discuss more below. Precipitation and specific humidity are represented by P and q, respectively. $\mathbf{v}$ is the two-dimensional wind. s is dry static energy (DSE) and m is moist static energy (MSE). L_v is the latent heat of vaporization, 2.5×10^6 J/kg. Finally, in N_{mode}, c_p is the wave's phase speed, c is the phase speed of a first baroclinic free gravity wave, τ relates the wave's speed and size, and τ_c is the convective moisture adjustment time scale, which is found via Eqn. 2.1. For c, we used the same value as used in Adames et al. (2019) and Núñez Ocasio and Rios-Berrios (2023), 50 m/s. The other variables were calculated from the TEW tracks and near-TEW fields.

We are assessing these criteria along objectively identified TEW tracks, and calculated each term, its anomaly, and its standardized anomaly for each point in the 500 km radius surrounding each TEW track point. This is a larger area than that used in Núñez Ocasio and Rios-Berrios (2023), but corresponds with the near-TEW precipitation from Hollis et al. (2024b). Across all of the moisture mode criteria, results are

sensitive to the data used, especially precipitation, which we will discuss more below. When testing the near-TEW radius and which TEWs were included in our analysis, we found that results were less sensitive to either a smaller radius around the TEW or restricting to TEWs between 5-25° latitude than they were to dataset choices, hence we chose to use the full geographic extent of the TEW database.

Recent literature assessing these criteria for easterly waves have used various approximations to calculate Q_1, though all of these can be traced back to Yanai and Johnson (1993). Núñez Ocasio and Rios-Berrios (2023) explicitly calculated the apparent heating using DSE calculated from their simulation's output. On the other hand, Mayta et al. (2022) used the precipitation rate and radiative fluxes to estimate Q_1. Other recent literature on TEWs calculated Q_1 using MERRA-2's temperature tendency variables, DTDTMST, DTDTRAD, and DTDTTRB, which are the temperature tendencies due to moist processes, radiation, and turbulence, respectively, and correspond to latent, radiative, and sensible heating (Lewis-Merritt et al., 2024; Hollis et al., 2024b).

While all three methods of calculating Q1 described above should yield similar results, and the climatologies for each are qualitatively similar, we noted quantitative discrepancies between them, especially when the rain rate and radiative fluxes were used, that may impact the moisture mode criteria. Hollis et al. (2024b) showed that while MERRA-2 captures the general structure of near-TEW precipitation, the reanalysis's bias-corrected precipitation underestimates rain rates, especially near the TEW's CV-tracked center, while rain rate estimates using vertically-integrated latent heating yields results that were more consistent with IMERG. To further verify this, we performed a simple linear correlation between IMERG and MERRA-2 near-TEW precipitation, we found a slope of approximately 0.75, but an r-value of only 0.32, further supporting that MERRA-2 bias-corrected precipitation adequately captures the

	Temp. Tend.	P-MERRA2	P-IMERG	DSE
Temp. Tend.	-	0.34	0.22	0.86
P-MERRA2	0.34	-	0.35	0.35
P-IMERG	0.22	0.35	-	0.23

Table 2.1: Table reporting correlations between various methods to calculate apparent heating, Q_1. Methods are abbreviated as follows: Temp. Tend. is an approximation using MERRA-2's temperature tendency variables; P-MERRA2 is an approximation using surface fluxes and MERRA-2 precipitation; P-IMERG is an approximation using surface fluxes and IMERG precipitation; DSE uses DSE tendencies and transport calculated from MERRA-2 wind and temperature data.

general structure of precipitation but is unable to adequately represent all possible rain rates.

Given the discrepancies in near-TEW rain rates, we calculated Q_1 using all of the methods outlined above, including using both IMERG and MERRA-2 bias-corrected precipitation, to thoroughly compare the different methods. For all methods, we calculated Q_1 globally before extracting the near-TEW fields. We then calculated the correlation of the near-TEW fields for the different methods, shown in Table 2.1. The only methods that showed high correlation were using the temperature tendency terms and explicit calculations of the DSE tendency, with an overall correlation of 0.86. The lower correlations for combinations involving the surface fluxes and precipitation, ranging from 0.2-0.4, may be a result of a few factors. When using MERRA-2 bias-corrected precipitation, which Hollis et al. (2024b) showed is lower than either IMERG observations or estimates derived from latent heating, Q_1 is likely underestimated. Meanwhile, using IMERG precipitation, even after regridding to the same resolution as MERRA-2, there may be some discrepancies between where IMERG has the highest precipitation and where MERRA-2's radiative fluxes are optimized. Given these results, we will use Q_1 calculated with the MERRA-2 temperature tendencies in evaluating how closely TEWs resemble moisture modes for the main body of this paper, and include the other methods in Appendix B.

2.2.4 Near-TEW Fields

We extracted zonal and meridional vertical cross sections centered on the TEW track points from MERRA-2. These cross sections cover all available vertical levels, and span 10° north and south (east and west) of the TEW center for zonal (meridional) cross sections. Along the cross sectional path, data for 2.5° on either side of the path was averaged. Similar averaging along the cross sectional path has also been done in studies including Núñez Ocasio et al. (2024), Russell et al. (2020), and Schlueter et al. (2019), averaging data within approximately 2.5-3° of either side of the cross section.

To more easily compare between different regions and times of year, we extracted cross sections of the raw data and calculated standardized anomalies for those cross sections. Because the TEW track database covers the full year, standardized anomalies were calculated using a monthly climatology to account for seasonal variations. Where precipitation anomalies are presented, these anomalies are also standardized relative to the monthly climatology. For both MERRA-2 fields and IMERG precipitation, the monthly climatology was calculated using 2001-2020. While not a full 30-year climatology, this ensures that the climatology period for all variables is consistent.

2.3 Results

2.3.1 Moisture and Precipitation Comparisons

While studies like Mayta et al. (2025a) have found that TEWs in certain regions are moisture modes, because we aim to examine TEWs across the global tropics, comparing near-TEW precipitation and specific humidity (q) is a useful starting point. While we anticipate that increased precipitation and anomalously high specific humidity are correlated for TEWs across the tropics, examining composites of these two variables is

helpful for developing a preliminary understanding of whether TEWs in more parts of the tropics than have been considered in existing literature may be moisture modes. If TEWs across the tropics behave at least partially like moisture modes, we should expect to see increased precipitation and atmospheric moisture co-occurring in these composites for all regions.

While only hemispheric averages are shown in Fig. 2.3 for each tracking level, we generally see, across all combinations of tracking level, hemisphere, and wave location, that moisture is typically enhanced near TEWs and especially near the wave's CV center, and approximately corresponds with the greatest rain rates, as expected. TEWs tracked at 850 hPa, which have a higher composite mean rain rate, also have larger standardized anomalies of q, with the composite mean exceeding one standard deviation near the TEW center for TEWs tracked at 850 hPa in both the northern and southern hemisphere. For TEWs in certain longitudinal groupings (shown below) where near-TEW precipitation has the highest average rain rates, standardized anomalies of q exceed 1.5 standard deviations.

While climatological increases in moisture towards the equator dominate the spatial patterns when using raw values of q (not shown), the increased moisture near the TEW's center results in less anomalously moist environments equatorward of the wave's CV center. However, when examining the composite precipitation/moisture anomaly structures for TEWs in certain locations, such as those shown in Fig. 2.4, we find that this increase is variable in both structure and magnitude. For some regions, such as the northern Indian Ocean and over the Maritime Continent and northern Australia (Fig. 2.4c and f, respectively), the increased precipitation and moisture are approximately collocated, while for other regions, such as West Africa (Fig. 2.4b), precipitation and moisture are slightly out of phase.

Comparing Fig. 2.4 a and b, composites for TEWs in the Caribbean and near

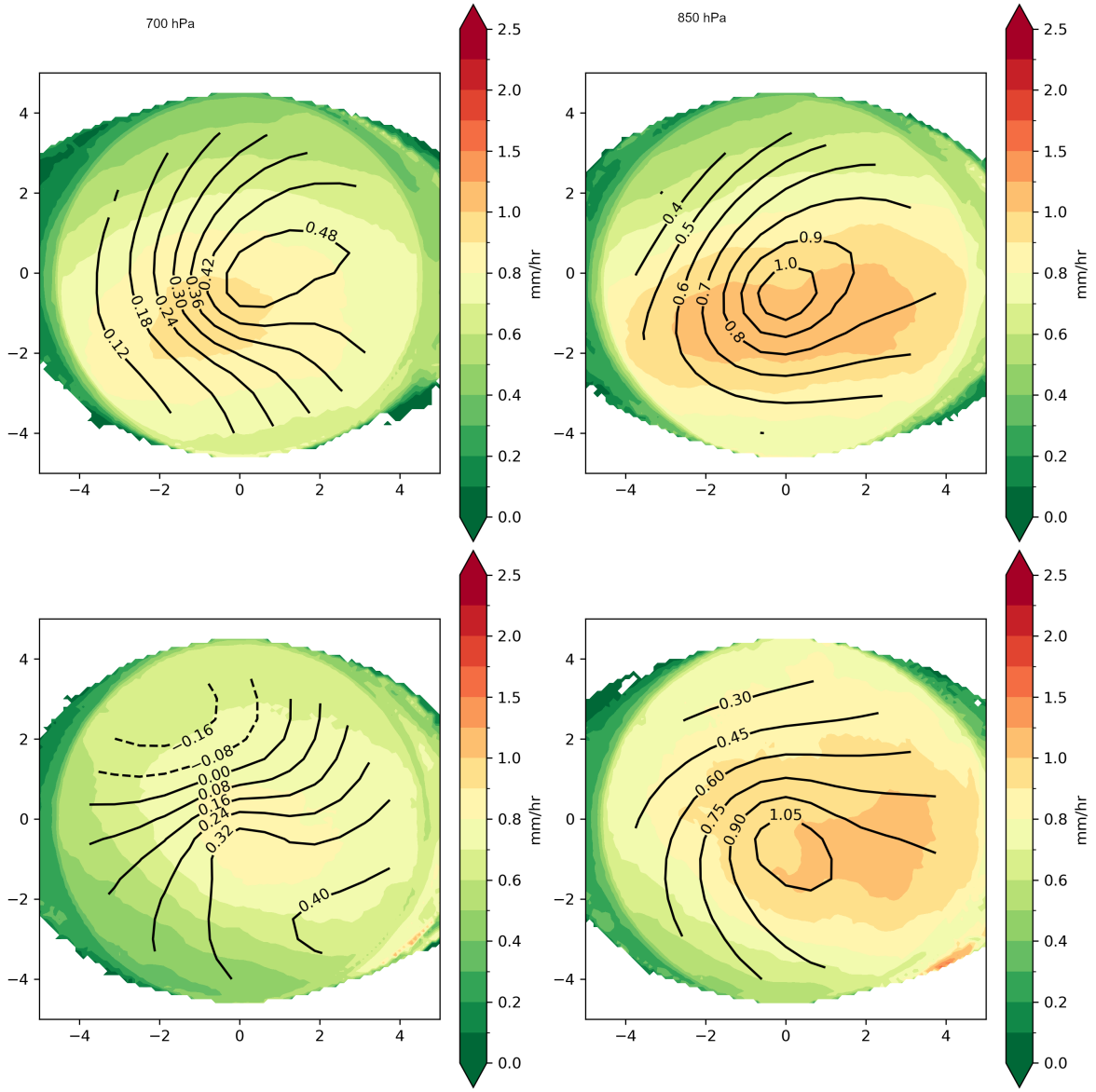


Figure 2.3: Contoured plots showing the composite mean precipitation (shaded) and standardized anomalies of q (black solid and dashed lines) for the 500 km radius around TEWs in the NH (top row), SH (bottom row), tracked at 700 hPa (left column) and 850 hPa (right column).

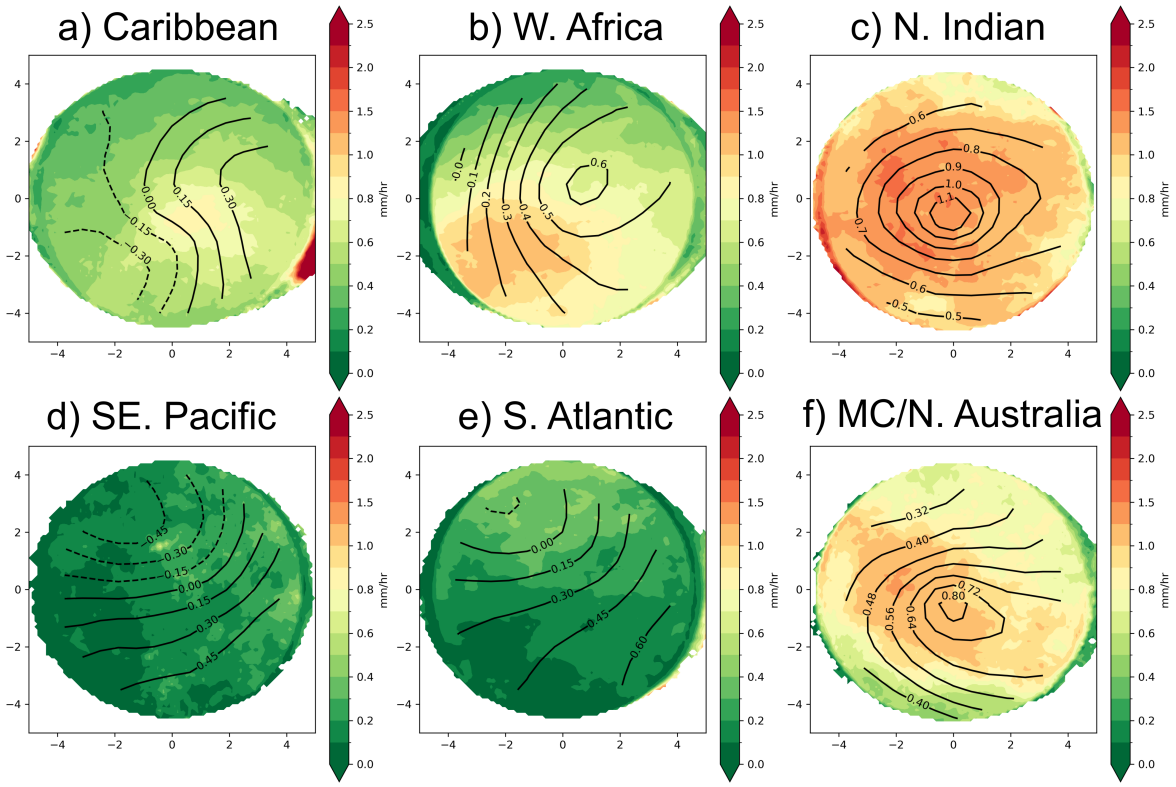


Figure 2.4: Contoured plots showing the composite mean precipitation (shaded) and standardized anomalies of q (black solid and dashed lines) for the 500 km radius around 700 hPa TEWs in selected hemisphere/longitude bin combinations.

the coast of West Africa, shows some of the changes that occur in AEWs as they cross Africa and the North Atlantic. While AEWs are near the coast of West Africa, on average, the enhanced precipitation leads the AEW's CV center and the most enhanced moisture. As the waves reach the Caribbean, the precipitation comes closer into phase with the CV center and enhanced moisture, though the precipitation still leads the most enhanced moisture. These differences between the two sides of the Atlantic provide additional motivation for separating TEWs even within basins.

While Fig. 2.4 only shows results for TEWs tracked at 700 hPa, results for TEWs at 850 hPa (in Appendix C) similarly show the greatest rain rates occurring near TEWs in the Indian Ocean and across southeast Asia. However, for TEWs in other regions, especially the southeastern Pacific and South Atlantic, we see more differences between TEWs tracked at each level.

With increased precipitation and anomalously high moisture co-occurring around TEWs in some but not all regions, a more through investigation of whether TEWs in various locations are, on average, moisture modes, appears warranted.

2.3.2 Moisture Mode Assessment

As shown in the previous section, enhanced precipitation and anomalous moisture are approximately in-phase around TEWs in many parts of the world, which suggests that many TEWs behave at least partially as moisture modes. We will examine this relationship more quantitatively below, as well as the other moisture mode criteria, concerning weak temperature gradient and the dominance of moisture in the wave's thermodynamics, both in the global average and for individual longitude bands, and separating TEW points by whether they are over land or ocean.

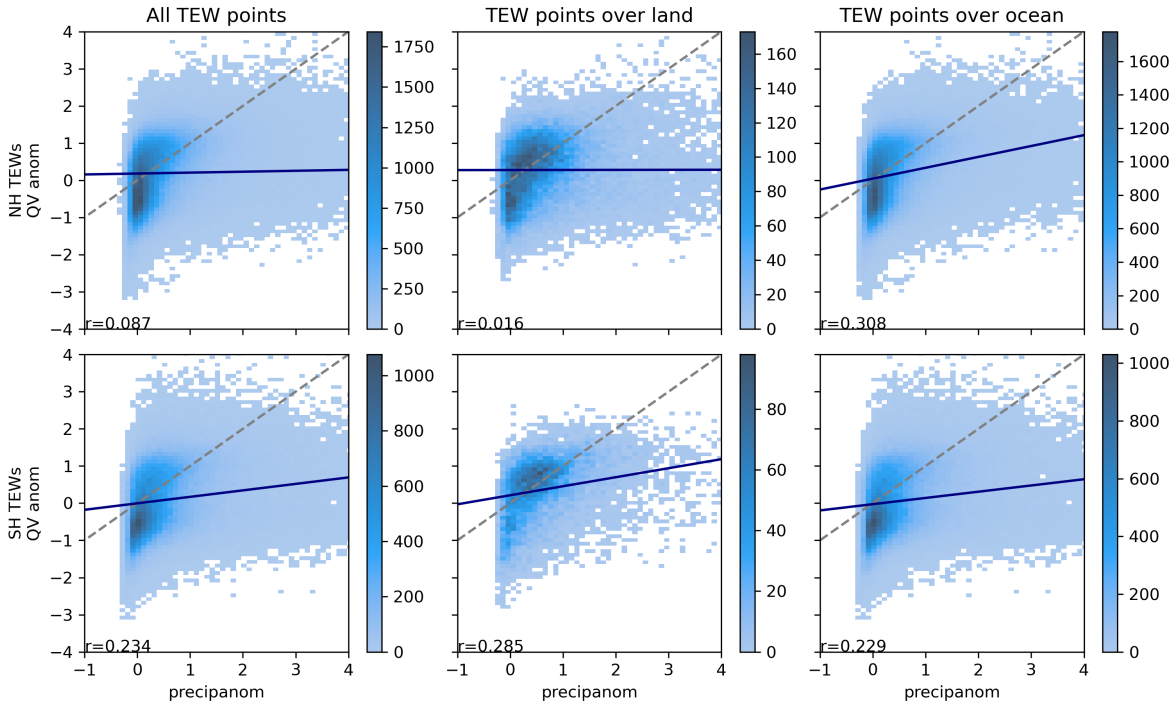


Figure 2.5: Heatmaps of area-average standardized anomalies of precipitation (x-axis) and column-integrated specific humidity (y-axis) for TEWs a) all NH b) NH land c) NH ocean d) all SH e) SH land f) SH ocean. In each panel, the linear best fit is shown in solid dark blue, while x=y is shown in dashed grey. The correlation is given in the lower left corner of each panel.

2.3.2.1 Criteria 1: Precipitation and Moisture

Even with a broad qualitative correlation between enhanced precipitation and specific humidity, the quantitative relationship between the two variables varies across the tropics. Heatmaps showing the standardized anomalies of column-integrated specific humidity against standardized anomalies of precipitation are shown in Fig. 2.5, separated by hemisphere and whether the TEW points are over land or ocean. The heatmaps for individual longitude bins across the tropics display similar shapes, and the slopes and correlations for individual longitude bins are summarized in Fig. 2.6. Subgroups with fewer than 100 TEW points have been excluded (grey dashed line in Fig. 2.2).

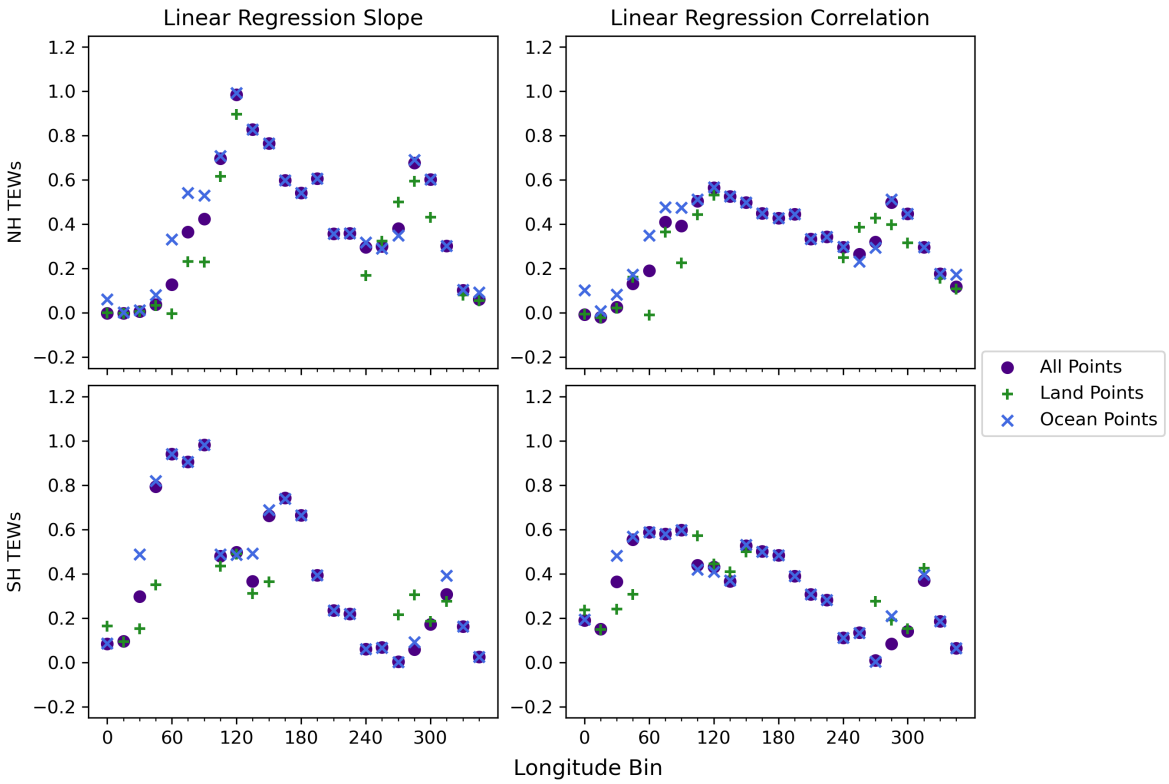


Figure 2.6: Scatterplot of the slope (left column) and correlation (right column) for the linear regression between standardized precipitation anomalies and column-integrated specific humidity for 700 hPa TEWs in the NH (top row) and SH (bottom row) t

Among all TEW points, the correlation between precipitation and moisture is relatively weak, though slightly stronger in the SH. However, the low correlation in both hemispheres may be in part due to large outliers on the precipitation axis, a small number of which exceed the axis limits. Because precipitation has much larger outliers than moisture, this in turn gives the linear fit a flatter slope. These extreme outliers arise from the exponential relationship between precipitation and moisture, where minor increases in moisture can result in large increases in precipitation. When considering only the anomalies representative of most TEWs, shaded in darker blues in Fig. 2.5, the relationship between precipitation and moisture appears slightly stronger.

In the NH, when grouping the waves by the surface their CV centers are over, the correlation between precipitation and moisture is greater for TEWs over ocean than land. The linear fit for NH TEWs over ocean also has a slope closer to 1 than the fit for NH TEWs over land. This suggests that for NH TEWs, precipitation and moisture are more closely related in oceanic TEWs than those over land, consistent with prior literature.

In the SH, which has fewer TEWs overall and many fewer TEWs over land, the differences between TEWs over land and ocean are less pronounced. The correlations for TEWs in the SH over both land (0.285) and ocean (0.229) are less than oceanic TEWs in the NH, but greater than land-based TEWs in the NH.

For some longitude bins, especially in the Indian and West Pacific Oceans (the longitude bins 75-120°E), the slopes are similar to the slope for TD-like systems identified in Mayta and Adames Corraliza (2024), 0.6 (Fig. 2.6, left panels). TEWs in the Caribbean and eastern North Pacific also show a comparable relationship between precipitation and moisture (NH longitudes 270-300°E). However, the correlation values we found are much less than those obtained in either Mayta et al. (2022) or Mayta et al. (2025a), whose correlation values ranged from 0.8-1. Both of those studies used

spectral filtering to identify their waves, so the differences between filtered waves and objective tracks may contribute to differences in the strength of the correlation. Our correlation values broadly fall between the values found in Núñez Ocasio and Rios-Berrios (2023), which objectively tracked a single AEW in both ERA5 and an MPAS simulation.

In addition to the hemipherically-averaged results from Fig. 2.5, Fig. 2.6 further shows that the relationship between precipitation and moisture is frequently stronger for TEWs over ocean than land, with almost all longitude groups having higher slopes and correlations for oceanic TEWs. Interestingly, exceptions to this pattern mainly happen in the SH. For these locations, the 270-300°E groups (the eastern South Pacific and South America) and the 0°E group (eastern South Atlantic and far western southern Africa), smaller sample sizes may play a role, as these regions have fewer TEWs over land than other regions even in the SH.

The slope of the linear regression also indicates the convective moisture adjustment time, τ_c in Eqn. 2.4. Our values for TEWs are approximately between 0.5-1 days in the Caribbean, western North Pacific, northern and southern Indian Ocean, and the southwestern Pacific, which is consistent with various literature (e.g., Mayta et al., 2025a; Núñez Ocasio and Rios-Berrios, 2023; Adames et al., 2019). These regions also have higher positive correlations, suggesting that TEWs in these places on average meet the first moisture mode criteria and have their enhanced precipitation and moisture in-phase.

For other regions, including Africa and the eastern Atlantic, the slopes are less than 0.5, with some near or even below 0. The significance values of the linear regression for these places tends to be much greater than 0.05, indicating that the weak relationship in these locations is not statistically significant. Based on Núñez Ocasio and Rios-Berrios (2023), a weaker relationship between precipitation and moisture for waves over land

is not surprising, as they found a relatively weak relationship between the two when using reanalysis data. The inclusion of the eastern North Atlantic in this group is at first surprising, but may indicate a longer transition time from mixed-type systems to more more moisture mode-like systems as AEWs translate across the Atlantic.

Finally, the weaker correlations for objectively tracked waves, seen both here in our results and in Núñez Ocasio and Rios-Berrios (2023), compared to the filter-based methods like Mayta and Adames Corraliza (2024) indicate that the strength of the relationship between precipitation and moisture around TEWs, even those over ocean, is variable and sensitive to how wave activity is identified. While both methods agree that precipitation and moisture enhancements are at least partially in-phase around TEWs, the methods diverge on the strength of the relationship.

2.3.2.2 Criteria 2: Weak Temperature Gradient

The second criteria, concerning whether the environment around TEWs is approximately in WTG balance, raised many questions about heating in near-TEW environments and the data and methods used to evaluate them more broadly. As described in Section 2.22.2.3, we checked multiple techniques for calculating Q1 and tested the impacts of various near-TEW radius sizes, finding that Q1 approximations had a larger impact. While we will only show results calculated using MERRA-2 temperature tendency terms, for all methods of calculating Q1, heatmaps of Q1 against the column-integrated DSE flux divergence (hereafter simply "DSE"), heatmaps like Fig. 2.7 are qualitatively similar, with a generally positive relationship between Q1 and DSE that is similar between both hemispheres. If the near-TEW environment is in WTG balance, we expect linear regression slopes near 1, ideally with correlation values also near 1. For each hemisphere overall, despite the presence of large outliers, the majority of TEW points lie in a region near both the best fit and 1:1 lines. General patterns

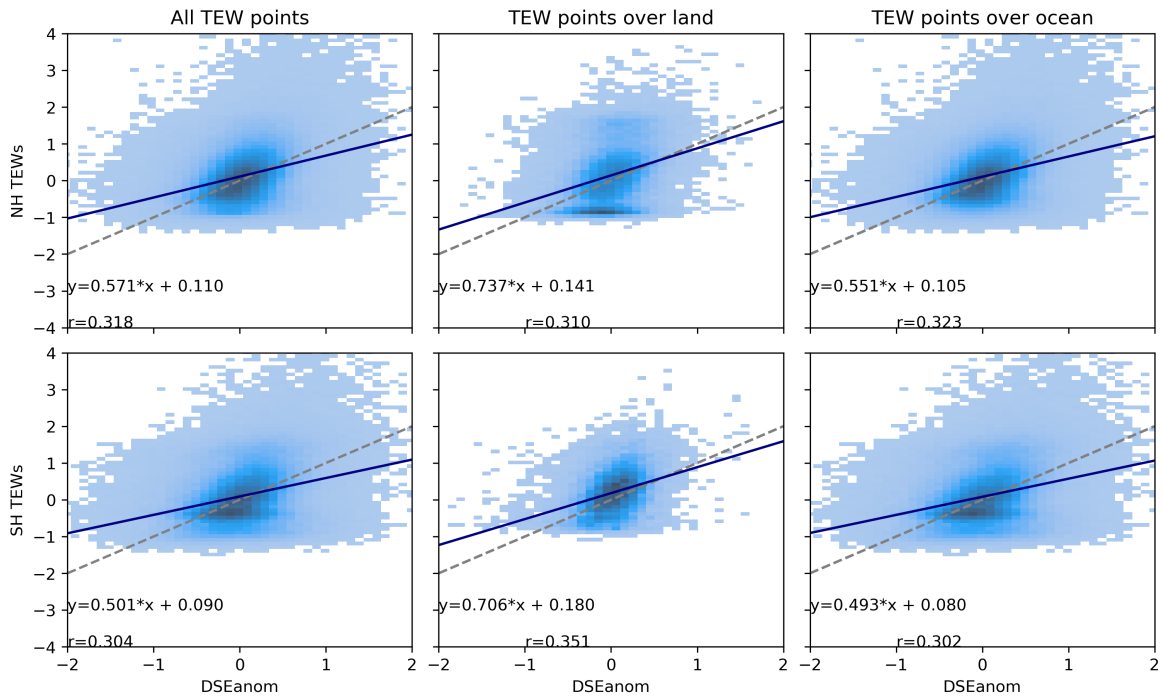


Figure 2.7: As Fig. 2.5 but for area-average standardized anomalies of the column-integrated DSE flux divergence (x-axis) and column-integrated Q1 (y-axis).

are similar in the NH and SH, with slopes between 0.5-0.6 and correlations near 0.3, supporting TEWs approaching WTG balance, even if not all TEWs completely meet this criteria.

When separating TEWs by surface type, TEW points over land in each hemisphere have slopes exceeding 0.7, indicating that these waves are closer to WTG balance than their oceanic counterparts, which for both hemispheres have slopes near 0.5. The oceanic TEW group contains more outliers than the land-based group, which may mean that many oceanic TEWs are slightly closer to WTG balance than the linear regression in Fig. 2.7 indicates. However, with correlation values between 0.3-0.4 for both surfaces and hemispheres, the approximation of WTG balance for TEWs in either hemisphere over either surface appears mixed, with many TEWs nearing WTG balance and many that do not.

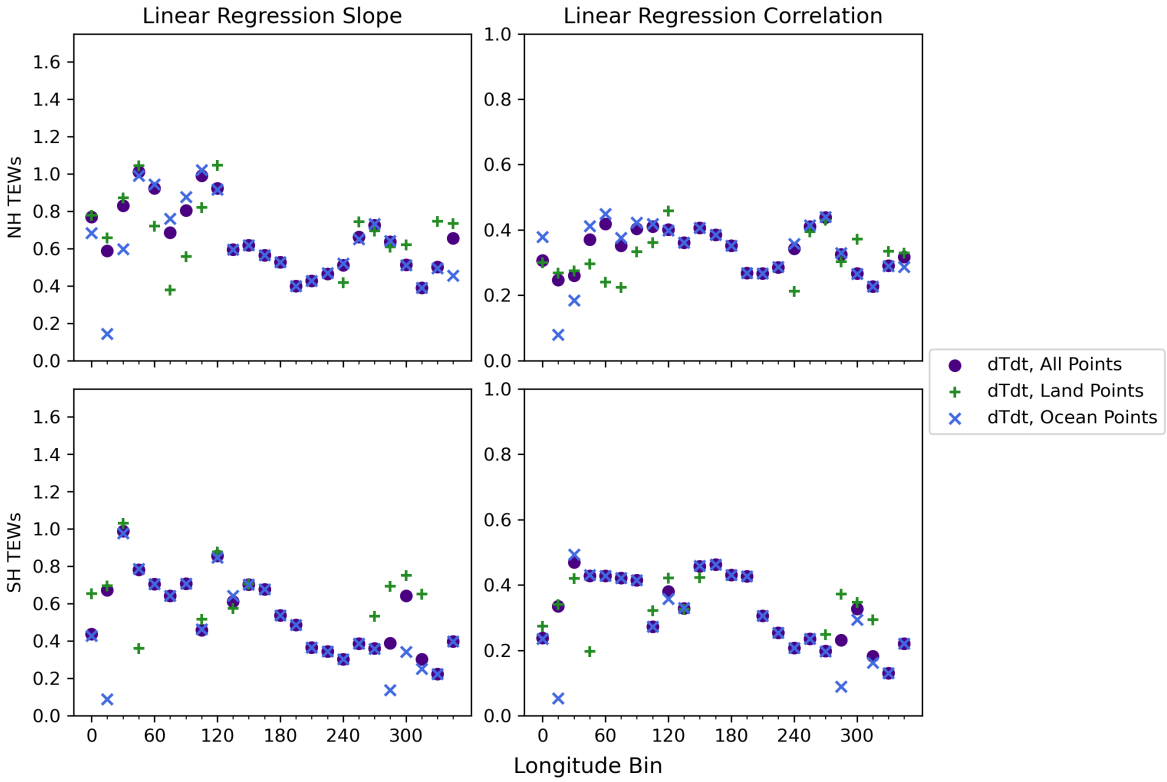


Figure 2.8: As in Fig. 2.6 but for the linear regression between standardized anomalies of the column-integrated DSE flux divergence and column-integrated Q1.

Further breaking down TEWs into longitudinally-based groups shows additional variation, with some regions being much closer to WTG balance than others. The slope of the linear regression between DSE and Q1 for land-based TEWs over western North Africa (longitude groups 0°E and 330-345°E) is near 0.8, which, while less than the case study in Núñez Ocasio and Rios-Berrios (2023) does agree that TEWs in this area are approximately in WTG balance. Interestingly, TEWs in the central North Atlantic (oceanic TEWs in longitude groups 300-330°E) are further from WTG balance than either those over western North Africa or the Caribbean and eastern North Pacific (longitude groups 255-285°E).

In the NH, the TEWs closest to WTG balance are broadly found in the Indian Ocean and far western North Pacific. For some longitude groups, land and ocean appear similarly close to WTG balance, such as the groups at 45°E and 120°E, which cover the far western Indian Ocean and the Philippines and waters immediately east, respectively. For the far western North Pacific in particular, the exact location of the TEW CV centers among islands may be a factor influencing apparent differences between TEWs over land and ocean. Not all TEWs in the broad Indo-Pacific region are close to WTG balance, however, as TEWs over land in the vicinity of the Bay of Bengal (longitude groups 75-90°E) are much further than those over ocean in the same region.

Fewer regions of the SH have TEWs very close to WTG balance, though TEWs in parts of the Indian Ocean basin (longitude groups 30-90°E) and near the Maritime Continent and northern Australia (longitude group 120°E), TEWs over both land and ocean approach it with slopes near 0.8.

For many longitudes of both hemispheres, correlation values are between 0.3-0.5, with lower values in both hemispheres in the central to eastern Pacific Ocean. Therefore, while the closeness to WTG balance varies across the tropics, the strength of this

relationship is largely consistent.

Results using other methods of calculating Q1 are similar, and are shown in Appendix B. Furthermore, TEWs tracked at 850 hPa (Appendix C) are generally closer to WTG balance, with DSE-Q1 linear regression slopes closer to 1 than those shown in Fig. 2.8. Discrepancies between levels are not surprising, as Hollis et al. (2024b) showed differences in near-TEW precipitation between TEWs tracked at 850 and 700 hPa, and furthermore between TEWs where the wave was only identifiable at one level or at both levels.

2.3.2.3 Criteria 3: Importance of Moisture

While weak temperature gradient is not consistently met around TEWs, Fig. 2.9, which shows the relationship between anomalies in moisture and anomalies in column-integrated MSE (hereafter simply "MSE"), indicates that moisture is a leading component in thermodynamic variations in TEWs. The strong linear relationship is present for TEWs over both land and ocean, indicating that moisture is critically important for most or all TEWs. Given the convective coupling of most TEWs and the relationship between precipitation and moisture shown above, a strong relationship between moisture and MSE is to be expected. Correlation values for almost all combinations of level, hemisphere, and longitude bin are greater than 0.7, and in many cases, correlations are greater than 0.9, which is closer to correlations reported in existing studies. The slopes and correlations for all combinations of subgroupings are summarized in Fig. 2.10.

Interestingly, while we see a strong linear relationship between moisture and MSE, the slopes found here differ from those in other recent literature. However, unlike those studies, we use standardized anomalies to aid intercomparison between regions, as climatological means and standard deviations vary across the tropics.

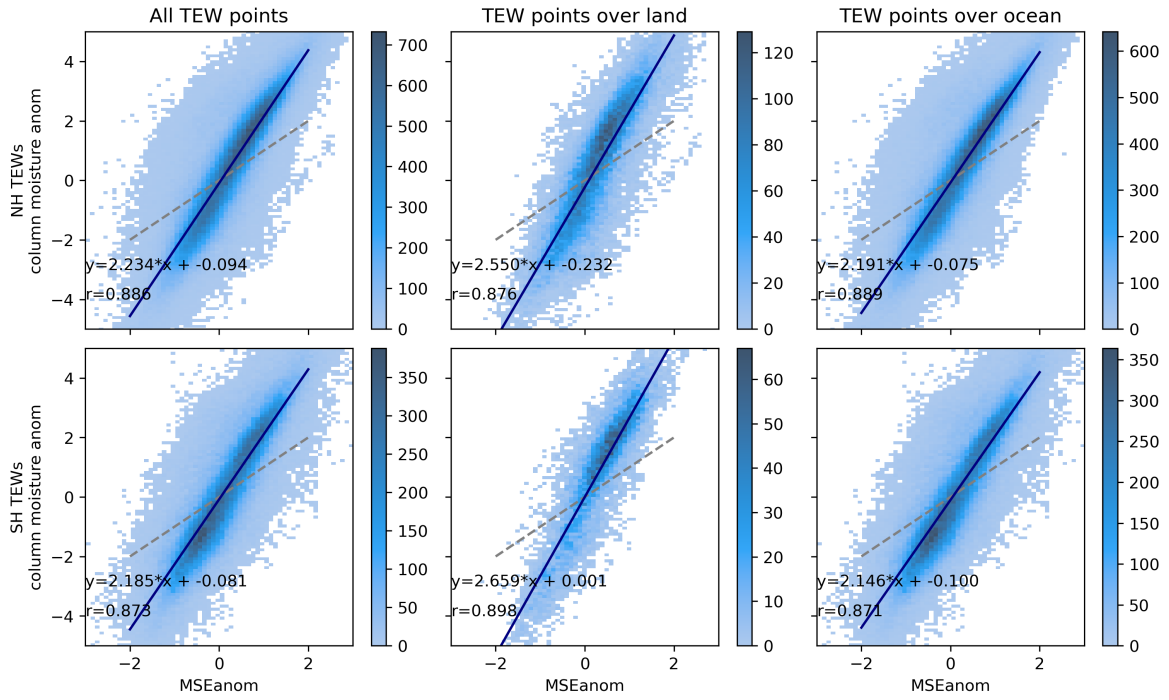


Figure 2.9: As Fig. 2.5 but for area-average standardized anomalies of MSE (x-axis) and column-integrated moisture (y-axis).

2.3.2.4 N-mode Parameter

In addition to the strong linear correlations shown in Figs. 2.9 and 2.10, the N-mode parameter can be used to assess the importance of moisture to a system. This parameter gives a more accurate assessment of whether thermodynamic variations are due to moisture. For moisture modes, N-mode should be much less than 1. Averaged over all TEWs in each hemisphere, N-mode has values of 0.379 in the NH and 0.050 in the SH. However, these values include TEWs over both land and ocean. Over ocean, N-mode is smaller for TEWs in both hemispheres, 0.032 in the NH and 0.052 in the SH. These oceanic values are consistent with Mayta and Adames Corraliza (2024), and are sufficiently small to meet the criteria for moisture modes. In the SH, land-based TEWs also have sufficiently small N-mode, 0.033, while land-based TEWs in the NH do not, with a hemisphere-average value of 5.305.

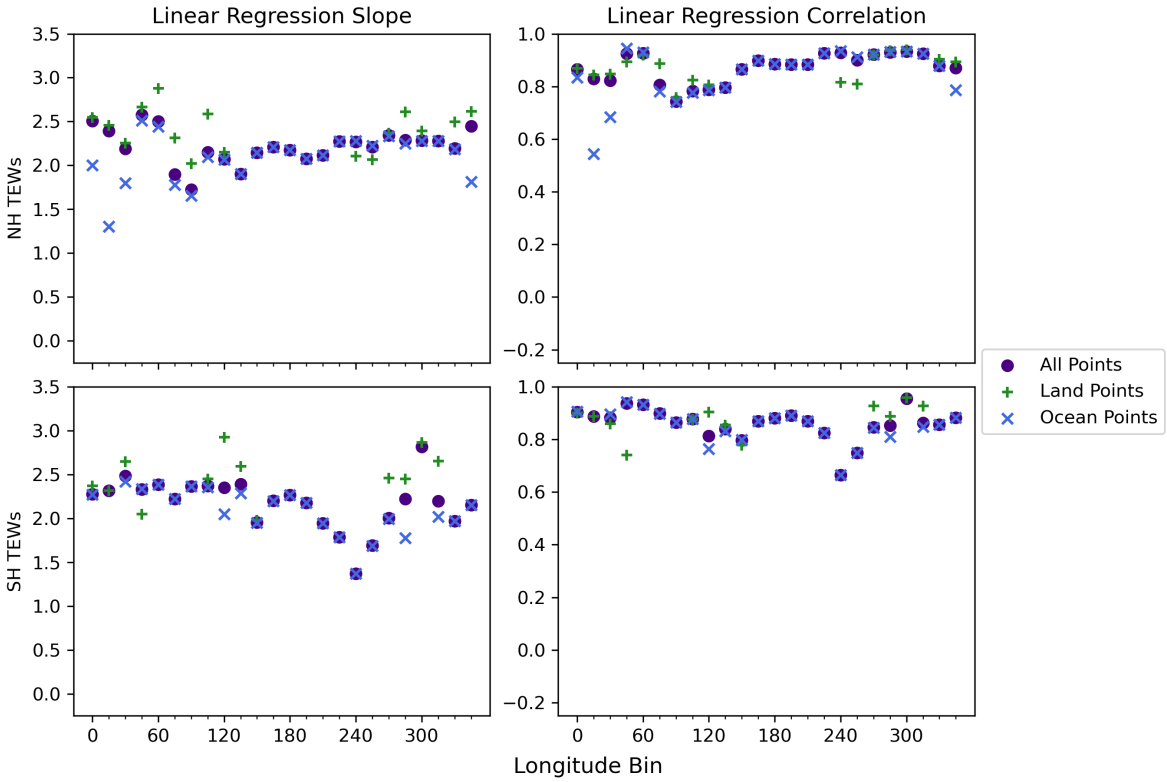


Figure 2.10: As Fig. 2.6 but for for the linear regression between standardized MSE anomalies and column-integrated moisture.

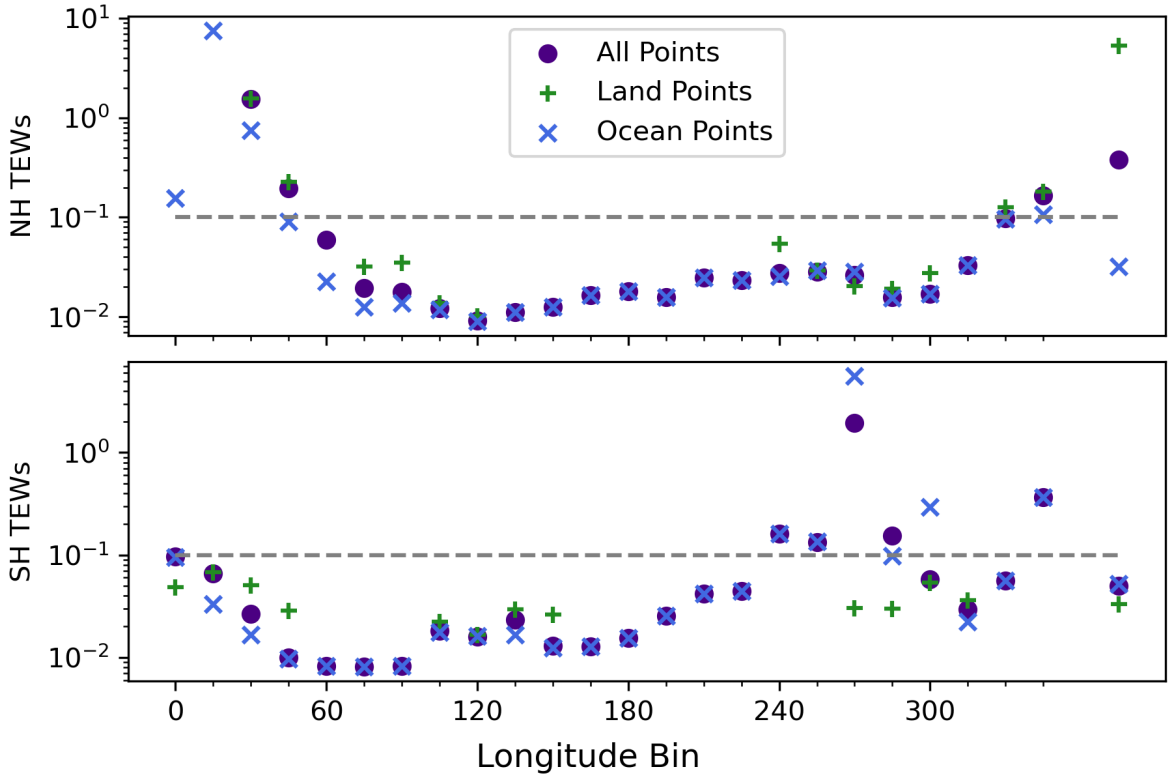


Figure 2.11: Scatterplots showing the values of the N-mode parameter for TEWs in the NH (top) and SH (bottom). The horizontal grey dashed line denotes the threshold for small N-mode values, 0.1. Subgroups with fewer than 100 TEW points have been excluded. The rightmost points in each panel, which do not have a tick beneath them, are the global averages.

While the global average value of N-mode for NH TEW points over land is not sufficiently small, it is in some longitudes. Shown in Fig. 2.3.2.4, values of N-mode are sufficiently small for land-based TEWs in areas adjacent to the Indian Ocean (longitude groups 75-120°E) and in the tropical Americas (longitude groups 240-300°E). We also note that in addition to the exclusion of subgroups with 100 points, values for N-mode are not shown for locations where τ_c was negative (longitude groups 0-15°E). The negative values of τ_c in these locations were very close to zero, so these TEWs did not meet Criteria 1 and the magnitude of N-mode is greater than 1. Therefore TEWs in these locations are much less moisture mode-like than other parts of the tropics.

In the SH, TEWs in most longitude groups have sufficiently small N-mode, including TEWs over land. The locations where N-mode is not sufficiently small are in the southeastern Pacific Ocean (longitude groups 240-285°E) and parts of south Atlantic (longitude groups 300 and 345°E). These TEWs are often only trackable at 700 hPa (Hollis et al., 2024a), whereas TEWs in other parts of the tropics are more frequently identifiable at both 700 and 850 hPa. However, N-mode values for 850 hPa TEWs in these regions are not sufficiently small (Fig. C.9), so differences in waves at the two levels and their vertical development do not fully explain the larger N-mode values in these regions.

While these results broadly indicate the importance of moisture to TEWs, the estimation of key components of N-mode, especially τ_c, leave some uncertainties. Because we showed a nonlinear relationship between extremes in precipitation and moisture when evaluating the first moisture mode criteria (Fig. 2.5), the linear assumption used to estimate τ_c may not provide the most accurate convective moisture adjustment timescale. Furthermore, because we used basin and regional averages for both τ_c and the wave phase speed, rather than calculating N-mode for individual waves, these results are only indicative of an average behavior of TEWs in a given region, and

moisture may be more or less important to individual TEWs.

2.3.3 Longitudinal Variations in Structure

The variations in whether and how strongly TEWs meet moisture mode criteria across different longitudes suggest variations in TEW structure across the tropics, both between TEWs over land and ocean, and especially across tropical basins. Here, we will highlight the similarities and differences across a few key regions of the tropics. In general, the composites shown for the selected longitude bins are approximately representative of adjacent longitudes, so while there are minor variations across smaller regions, we will focus on the larger differences.

As discussed above, Fig. 2.4 shows that the magnitude of near-TEW precipitation varies greatly across the tropics. Considered together with the regional moisture mode results above, it appears that there may be a precipitation threshold below which TEWs do not behave as moisture modes: moderately precipitating TEWs in the Caribbean (Fig. 2.4a) approximately met moisture mode criteria, but southeastern Pacific and South Atlantic TEWs, which have much lower composite rain rates, did not on average meet the criteria.

As our TEWs were dynamically tracked, and a cyclonic circulation is a key feature of TEWs, we ought to consider the structure of their circulations. In addition to having the greatest rain rates and moisture anomalies, the streamlines in Fig. 2.12 show that TEWs in the eastern Indian and western Pacific Oceans also typically also have a more closed circulation than TEWs in other regions. Even without a closed circulation, the open wave composite structure for AEWs near the West African coast would still advect anomalously moist air shown in Fig. 2.4 towards the area of enhanced precipitation.

Underlaid beneath the streamlines, the column-integrated MSE near TEWs shows a number of variations across regions. Between regions, there is variability in the

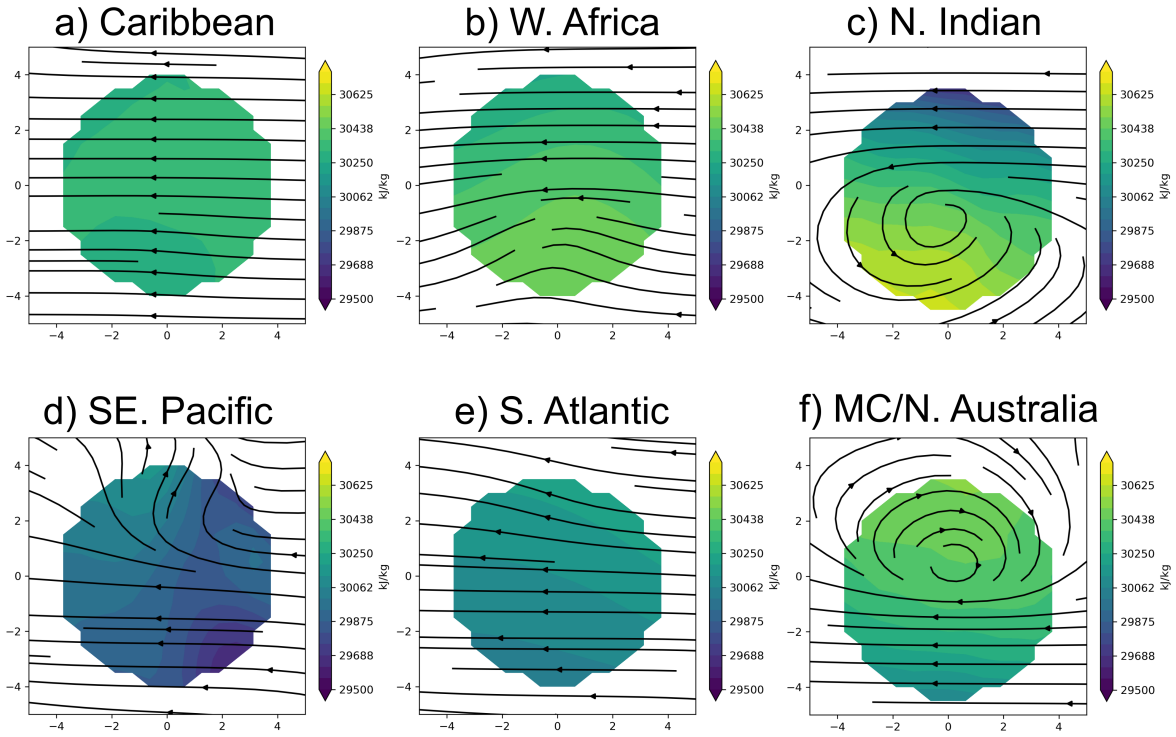


Figure 2.12: Plan view of MSE (shaded) and streamlines (black lines) for a 1000 km sided box around TEWs tracked at 700 hPa over the a) Caribbean (285-300°), b) West Africa (330-345°), c) North Indian Ocean (90-115°), d) southeastern Pacific (270-285°), e) South Atlantic (345-360°), and f) Maritime Continent/northern Australia (120-135°)

magnitude of the near-TEW MSE field, with the greatest average values near TEWs in northern Indian Ocean and the lowest values for TEWs in the southeastern Pacific. In most regions, MSE is greatest on the equatorward side of the TEW. For TEWs in the Caribbean, however, this area has lower MSE values than the area nearer the TEW's CV center. It is unclear whether this is related to the notably weaker circulation discussed above, or to other features of TEWs in this region. Though not shown here, both MSE and cyclonic circulations are stronger for TEWs in the eastern North Pacific than in the Caribbean. This further suggests an important relationship between moisture and the dynamic structure of TEWs, at least in these regions.

The weaker cyclonic curvature to the flow around TEWs in the Caribbean is consistent with challenges many TEW tracking algorithms have tracking TEWs in the Caribbean (e.g., Downs et al., 2025). Such tracking challenges are evident in the tracks we use, as shown in Fig. 2.1, where, relative to the North Atlantic, there are fewer TEWs in the Caribbean. We also note that some of the reduction in TEWs in the Hollis et al. (2024a) database can be attributed to the development and subsequent removal of TCs in this region.

In the vertical, TEWs across the tropics exhibit a clear anomalously cyclonic low-level circulation, illustrated by the meridional cross sections of the u-component of wind shown in Fig. 2.13. All of these selected composites are for TEWs tracked at 700 hPa, and feature a cyclonic circulation that maximizes near that level. As expected, the easterly anomalies are on the poleward side of the TEW's CV center (positive x-axis for panels a-c, negative x-axis for d-f). For all regions, this poleward side with the easterly anomalies is as strong as or stronger than the westerly anomalies on the equatorward side. While we expect the strength of the circulation and precipitation intensity to be related for convectively coupled waves, the exact relationship is not well quantified across the whole tropics and will be discussed more in Chapters 3 and 4. Here, we show

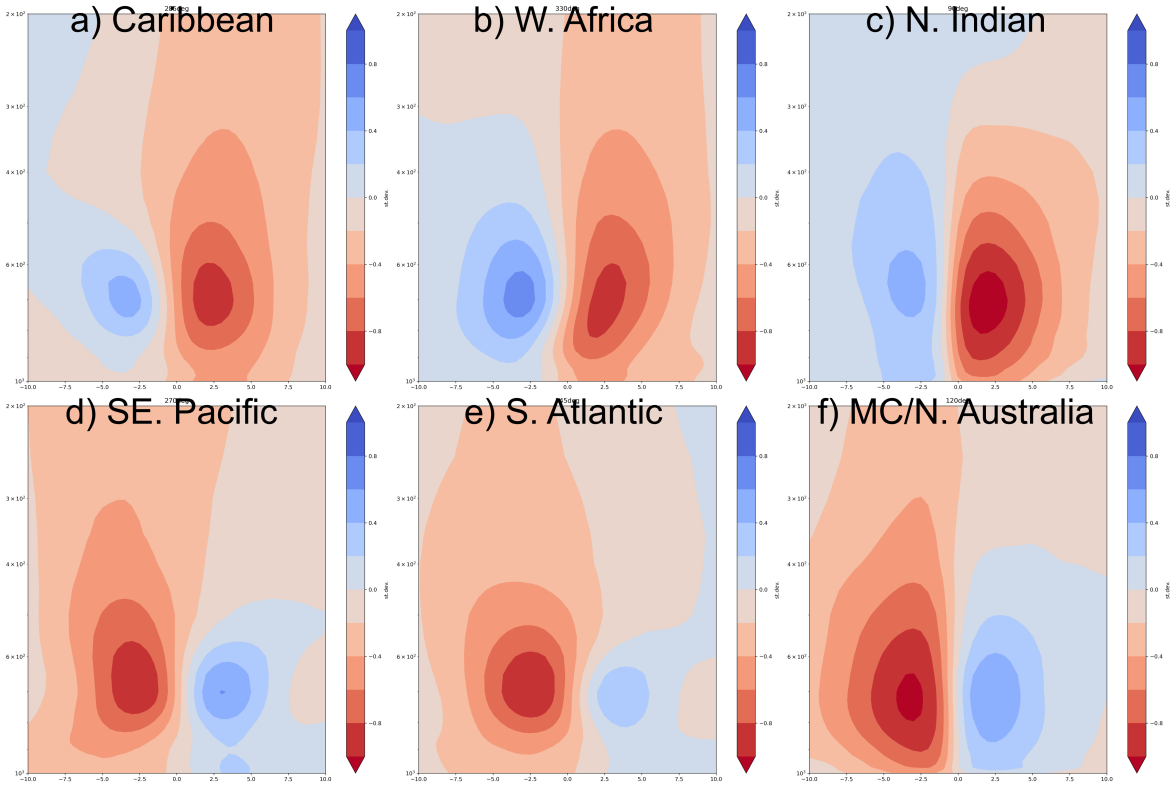


Figure 2.13: Meridional cross sections of u-wind for TEWs tracked at 700 hPa over a) the Caribbean (285-300°), b) West Africa (330-345°), c) North Indian Ocean (90-115°), d) southeastern Pacific (270-285°), e) South Atlantic (345-360°), and f) Maritime Continent/northern Australia (120-135°)

that regions with the greatest precipitation also have stronger circulations than those with less precipitation. Consistent with the streamlines shown above, the cyclonic anomalies are somewhat weaker for TEWs in the Caribbean and South Atlantic.

Across the selected regions shown, the depth and orientation of the cyclonic circulation shows some distinct differences. In the lower half of the atmosphere, the TEWs across the Indian and western Pacific region (Fig. 2.13 c and f) feature circulations that are very close to vertically stacked. The cyclonic anomalies in this region are also typically relatively vertically deep when compared to the circulations near TEWs in other parts of the SH (Fig. 2.13 d-e).

For TEWs near the coast of West Africa (Fig. 2.13b), however, the structure is less

symmetric about TEW's CV center, with the strongest westerlies in a more compact area than the strongest easterlies and vertical tilts in the cyclonic circulation below 700 hPa. In these lowest levels of the atmosphere, the cyclonic circulation is slightly equatorward (south, negative x-axis) of the 700 hPa circulation. While TEWs at 850 hPa are more commonly further north than those at 700 hPa (Hollis et al., 2024a), this cross section suggests a slight north/south tilt to more vertically developed AEWs. As seen with precipitation, wave structure changes as AEWs cross the North Atlantic. Caribbean easterly waves on average have a slightly weaker and less deep circulation whose tilt has become more vertically stacked below 700 hPa. While the Caribbean low-level jet is strongest lower to the surface, around 900 hPa (Wilson et al., 2025), it does not appear on average that its presence results in deeper circulations around TEWs or contributes to a notable low-level tilt.

Stronger westerly anomalies are also present closer to the surface for AEWs than for TEWs in other regions, though TEWs near Australia and the Maritime Continent also have deeper westerly anomalies. Some work has attempted to compare TEWs in these two regions, though results are mixed whether TEWs in these two places have similar or different influences. Dickinson and Molinari (2000) found that there is a similar climatological PV gradient along the Sahel region of Africa and the northern coast of Australia, but that Australia lacked comparable wave activity when using variance filtered wind and OLR to detect TEW activity. Later, Berry et al. (2012) objectively tracked PV features over northern Australia, finding westward-propagating convectively-coupled synoptic-scale cyclonic disturbances with TEW-like phase speeds. They attributed their differing results to the different methods for identifying wave activity, as they further found that the return period for the waves in the Australian region was less regular than for AEWs.

The moisture mode analysis above used area-averaged column-integrated moisture

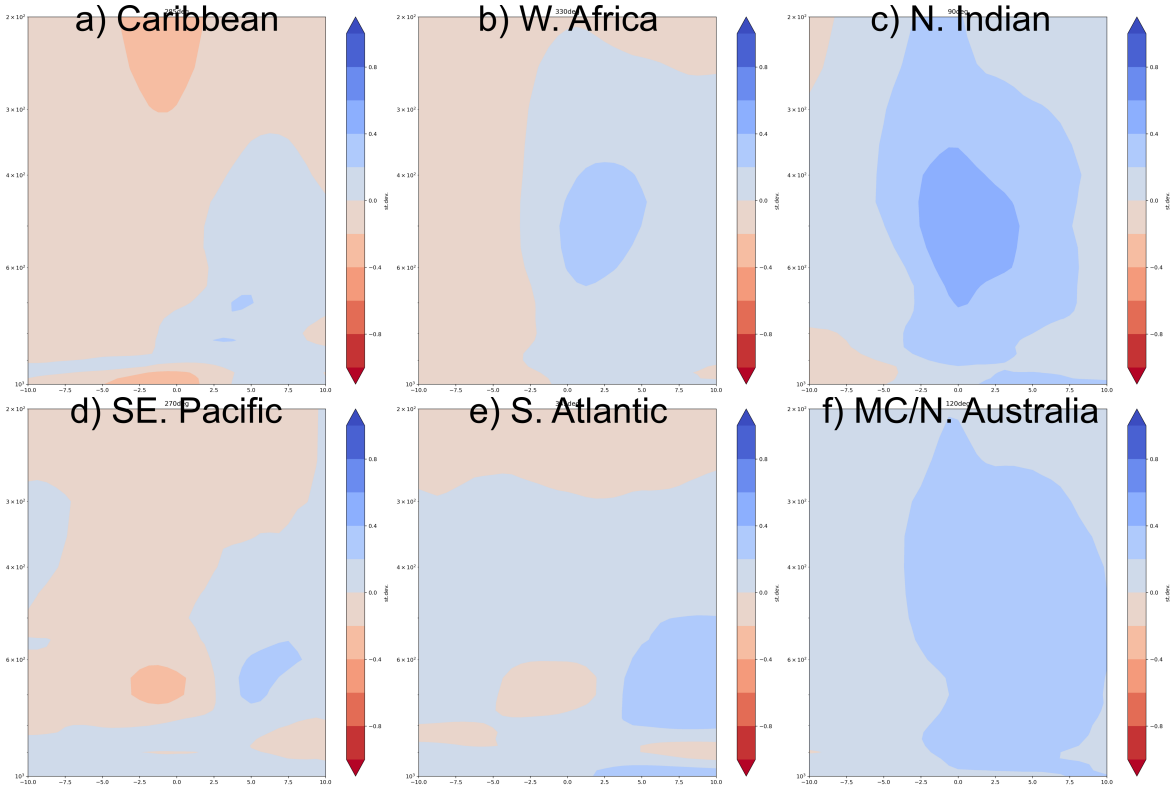


Figure 2.14: Zonal cross sections of q standardized anomalies for TEWs tracked at 700 hPa over a) the Caribbean (285-300°), b) West Africa (330-345°), c) North Indian Ocean (90-115°), d) southeastern Pacific (270-285°), e) South Atlantic (345-360°), and f) Maritime Continent/northern Australia (120-135°)

anomalies, and Figs. 2.3 and 2.4 showed plan view column-integrated anomalies. Here, we present zonal cross sections of near-TEW moisture to further examine the structure of moisture near TEWs. Similar to Fig. 2.4, the strongest moisture anomalies are found near TEWs in the northern Indian Ocean (Fig. 2.14c), with more strongly enhanced moisture also present for AEWs (Fig. 2.14b) and the Maritime Continent/northern Australia region (Fig. 2.14f). Similar to the plan views shown in Fig. 2.4, the enhanced moisture is near and/or behind the CV centers of the waves.

These zonal cross sections, however, give additional insight into where in the column moisture is most enhanced. While the cyclonic circulations were strongest at the wave tracking level, moisture enhancements exist across a deeper portion of the atmosphere

for many regions, between the surface and 400 hPa, and in some regions extend through the entire column. Moistening in the lower portions of the column behind (east of) the CV center is expected with the cyclonic circulation around TEWs, and is additionally consistent with the latent heating observed in Lewis-Merritt et al. (2024).

While TEWs appear to leave moistened atmospheric columns in their wakes, resulting in asymmetrical zonal cross sections, the same cross sections for temperature are typically more symmetric. Across most regions, the temperature structure near TEWs, shown in Fig. 2.15 follows a broad pattern of warm anomalies above 700 hPa, the tracking level shown, and cool anomalies below it, while the finer details vary notably by region. For example, comparing AEWs over West Africa and TEWs in the Caribbean, which includes some AEWs that have propagated across the Atlantic, warm anomalies exist through the atmospheric column above 600 hPa for the innermost 2.5° along the cross section for AEWs near West Africa (Fig. 2.15b), while the warm anomalies are constrained to a smaller pocket between 700-400 hPa, with weak cold anomalies in the uppermost levels of the atmosphere. This smaller pocket of warm anomalies is also above stronger low-level cool anomalies (Fig. 2.15a), averaging 0.8 standard deviations cooler than average near the TEW's CV center.

Unlike other fields, where TEWs over the northern Indian Ocean and near the Maritime Continent and Northern Australia shared many similarities, their composite temperature structures are less similar, though both have a much deeper vertical extent to their mid-level warm anomalies. TEWs over the northern Indian Ocean (Fig. 2.15c) have weaker low-level cool anomalies, and an asymmetrical structure, with the cool anomalies near 700-600 hPa being stronger ahead (west of) of the TEW's CV center. In contrast, the temperature structure for TEWs near the Maritime Continent and Northern Australia resemble some elements of those over West Africa and the Caribbean, with stronger, symmetrical low-level cool anomalies, similar to Caribbean

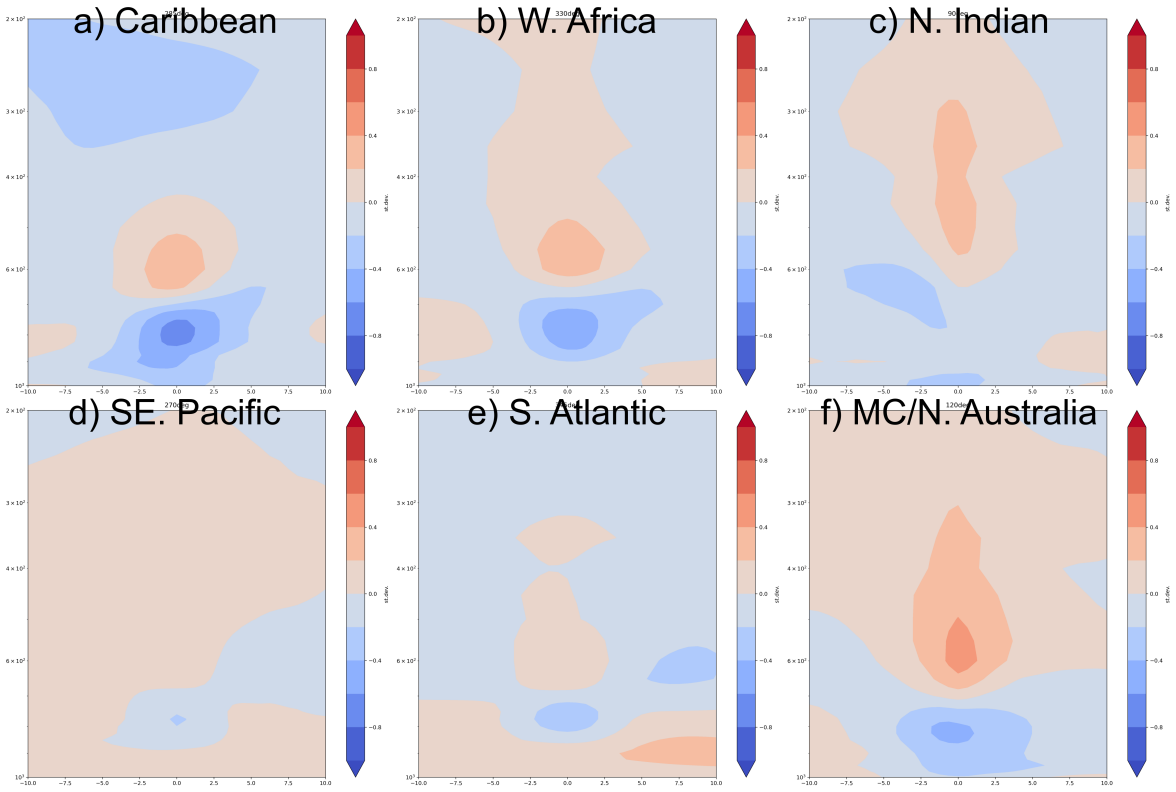


Figure 2.15: As Fig. 2.14 but for temperature.

TEWs, and warm anomalies both above and ahead of the wave, similar to AEWs near West Africa. This apparent hybrid of features may be due to the inclusion of TEWs over both land and ocean in these composites. Additionally, we showed above that TEWs in this longitude bin (120°) over ocean more closely met the first moisture mode criteria than those over land.

2.4 Discussion and Conclusions

In exploring whether TEWs across more parts of the tropics may be considered moisture modes, we have investigated the importance of moisture to TEWs, as well as some of the differences that arise in near-TEW structures across different regions. Our analysis of whether TEWs meet moisture mode criteria did not find that all TEWs can broadly be assumed to be moisture modes, but we have found that TEWs in some regions, especially TEWs over oceans, are likely moisture modes. Regardless of whether TEWs are moisture modes, however, we have reaffirmed the importance of moisture for processes happening around TEWs. In particular, we found that enhanced column moisture and precipitation are often approximately correlated, and that moisture variations are at least as important as temperature variations for most TEWs.

In addition to the regional and surface-based differences in TEWs and their resemblance to moisture modes, how closely a TEW resembles a moisture mode may vary over the wave's life. Some of these changes are implied by the changes in slope and correlation crossing the North Atlantic (Figs. 2.6 and 2.8, longitude groups 285-345°), which gradually increase with westward progress across the basin implying that AEWs crossing the Atlantic become more moisture mode-like over the course of their lives. Changes across basins are likely the result of changing dynamic and thermodynamic environments. In the case of AEWs crossing the Atlantic, the systems are more mixed

over the African continent, consistent with the case study in Núñez Ocasio and Rios-Berrios (2023), which is also physically consistent with the relationship between AEWs, the AEJ, and the temperature and moisture gradients in the Sahel. Our results show that these waves become more moisture mode-like with time and propagation over the tropical North Atlantic, where there is no temperature-driven easterly jet. Therefore, while wave life-related changes cannot be entirely divorced from regional differences, the moisture and temperature dependence of TEWs varies over their lives. Other aspects of wave evolution will be explored in Chapter 4.

Across the moisture mode criteria, especially the first two criteria, differences with prior literature arise in part due to TEW identification methods. Studies like Mayta and Adames Corraliza (2024) used spacetime filtering of a convective proxy variable, brightness temperature, to identify TEW activity. As such, they require TEWs to be convectively active, but do not prescribe a dynamical strength to the waves. In contrast, by using objective TEW tracks derived from CV, some of our TEWs may be less convectively active, but are required to have a certain dynamical strength. As a result, spacetime filtered TEW activity includes dynamically weaker but convectively active TEWs, while objective tracks include dynamically stronger but less convectively active TEWs. These two approaches can be complementary, with the spacetime filtered results giving a broad picture of oceanic TEWs as moisture modes, while the objective tracks help show variations across even specific basins.

With regards to near-TEW structures, while our methods differ significantly from those used in other studies like Hurley and Boos (2015), when we compare our TEW cross sections to their monsoon low pressure systems, we see some similarities. Both find strong cyclonic signatures, maximized in the lower half of the atmosphere but extending through a significant portion of the column. We also similarly find that temperature anomalies away from the TEW center tend to be relatively weak.

For AEWs near the West African coastline, Sakaeda et al. (2025) found that positive interactions between AEWs and MCSs are stronger when the AEW is slightly east of the MCS. These interactions result in stronger precipitation in the MCS, west of the AEW trough, though the strength of this relationship additionally depends strongly on the locations of both the AEW and MCS relative to the coastline. This is consistent with our composite in Fig. 2.4, where the greatest rain rates were found ahead of the TEW's CV center.

While field campaign observations are only available to compare to some of the regions presented here, we do note some similar findings. In cases from the CPEX-CV field campaign, Sakaeda et al. (2025) noted that the coastal MCS with an accompanying AEW featured more easterly and northeasterly flow to the north and northwest of the AEW, transporting warm, dry Saharan air into the environment ahead of the wave. Such patterns may help explain the anomalously warm region seen ahead of AEWs in Fig. 2.15b.

The presence of convection near to ahead of the CV center in many regions also suggests that moisture-vortex instability (MVI; Adames and Ming, 2018) applies to TEWs. Under MVI, the combination of a low-level cyclonic circulation and convection work together to import moisture towards the area just ahead of the cyclonic circulation, enhancing convection in this region and supporting westward propagation of the system.

It is important to note that our analysis is a very large-scale analysis, treating TEWs in each longitudinal and surface grouping as a composite average, and does not answer whether a specific TEW is behaving as a moisture mode. Case studies of individual or small groups of TEWs may still find value in assessing whether those specific waves behave as moisture modes or how an individual wave behaves over time, even in regions that less closely adhered to moisture mode criteria.

Beyond the question of whether TEWs are moisture modes, our findings of discrepancies between different methods to calculate Q_1 suggest a need to carefully evaluate the appropriateness of different apparent heating approximations and data sources within the broader context of the research problem being addressed. This sensitivity appears to be closely related to heating and moisture in reanalysis data, as the composite structures we showed in Section 2.32.3.3 generally agree with established literature. More investigation is needed to determine potential sources of these discrepancies and their impact on our understanding of the relationship between TEWs and moisture.

Chapter 3

Diurnal Cycle in TEW Strength and Precipitation

3.1 Introduction

Tropical easterly waves (TEWs) are westward-propagating, off-equatorial, synoptic-scale waves that are important components of precipitation variability in the tropics. TEWs occur year-round in both hemispheres, but in each hemisphere are most frequent during the warm season (Hollis et al., 2024a), where they are a notable part of the seasonal precipitation and contribute to extreme rainfall events (e.g., Dominguez et al., 2020; Fink and Reiner, 2003; Hollis et al., 2024b).

In the tropics, there are two general patterns to the diurnal cycle. Over land, precipitation often peaks in the late afternoon, especially in places dominated by sea breeze circulations, such as coastal areas and islands. Meanwhile, over oceans, both coastal waters and the open ocean, precipitation typically peaks in the early morning hours. These patterns are seen across the tropics, from West Africa to the Caribbean to the Maritime Continent.

Convectively coupled waves, including TEWs, can modify the intensity and timing of the diurnal cycle of precipitation. During the boreal summer, TEWs over Central America magnify the diurnal cycle, with the convectively active phase of TEW passage

resulting in increased precipitation (Wiggins et al., 2023). This TEW-related amplification of the diurnal cycle primarily occurred as an increase in the daily maximum intensity of rainfall. TEWs may also slightly shift the timing of the precipitation maximum and contribute to slightly rainier conditions throughout the day when they are passing a given location.

Currently, TEW-related effects on the diurnal cycle are not well understood for many parts of the tropics. This can affect our ability to forecast TEW-associated precipitation and changes in strength. The availability of global objective TEW tracks with sub-daily temporal resolution presents a larger sample of TEWs for attempting to quantify how TEWs affect the diurnal cycle. With consistent methods used to identify TEWs across the global tropics, such databases allow for the comparison of TEW-related diurnal cycles across multiple locations without discrepancies between TEW identification methods or data sources, which multiple studies have shown can affect results and complicate comparisons (e.g., Downs et al., 2025; Hollis et al., 2024a; Belanger et al., 2016).

Results like Wiggins et al. (2023) suggest that TEWs typically modulate the intensity of the diurnal cycle and only slightly shift its phasing. Therefore, we hypothesize that similar patterns will hold across the tropics, with TEW-related precipitation peaking in the early morning for TEWs over the ocean and late afternoon for TEWs over land. TEWs most likely amplify the existing diurnal cycle, though the degree of amplification likely varies by location, especially as the available moisture is highly variable across the tropics and TEWs in some locations may interact with other features like MCSs and the ITCZ.

3.2 Data and Methods

3.2.1 Data

This study relies on the global database of TEWs described in Hollis et al. (2024a) and extended to include 2022 and 2023 in this dissertation. Fig. 3.1 shows the spatial distribution of TEW tracks for the years used in this study, split between seasons. The TEWs in this database were objectively identified using TRACK (Hodges, 1995), and further filtered to TEWs using motion-based criteria. Within TRACK, cyclonic features met an initial curvature vorticity (CV) threshold of $1 \times 10^{-5} s^{-1}$ and persisted for at least two days. To filter TRACK output to TEWs, features were further required to propagate westward at least 15°. Additionally, Hollis et al. (2024a) removed the TC portions of TEW tracks to focus their study on TEWs. These criteria may have excluded some weaker or shorter-lived TEWs, but this database uses consistent methodology across the globe, enabling comparisons across regions.

The TEW database contains tracks from two levels, 850 and 700 hPa, however results presented here will mainly focus on TEWs at 700 hPa, with selected figures for 850 hPa TEWs available in Appendix C. TEWs at each level were tracked independently from the other level, which allows the database to capture a wider variety of TEWs. Differences in TEW structure affect the strength of CV at different heights, and therefore the trackability of TEWs at different heights. Hollis et al. (2024a) compared the differences in TEW occurrence for the two levels, and identified the times and locations where a TEW was trackable at both levels, but did not examine the structures of other variables in and around the TEWs.

To maintain consistency with the CV used to develop the TEW database, this study will use dynamic and thermodynamic fields from the Modern-Era Retrospective

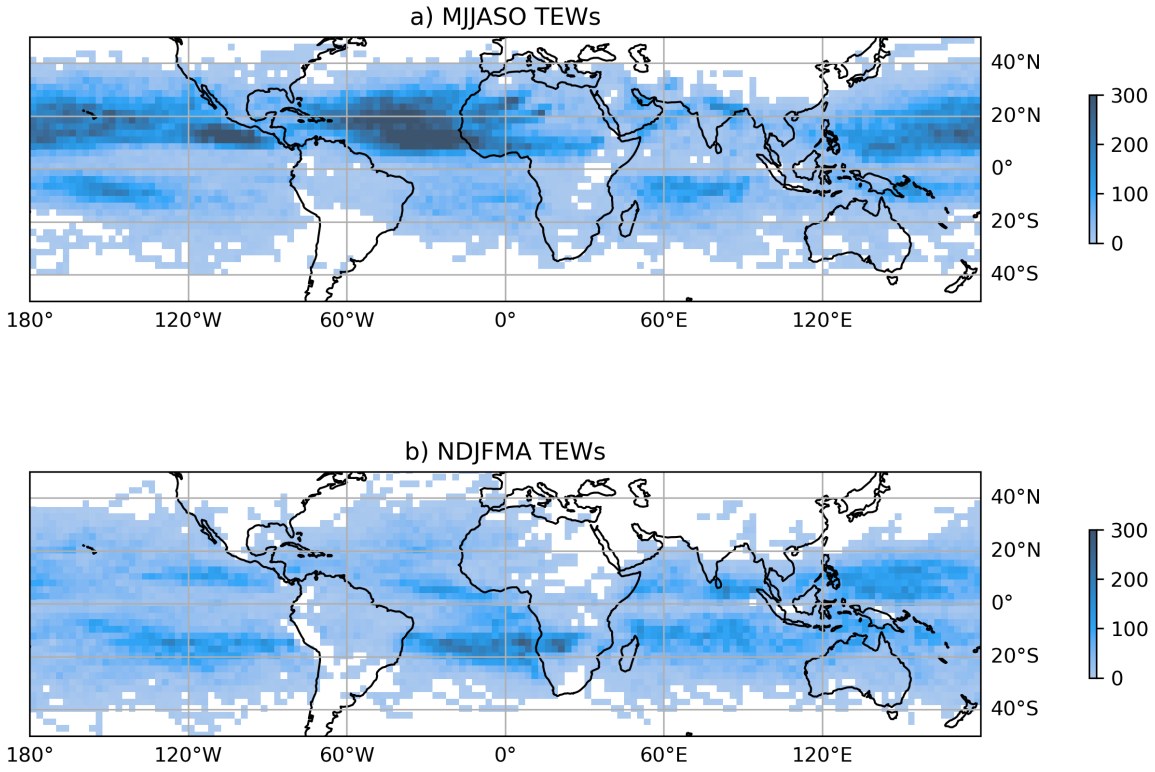


Figure 3.1: Maps of TEW track points in 2.5° grid boxes for TEWs tracked at 700 hPa during a) boreal summer (MJJASO) and b) austral summer (NDJFMA).

Analysis for Research and Applications, Version 2 (MERRA-2) (Gelaro et al., 2017) to analyze TEW structures. Additionally, we will use calibrated precipitation from the Integrated Multi-satelliE Retrievals for the Global Precipitation Measurement (IMERG) (Huffman et al., 2019), for near-TEW precipitation. As done in Hollis et al. (2024b), we use three-hourly averaged rain rates and a 500 km radius for associating precipitation with TEWs.

While time steps in the TEW tracks, MERRA-2, and IMERG all natively use UTC, we additionally consider the approximate local solar hour in our analysis of the diurnal cycle in and around TEWs. We converted from UTC to local solar hour using the TEW's longitude, retaining only the hour. As the average TEW travel distance in this database is over 2000 km (Hollis et al., 2024a), we found the local solar offset for each track point independently, rather than determining an offset based on the first track point and applying it to the whole track. Therefore, as TEWs cross from one longitude bin to the next, the local solar hour used here is within an hour of the true local solar time.

3.2.2 Wave Subgroupings

As shown in Chapter 2, TEW structures vary across the tropics. Therefore, as done in Chapter 2, we have separated TEWs into 15° wide longitude bins for parts of our analysis. Grouping TEWs into these longitude bins ensures that the TEWs in the group have a similar local solar time, allowing them to be averaged together to create composite diurnal cycles.

Following Chapter 2, also we separate TEWs by the surface their CV centers are over using the IMERG land/sea mask. Because TEWs are not points but meso/synoptic scale atmospheric waves, this method is not perfect, and does not account for complex interactions at coastlines. However, it is sufficient for our large-scale analysis and as

we ask how diurnal cycles vary across surface types.

To examine how TEWs affect the diurnal cycle of precipitation, we will look at how the daily maximum, minimum, and range vary when TEWs are or are not present. Daily maxima, minima, and ranges are found for every grid point, using UTC-defined days. Daily ranges are the daily maximum - daily minimum at each grid point. The presence of TEWs is determined using a corresponding daily global TEW mask, computed in two steps. Firstly, all points within 500 km of TEW CV centers are considered as being near the TEW, matching the radius used for TEW-associated precipitation. Then, all near-TEW points for each UTC day were combined into one mask for that day. Therefore, for a given day, the swath considered to be near-TEW includes the 500 km radius for each time step of the day.

Comparisons of TEW-associated and non-TEW daily maxima, minima, and ranges are done for the whole year and for halves of the year, one spanning May-October (MJJASO) and the other November-April (NDJFMA). These halves of the year encompass each hemisphere's warm season, which is also when TEWs are typically most active.

3.3 Results

3.3.1 Diurnal Variation in TEW Counts

Before comparing diurnal cycles near TEWs, we first ask whether there are preferred times for the initiation of TEW tracks. When we convert the TEW track initiation times from UTC to approximate local solar, there is no globally preferred local time for TEW tracks to initiate (Fig. 3.2). Rather, slightly more tracks are initiated at 00 and 12 UTC, a pattern that appears in both the 850 and 700 hPa tracks. This suggests that the additional data available for assimilation at those times contributes

to analyses that meet tracking thresholds. It is important to note that these times are when the TRACK algorithm initiates a track. In manual operational analysis, TEWs may preferentially form or become identifiable at a particular local time. While only bulk statistics for each hemisphere are shown here, this pattern holds in each hemisphere and longitude bin.

For most combinations of level, hemisphere, and longitude band, the percent of tracks starting at each time is within one standard deviation of the mean for the respective level and hemisphere combination (not shown). Among the longitude bins where some local times account for higher percents of tracks, there is no clear pattern to the local times. That is, there is no preference towards TEWs meeting tracking thresholds in early morning hours or another time of day.

The TEW tracks are required to persist for at least two days in the initial tracking, but may be shorter due to the removal of TCs (Hollis et al., 2024a). Therefore, when using all track points rather than only track initiation points, we find that TEW track points at each level are approximately equally distributed throughout the day, whether using UTC or local times (not shown). Slightly more track points occur at some local times. However, because these very slightly preferred local times are every three hours, this is most likely a byproduct different levels of TEW activity in different longitude groups. For example, with many more TEW points in the eastern Atlantic than over West Africa, the local equivalent times for the longitude group immediately west of the African coastline will have more points than the group immediately east of it.

3.3.2 Wave-focused Diurnal Variations

Across longitude bands, near-TEW precipitation following the wave shows a strong diurnal cycle. To more easily compare across longitudes, as precipitation amounts vary across the tropics, Fig. 3.3 shows the fraction of the daily maximum of total

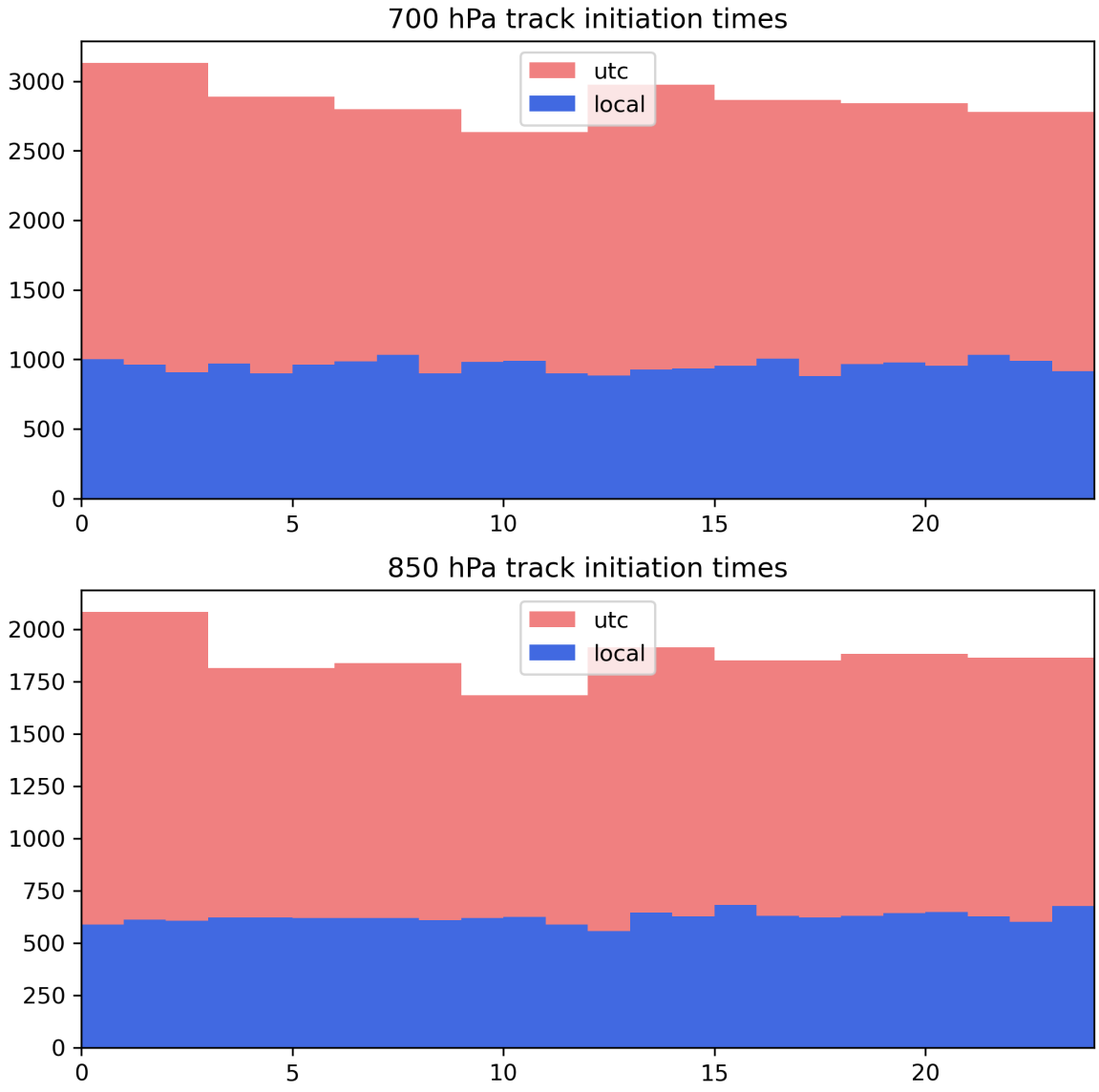


Figure 3.2: Local and UTC times of initial track points of TEWs, aggregated globally for each level, for TEWs tracked at a) 700 hPa and b) 850 hPa.

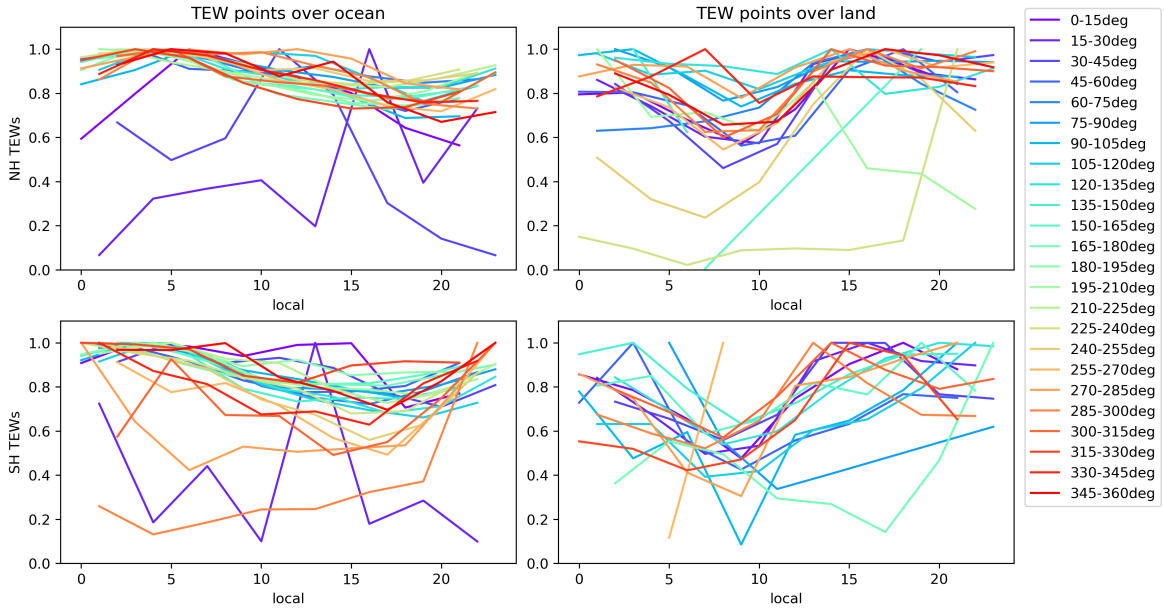


Figure 3.3: Line plots showing the diurnal cycle of TEW-associated rainfall, as a percent of the daily maximum, for each longitude bin, for TEWs in the top) NH and bottom) SH, and for TEWs over left) ocean and right) land.

accumulated precipitation in the 500 km radius of the TEW center by local time. Like the general diurnal cycle of precipitation in the tropics, land and ocean TEWs have different precipitation diurnal cycles. For TEWs over ocean (Fig. 3.3a,c), TEW-associated precipitation peaks in the early morning for most longitude bands, between 0300-0600 LST. The oceanic longitude bands whose peaks are at other times of day typically have some combination of coastal geography and fewer points (e.g., 0-30° bands in both hemispheres).

Over land, diurnal patterns in precipitation are noisier than those over ocean, but TEW-associated precipitation typically peaks later in the day, between 1200-1800 LST, for most longitude bins. Exceptions to this, such as NH TEWs in the 330-345° longitude bin (red line with local maximum at 0600 LST in Fig. 3.3b), are once again mostly in places where TEWs transition between surface types. Groups with very few TEWs over land, such as in the eastern South Pacific (yellow-oranges in Fig. 3.3d), do not

have enough data to meaningfully contradict these patterns.

In addition to the differences in the timing of peak precipitation, the relative magnitude of the diurnal cycle also varies between land and ocean. For most oceanic TEWs, total area accumulated precipitation at each time step is within approximately 70% of the daily maximum, indicating that oceanic TEWs are persistently rainy throughout the day. TEWs in the eastern South Pacific (yellow-oranges in Fig. 3.3c and parts of the South Atlantic (reds and purples in Fig. 3.3c) are the primary exceptions to this pattern, with some of these areas seeing near-TEW precipitation decrease to half or less of the daily maximum.

TEWs over land typically show more variation in the relative magnitude of their diurnal cycle in precipitation, with maximum-relative precipitation dropping to approximately 60% of the daily maximum for many longitude bins, and below 40% for a few longitude bands. We note that many of these longitude bands with much lower minima are in the Pacific Ocean, where there is relatively little land and therefore very few TEW points over land.

TEW strength, as measured by CV, does not vary diurnally to the same degree as precipitation. Fig. 3.4 shows the daily evolution of CV, expressed as a percent of the daily maximum. For oceanic TEWs, With the exception of SH TEWs in the 15-30° longitude bin, CV does not vary greatly throughout the day, staying within 95% of the daily CV max.

Over land, however, CV has a slightly more apparent though still weak diurnal cycle, even excluding noisy longitudes in the Pacific Ocean (greens-yellows in Fig. 3.4b,d). For most of the remaining longitudes, CV typically falls to 80-90% of the maximum in the mid to late afternoon hours after peaking in the early morning.

The larger relative diurnal cycles in both CV and precipitation for TEWs over land suggests a possible relationship between the two variables. Additionally, the inverse

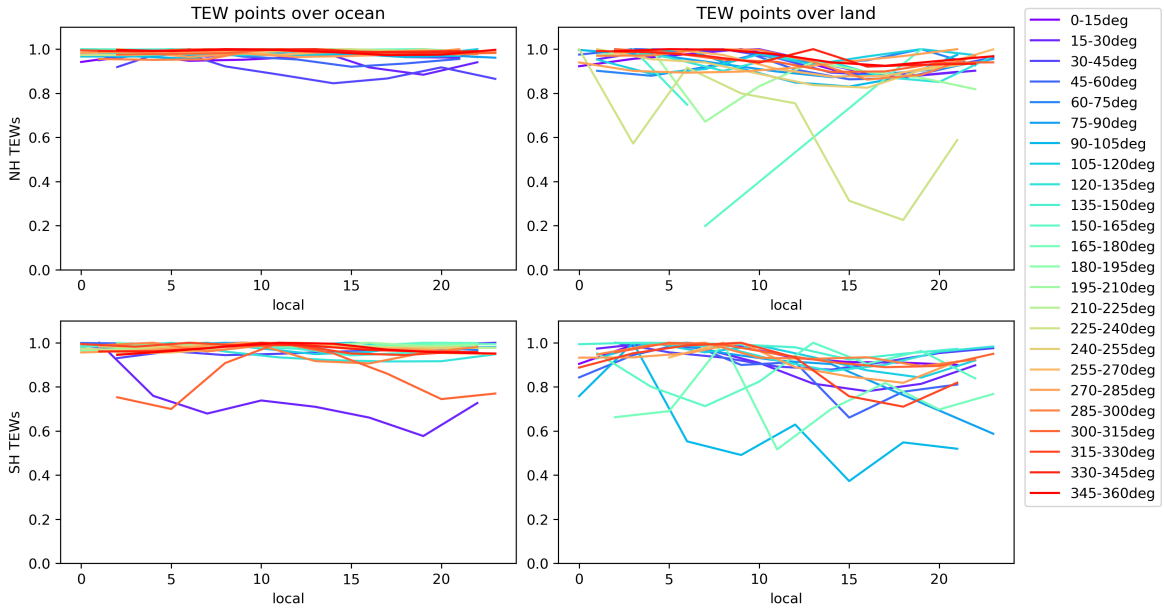


Figure 3.4: Line plots showing the mean percent of daily max CV for TEWs in each longitude bin (colors) for TEWs in the top) NH and bottom) SH, and for TEWs over left) ocean and right) land.

behavior between precipitation and CV poses interesting questions about whether such a relationship is out of phase. While we might expect increased cyclonic CV to be associated with increased convection through vortex stretching, Figs. 3.3 and 3.4 suggest that the relationship may be out of phase. Therefore, we examine the ratios of values from these two figures, shown in 3.5. If precipitation and CV changes are in phase, we would see the ratio stay close to 1 throughout the day. As above, there are two different diurnal cycles, depending on surface type, with stronger variation in TEWs over land. For these TEWs, the increase in CV in the morning hours corresponds with the minimum in precipitation. For TEWs over ocean, the diurnal cycle of the precipitation to CV ratio more closely resembles the diurnal cycle of precipitation, largely due to the lack of variation in CV.

With TEWs over land typically exhibiting a sharper increase in this ratio during the daytime, the hours between maximum CV and maximum precipitation, this may

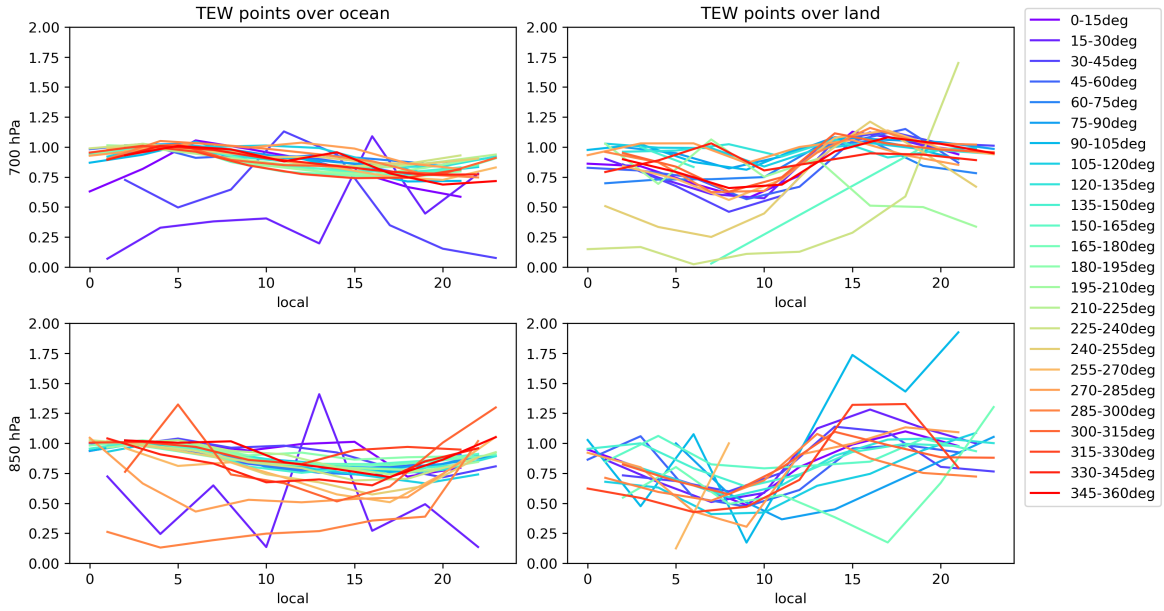


Figure 3.5: Line plots showing the ratio of values from Fig. 3.3 to Fig. 3.4 for TEWs in the top) NH and bottom) SH, and for TEWs over left) ocean and right) land.

be indicative of the increase in precipitation being a response to the increase in CV. However, more work would be needed to confirm such a relationship.

3.3.3 Effects of TEWs on Local Diurnal Cycles

While we have shown above that the diurnal cycle of precipitation near TEWs follows a similar pattern to what is typically observed across the tropics, with precipitation typically peaking over land in the late afternoon and over the ocean in early morning, the previous section does not consider how TEWs may affect the magnitude of the diurnal cycle relative to when TEWs are not present. Having now established that the phasing is similar and focusing on the amplitude, this section takes a spatial perspective to showing how TEWs affect the magnitude of the diurnal cycles.

When we compare the diurnal range in rain rates, as shown in panels a and b of Fig. 3.6, we find that the diurnal range in rain rates is dramatically increased when TEWs are present. Without TEWs, the average diurnal range in rain rates does not

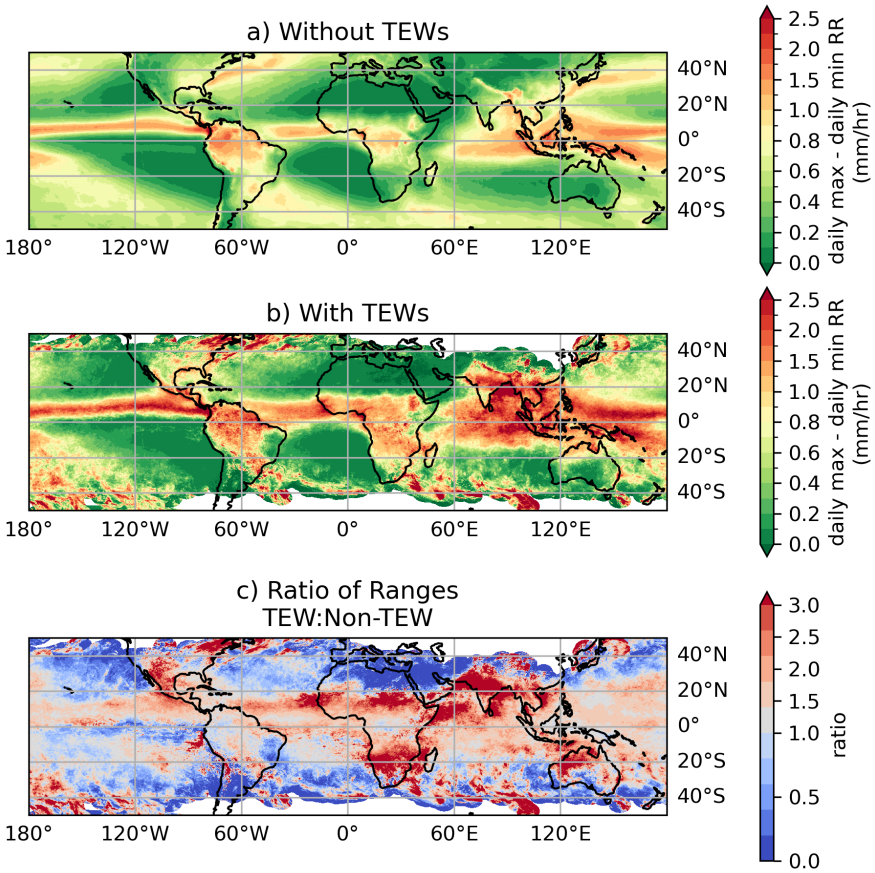


Figure 3.6: Maps showing a) the average diurnal range when 700 hPa TEWs are not present, b) the average diurnal range when 700 hPa TEWs are present, and c) the ratio of the diurnal ranges TEW:non-TEW

exceed 2.0 mm/hr for most of the tropics. When TEWs are present, however, many parts of the deep tropics have diurnal ranges exceeding 2.5 mm/hr. This behavior exists across the tropics where TEWs commonly occur, for both climatologically wet and dry locations over both land and ocean.

In most cases, the areas with the largest absolute diurnal ranges when TEWs are present also have larger diurnal ranges when TEWs are not present, such as the ITCZ, Central America, and southeast Asia. However, when TEWs are present, larger diurnal ranges are also present across much of sub-Saharan West Africa, portions of southern Africa near 20°S, and across the northern coast of Australia from approximately 120-

140°E. These regions are similar to locations noted in Hollis et al. (2024b) where TEW-associated precipitation accounts for more than 10% of the total annual rainfall.

To help contextualize the degree to which TEWs enhance the diurnal range, Fig. 3.6c shows the ratio of the TEW-associated diurnal range to the diurnal range when TEWs are not present. Large areas, including a significant amounts of land, have the magnitude of their diurnal ranges more than doubled when TEWs are present. These areas are not exclusive to the regions with either the most TEW activity or greatest total annual precipitation. While AEWs across the Sahel and North Atlantic more than double and in some areas triple the magnitude of diurnal range, TEWs in the central and western North Pacific do not enhance the diurnal range as strongly. Over northern Australia and southern Africa, as noted above, TEWs greatly enhance the diurnal range for these regions that climatologically see less precipitation.

However, both TEW activity and precipitation in the tropics more generally is seasonally dependent (e.g., Hollis et al., 2024a; Gomes et al., 2019; Dai et al., 2007). Therefore, when looking at the whole year in aggregate, as done above, the effects of TEWs may be exaggerated due to differences in both TEW activity and precipitation between the warm and cool season or the rainy and dry season. The cool or dry seasons may be over-represented in Fig. 3.6a and the warm or rainy seasons in Fig. 3.6b, resulting in exaggerated ratios that suggest TEWs affect the diurnal range more strongly.

When the year is split to each hemisphere's warm season, as done in Fig. 3.7, TEWs still enhance the magnitude of the diurnal range, including more than tripling it in some locations. For many parts of the tropics, TEW-related increases in the diurnal range appear to be seasonal, with greater enhancements during a location's respective warm season.

Across the North Atlantic and North Pacific, while summertime (MJJASO) TEWs

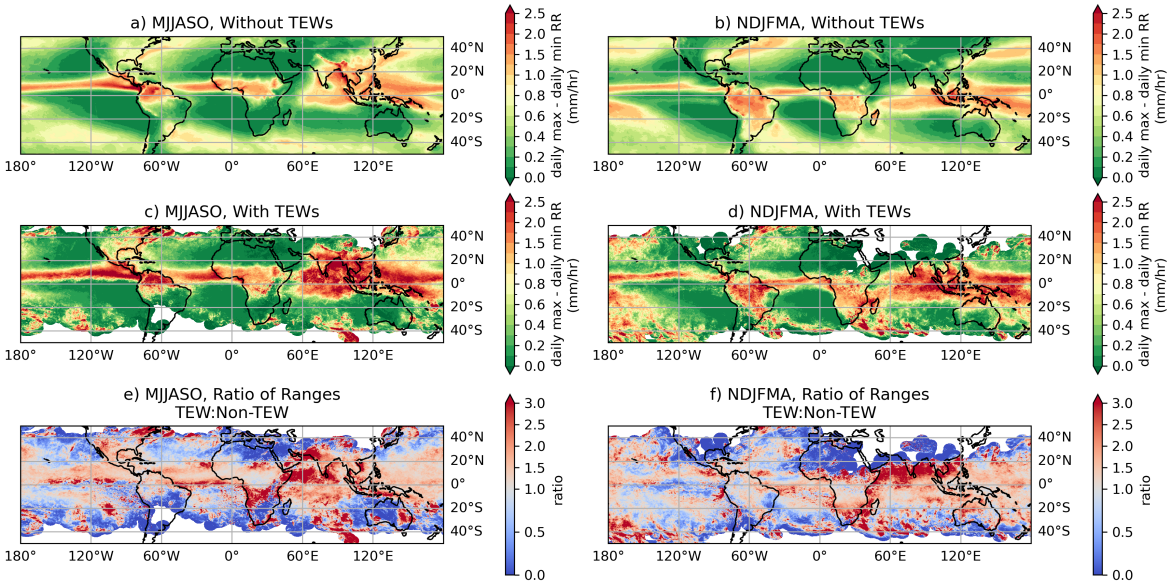


Figure 3.7: Maps showing a) the average diurnal range when TEWs are not present for MJJASO, b) the average diurnal range when TEWs are not present for NDJFMA, c) the average diurnal range when TEWs are present for MJJASO, d) the average diurnal range when TEWs are present for NDJFMA, e) the ratio of the diurnal ranges TEW:non-TEW for MJJASO and f) the ratio of diurnal ranges TEW:non-TEW for NDJFMA.

enhance the diurnal range across both basins, increases in the diurnal range are greater at the peripheries of the preferred TEW track regions rather than at their centers, especially the equatorward (southern) side (Fig. 3.7a,c,e). This may be related to the structure of near-TEW precipitation, which Hollis et al. (2024b) and Chapter 2 showed is not necessarily symmetric about the CV center, but rather for these regions favors increased precipitation on the equatorward side of the wave. These TEWs may also be interacting with the ITCZ, which multiple automated identification methods, such as Downs et al. (2025) and Mamalakis and Foufoula-Georgiou (2018), typically place near to slightly south of the maxima in TEW tracks.

During MJJASO, notable TEW-associated increases in the diurnal range also occur over much of the Indian Ocean and South Asia as well as the southwest US/northern Mexico. For western North America, prior work has shown that TEWs interact with the North American monsoon, affecting the which days have increased precipitation and where those increases occur (Adams and Stensrud, 2007; Seastrand et al., 2015). Fig. 3.7e appears to suggest that TEWs affect the diurnal range on days when they pass near the area.

Over southern Africa, TEWs enhance the diurnal range throughout the year for different locations. During MJJASO, the southern hemisphere's cool season, TEW-associated enhancements in the diurnal range mainly occur between 0-20°S for eastern portions of southern Africa. While there is comparatively little literature on TEW activity in the southern hemisphere, especially for southern Africa, results in Diedhiou et al. (2010) suggest multiple peaks in wave activity and wave-associated convection throughout the year. Conversely, during NDJFMA, TEW-associated changes to the diurnal range are more pronounced along and poleward (south of) 20°S, especially on the western side of southern Africa, likely associated with TEWs propagating across the southern Indian Ocean.

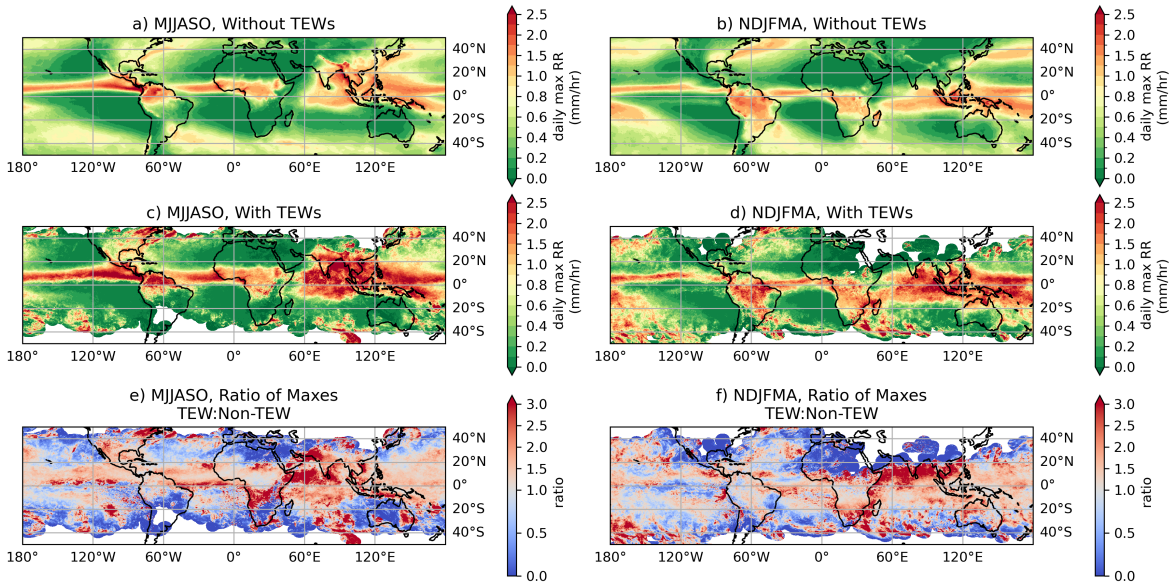


Figure 3.8: As Fig. 3.7 but for the daily maximum rain rate.

At the eastern side of the southern Indian Ocean, TEWs over and near north-central and northwestern Australia greatly magnify the diurnal range during NDJFMA. Both this area and southern Africa share that they climatologically receive less rainfall than many of the other regions where TEWs enhance the diurnal range and that TEWs are associated with at least 5% of the region's total annual rainfall (Hollis et al., 2024b).

To more thoroughly investigate how TEWs affect the diurnal cycle of precipitation, Figs. 3.8-3.9 compare the maximum and minimum rain rates when TEWs are or are not present for each hemisphere's warm season. Across the tropics, most of the absolute change in the diurnal range in the rain rate comes from changes in the maximum rain rate.

Throughout the year, in places where TEWs are most common, TEWs tend to at least moderately increase the daily maximum rain rate. As with the diurnal range, TEWs during a location's warm or rainy season have greater impacts on the daily maximum rain rate than those during the cool or dry season.

The daily minimum is not as greatly affected by the presence of TEWs, with mean

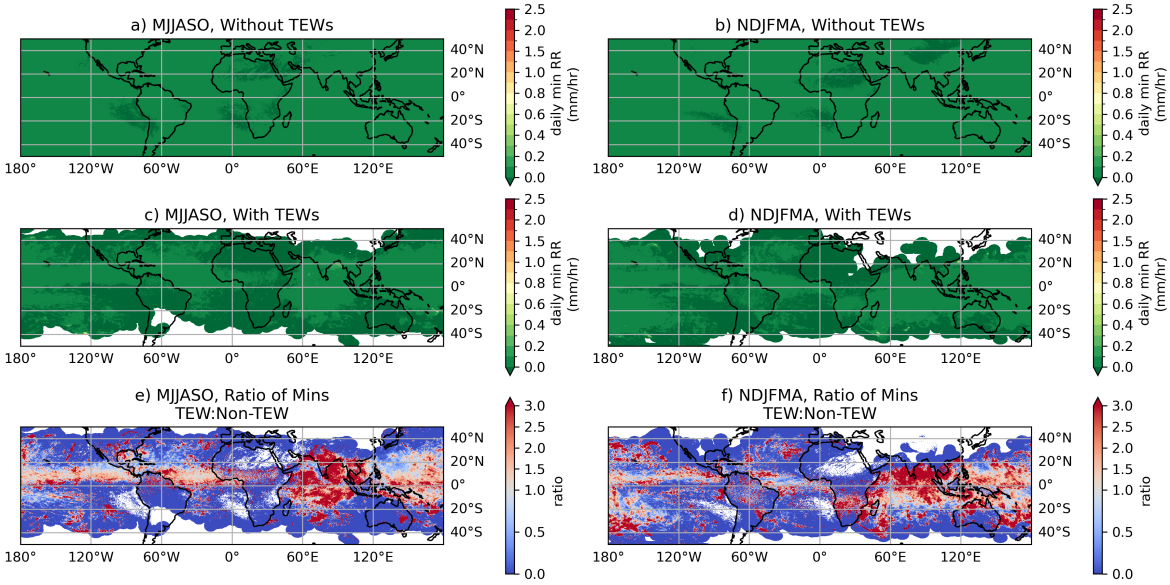


Figure 3.9: As Fig. 3.7 but for the daily minimum rain rate.

daily minimum rain rates remaining below 0.1 mm/hr nearly everywhere regardless of the presence of TEWs (Fig. 3.9), and a noisier field for the ratio of TEW-associated mean daily minimum rain rates to non-TEW rain rates. During MJJASO, the ratio of mean daily minimum rain rates is exceptionally noisy over Africa along approximately 10° latitude, where AEWs propagate, and over Central America and northern South America. Over much of the tropical North Atlantic and eastern North Pacific during this season, this ratio is near 1, indicating very small differences in the mean daily minimum rain rates.

Despite relatively little absolute change in the daily minimum rain rate, TEWs across the Indian Ocean basin and adjacent land areas relatively increase the daily minimum rain rate by a factor of 2-3. This enhancement is seen over the Indian Ocean throughout the year, but varies seasonally for land areas. Increases in the mean daily minimum rain rate for northern Australia and southern Africa, for example, only occur during NDJFMA, the warm and rainy season for those locations. Conversely, while TEW-associated increases occur over the northern Indian Ocean throughout the year,

over most of India TEW-associated increases in mean daily minimum rain rate occur during MJJASO, with NJDFMA increases only occurring for far southern India.

The increase in mean daily maximum rain rates coupled with minimal change in the mean daily minimum further indicates that TEWs affect the intensity of the diurnal cycle through increased daily maximum rain rates rather than by increasing the rain rate throughout the day. It may still be possible that TEWs increase the rain rate throughout the day in some locations, especially those in and adjacent to the Indian Ocean, but the relatively low change in absolute rain rate suggests that such changes are a slight increase in light rain rates. With small absolute differences in the mean daily minimum rain rate, it is also possible that these differences may be partially attributable to measurement or algorithm errors within IMERG.

3.4 Discussion and Conclusions

The diurnal cycle and TEWs are both key drivers of precipitation variability in the tropics at sub-weekly time scales. While the diurnal cycle of precipitation has been well established (e.g., Dai et al., 2007), the relationship of the diurnal cycle to TEWs has been less well quantified.

Across the tropics, we generally find that the diurnal cycle of near-TEW precipitation resembles the general diurnal cycle of tropical precipitation, with the daily maximum in precipitation occurring in the early morning over ocean and late afternoon over land. Longitude bands containing or near significant coastlines, such as West Africa (330-345° in the NH), showed more mixed results in their diurnal cycles of near-TEW precipitation. In addition to TEW-related impacts to the timing of diurnal maxima and minima in these places, our results may be further impacted by differences in IMERG performance for the different surface types (Derin et al., 2021). More

focused study of TEWs in coastal locations, potentially including ground-based gauge and radar observations, would be necessary to disentangle the influences of TEWs on the diurnal cycle vs data processing algorithms.

Despite a clear diurnal cycle in near-TEW precipitation, TEW CV intensity does not fluctuate as much at the daily scale. We also find that TEWs do not first meet tracking thresholds at any preferred local time. Instead, it appears that data assimilated into the reanalysis used for tracking has the most impact on TEWs meeting tracking thresholds, with more TEW tracks initiated at 0000 and 1200 UTC than the other times throughout the day. However, this is only indicative of when automatic objective tracking methods first detect the TEWs, and may also be sensitive to the choice of reanalysis. In operational settings, subjective analysis may preferentially favor certain local times.

The three hourly resolution of our data leaves open the possibility of a 1-2 hour phase shifting of the diurnal cycle, so our results do not necessarily contradict the slight delay found in Wiggins et al. (2023). Based on the clustering of the diurnal maxima and minima in Fig. 3.3, at least some of the longitudinal differences in timing found here are likely related to UTC to local time conversions, rather than TEWS significantly shifting the diurnal cycle out of phase from its climatological average. Nonetheless, revisiting this question with higher temporal resolution TEW tracks could yield interesting results.

While TEWs do not appear to significantly change the phasing of the precipitation diurnal cycle, they do amplify its magnitude, mainly through increasing the daily maximum rain rate. We find that these enhancements are seasonal, with stronger enhancements of the diurnal range typically during a given location's rainy season. TEW-associated amplification of the diurnal cycle is also more pronounced over land and at the peripheries of preferred TEW tracks, rather than at the core of the areas

of peak TEW activity. In some cases, such as over the tropical Atlantic, this suggests that TEWs are a dominant component of the diurnal cycle in places where they most commonly propagate, while their interactions with nearby features, such as the ITCZ, create relatively larger variations further away from the wave center.

The results here broaden our understanding of TEW-related impacts on the diurnal cycle across the tropics and throughout the year, complementing studies focused on specific locations and often for only the warm/rainy season. While our finding that TEW-related amplification of the diurnal range largely occurs during a location's warm/rainy season affirms the decision of many studies to focus on those months, the seasonal shifts themselves may be an interesting topic for further investigation, especially in the context of potential interactions between TEWs and other features like monsoons, the ITCZ, and MCSs. Analyzing the whole tropics also highlights understudied regions where more work is needed to understand TEW-related contributions to precipitation, such as southern Africa and northern Australia.

The larger diurnal cycles for TEWs over land further underscores their importance to the water cycle in the tropics. While multiple studies have established the annual and seasonal importance of TEWs to tropical precipitation (e.g., Hollis et al., 2024b; Dominguez et al., 2020) and their contributions to certain flooding events (e.g., Engel et al., 2017), the results here indicate that TEWs are key contributors to heavy rainfall in many parts of the tropics. Further understanding the role TEWs play in extreme rainfall events may be of particular importance given the expectation of increased tropical precipitation in a future, warmer climate.

It also remains possible that CV and precipitation have an out-of-phase relationship, especially over land, where the ratio between percent of daily maximum precipitation and CV varies the most. While not a direct measure of convective strength, increased vorticity at low levels is physically associated with increased convection. Furthermore,

this study did not examine how CV varies over the whole TEW life cycle, and how CV and near-TEW precipitation may be related at multi-day time scales. If CV changes more appreciably over multiple days, such changes may be related to multi-day changes in precipitation.

Chapter 4

Extremes in TEW-associated Precipitation

4.1 Introduction

Tropical easterly waves (TEWs), which are off-equatorial synoptic-scale waves, are key drivers of variability in the tropics at approximately the weekly timescale (e.g., Berry et al., 2012; Hollis et al., 2024b; Dominguez et al., 2020). TEWs are most active in the summertime, but Hollis et al. (2024a) identified TEW activity year-round in both hemispheres.

Typically convectively coupled, TEWs are most notable for their contributions to tropical rainfall (e.g., Dominguez et al., 2020; Hollis et al., 2024b; Schlueter et al., 2019) and for serving as precursor disturbances for tropical cyclones (TCs) (e.g., Landsea and Gray, 1992; Pasch and Avila, 1994). Various studies have estimated that anywhere from 30-80% of TCs develop from TEWs, depending on the basin (Du et al., 2025). Alternatively, Hollis et al. (2024a) found that, globally averaged over the nearly 40 years in their database of TEW tracks, about 20% of TEWs developed into TCs, where the exact values varied by year and tracking level.

Much recent work has been devoted to understanding the processes that influence TEWs undergoing tropical cyclogenesis, especially African easterly waves (AEWs) de-

veloping into Atlantic hurricanes (e.g., Núñez Ocasio and Rios-Berrios, 2023; Núñez Ocasio et al., 2024). Many of these studies have focused on the role of moisture in the maintenance and propagation of AEWs, finding that moisture is a leading factor in thermodynamic processes in AEWs.

TEW-associated rainfall accounts for a significant portion of summertime rainfall across much of the tropics (e.g., Berry et al., 2012; Dominguez et al., 2020), and between 10-30% of the total annual rainfall for much of the deep tropics (Hollis et al., 2024b). The maximum in TEW-associated precipitation shown in Hollis et al. (2024b) overlaps with the ITCZ, which suggests a relationship between the two.

Case studies have also shown that TEWs can cause or contribute to extreme rainfall in many locations, including sub-Saharan West Africa (Engel et al., 2017), the Caribbean (Jury, 2014), and South Asia (Sawaisarje et al., 2019). Such events can lead to landslides, urban flooding, and agricultural impacts. Additionally, these events sometimes occur outside of the typical rainy season, as was seen in the case described in Jury (2014).

Given the various impacts TEWs can have, especially extreme precipitation and seeding TCs, this study aims to quantify characteristics of these potentially impactful TEWs. Due to the importance of TEW-associated precipitation for some regions, we also consider the driest TEWs, as a lack of TEW-associated rainfall may also be impactful for some locations. Using a global database of objective TEW tracks, we will evaluate the climatology of the rainiest and driest TEWs and examine the relationship between TEW strength, TEW-associated precipitation, and TC genesis from TEWs.

Hollis et al. (2024b) showed that TEW-associated precipitation broadly follows the climatology of tropical rainfall, with bands of enhanced precipitation along the ITCZ in all basins. Among TEWs over land, the greatest quantity of TEW-associated rainfall falls in climatologically rainy locations, including West Africa, Central America, and

South/Southeast Asia, so we anticipate that many of the rainiest TEWs occur in these locations. They also showed that TEWs in less rainy locations, including southern Africa and northern Australia, are associated with approximately 10% of the region's total annual rainfall.

In general, TEW activity peaks during the warm/rainy season (Hollis et al., 2024a). Some studies, such as Sawaisarje et al. (2019) have found that TEW activity near India is often outside of the monsoon season. Different TEW identification methods may place more or fewer TEWs in each season, but the climatological presence of TEWs outside of the monsoon season further motivates a seasonally-divided year-round analysis of extreme precipitation associated with TEWs beyond individual case studies like Jury (2014).

On average, Chapter 2 showed that TEWs with more enhanced precipitation also had stronger cyclonic circulations. We build on this finding by further investigating the relationships between TEW strength, measured with curvature vorticity (CV), TEW-associated precipitation, and pre-TC TEWs. Though these relationships have not been well quantified, developing TEWs necessarily have stronger circulations, or attain higher CV. As the low-level cyclonic circulations of TEWs are also favorable locations for precipitation to occur, we expect that both pre-TC and exceptionally rainy TEWs will have higher CV than a non-developing TEW with more average associated precipitation.

4.2 Data and Methods

4.2.1 Data

This work leverages an updated version of the global database of objective TEW tracks introduced in Hollis et al. (2024a), as well as the methods for associating precipitation with TEWs described in Hollis et al. (2024b). At the time of writing, the full TEW track database spans 1981-2024. However, our choice of precipitation data, described below, is only available for the period 2001-2024, so our analysis will focus on those years. We use the TEW tracks that have had TC portions of tracks removed to focus specifically on TEWs and the pre-TC portion of developing TEWs.

Hollis et al. (2024a) tracked TEWs using cyclonic CV calculated from MERRA-2 u- and v-wind fields using the TRACK algorithm (Hodges, 1995). To maximize TEW detection, Hollis et al. (2024a) tracked TEWs independently at 850 and 700 hPa to allow for varying CV structures between different regions. The results presented herein will focus on TEWs at 700 hPa, and some preliminary work shows that general patterns are similar for TEWs at 850 hPa. For the studied years, the TEW database contains nearly 11000 tracks at 700 hPa.

For all precipitation fields, including TEW-associated precipitation and the background climatology, we use NASA's IMERG, version 7, final run. All precipitation data was reprocessed to a three-hourly temporal resolution to match the TEW tracks before any analysis was performed. As in Hollis et al. (2024b), TEW-associated precipitation is defined as all precipitation within a 500 km radius of the TEW's CV center.

4.2.2 Defining Impactful TEWs

For this study, we use three categories of potentially impactful TEWs, some of which overlap. The first category, extremely rainy TEWs, is broadly defined as points along TEW tracks that exceed a given percentile for rainfall among TEWs in particular subgroupings, which will be described more below. The second category, the driest TEWs, serves as a point of comparison against the rainiest TEWs. The third, pre-TC TEWs, consists of the TEW portion of the tracks that develop into TCs. Importantly, the pre-TC category is not mutually exclusive with the rainiest or driest categories. However, as pre-TC TEWs tend to be stronger and more well organized, we anticipate that the overlap between the pre-TC TEWs and the rainfall extremes will be with the rainiest TEWs.

While TEW-associated precipitation includes variable rain rates across a broad area, to simplify the determination of which TEWs are the rainiest, we will accumulate all of the precipitation in the 500 km radius at each time step. This choice was made for two reasons. Firstly, as seen in Hollis et al. (2024b) and Chapter 2, the greatest rain rates associated with TEWs are often slightly offset from the TEW's CV center, preventing the use of the rain rate for the grid point nearest the CV center. Secondly, this prevents TEWs with extremely high rain rates at one point from dominating the highly precipitating subset, allowing for the inclusion of TEWs with broad coverage of moderate rain rates.

Because most TEWs occur over ocean, where impacts from extreme precipitation are lesser, we further divide the TEW points by whether the CV center is over land or ocean before identifying the rainiest waves. While the TEW tracks were derived from MERRA-2, we use the land/sea static mask corresponding with our IMERG precipitation data (Huffman et al., 2019) for its higher resolution. Even though coastal

processes are important to TEWs (e.g., Sakaeda et al., 2025, and Chapter 2), to maintain sufficiently sized populations of waves, we will simply assign TEWs in grid boxes with greater than 50% ocean coverage to be ocean, and those with less to be land.

Once near-TEW precipitation has been accumulated and surface type assigned, percentiles are assigned in three ways, with the 90th percentile as the threshold for rainy and 10th percentile for driest. The simplest method to assign percentiles only considers the surface type of each TEW point, and so only has two sets of thresholds, one for TEW points over land and the other for those over ocean. The second method for assigning percentiles does not separate surface types, but instead considers whole tracks by further accumulating the precipitation along the track and normalizing by the track's temporal length. The third method assigns percentiles in a more locally aware manner, by assigning percentiles based on the TEW's hemisphere, surface type, and longitude. As done in Chapter 2 we group TEW points by longitude with 15° wide longitude bins. While this still does not fully account for climatological differences in precipitation across different parts of the tropics, it helps account for these differences.

4.3 Results

4.3.1 Globally Rainiest TEWs

When the threshold for rainiest TEWs is set using the global population of TEWs over each surface type, a large proportion of the rainiest TEWs are, unsurprisingly, in places with higher climatological TEW activity and rainfall, such as West Africa and South/Southeast Asia for land (Fig. 4.1a) and across the tropical North Pacific for ocean (Fig. 4.1b).

TEWs in less climatologically rainy locations also meet these globally set thresholds,

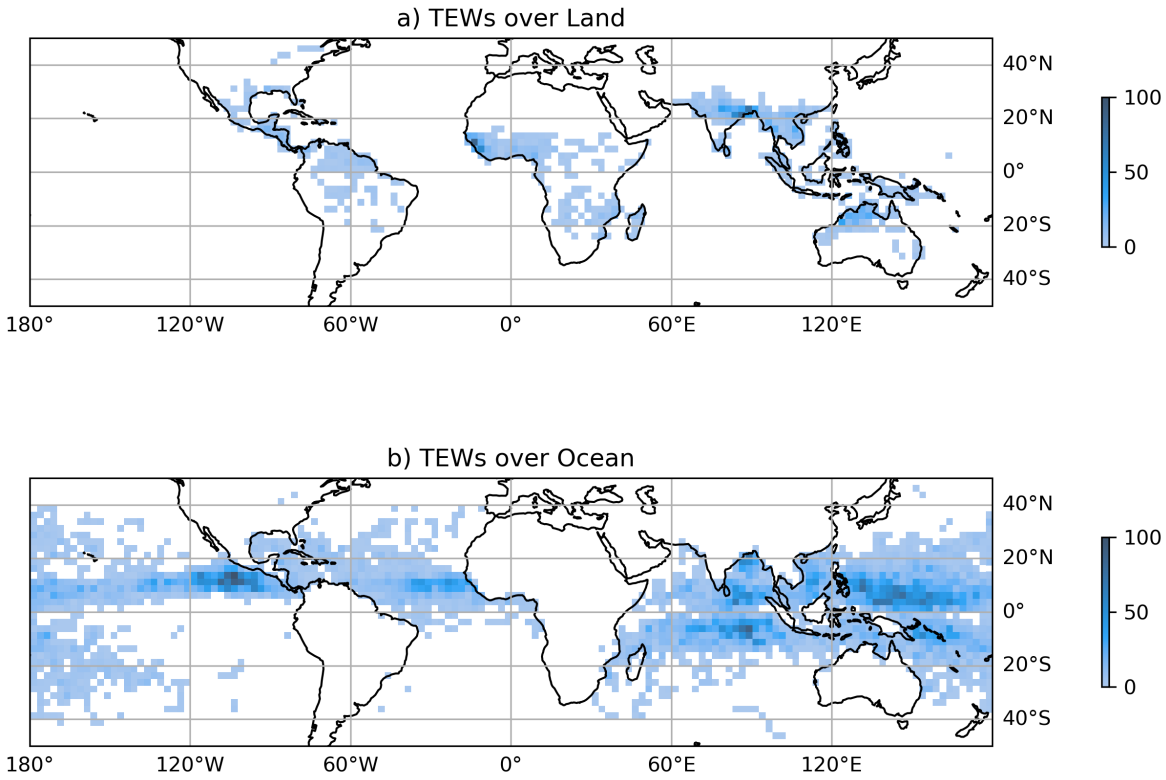


Figure 4.1: Maps of the locations of TEW points with the highest area total accumulations for 700 hPa TEWs a) over land and b) over oceans.

including some TEWs over the northwestern coast of Australia and southern Africa. While less numerous, these waves also warrant attention, as the rainfall associated with these TEWs may be more impactful than the same amount of rain in other places.

In a similar but contrasting pattern, many of the globally driest TEWs occur over climatologically drier locations, especially for TEWs over land, for which the largest concentrations are over the Sahara, Arabian Peninsula, and inland Australia. (Fig. 4.2). Among the driest TEWs over ocean, very distinct hotspots exist along the eastern edges of most basins. The cells over Central Africa in Fig. 4.2b are TEWs whose CV centers are located over lakes whose size is sufficient to have at least 50% water coverage for a grid point in the IMERG land-sea mask, and can either be disregarded or considered as points that should be included in Fig. 4.2a.

For the North Atlantic and North Pacific, the hotspots for dry TEWs are near the areas with the globally rainiest waves, but displaced slightly poleward, where SSTs are typically lower and therefore less conducive to TEW-associated convection and precipitation. For the North Atlantic, these waves likely originate over the Sahara or are influenced by Saharan dust outbreaks over the eastern Atlantic (Burgess and Oyola-Merced, 2024). AEWs can contribute to the transport of Saharan dust, but can also be negatively impacted by excessive dust. Land-based sources or influences on dry TEWs in the eastern North Pacific are less clear, especially as some of these TEWs may be sourced from the Caribbean. Difficulties tracking TEWs in the Caribbean region in many datasets (e.g., Downs et al., 2025) therefore complicate any hypotheses or conclusions about the origins of these waves.

Comparing the spatial distribution of the globally rainiest and driest waves, some patterns begin to emerge to suggest influences on TEWs and their associated precipitation. As the distribution of the rainiest TEWs is similar to the general distribution of TEWs, with a slight weighting towards climatologically rainy locations, environments

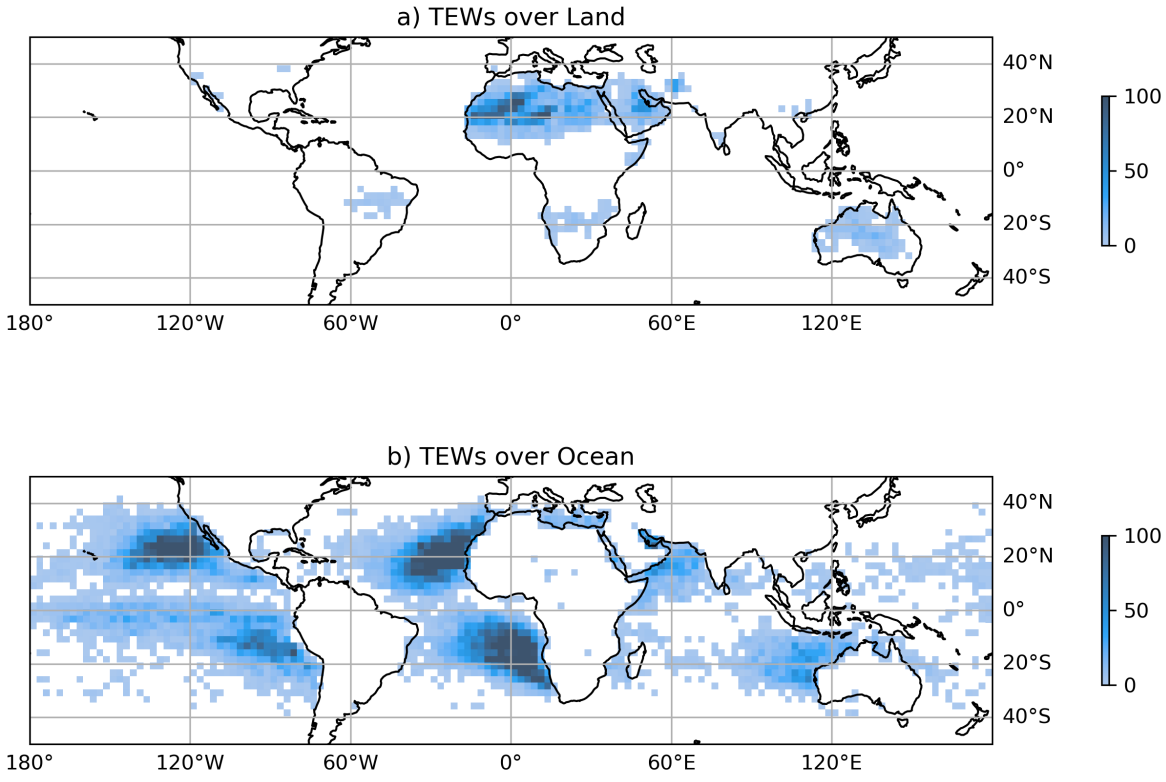


Figure 4.2: As Fig. 4.1 but for the globally driest TEWs.

most favorable for TEW development are also favorable for greatly enhanced TEW-associated precipitation. The locations of the driest waves reinforces this hypothesis, as dry TEWs over Africa are almost exclusively north (poleward) of 10°N, and there are very few dry waves in the western North Pacific and eastern Indian Ocean, some of the climatologically rainiest places on the planet.

The globally rainiest waves typically occur during each hemisphere's warm season (Fig. 4.3), approximately mirroring the overall seasonal activity of TEWs. The prevalence of rainy TEWs in the warm season also aligns with monsoon activity, For both hemispheres, the seasonal pattern is more pronounced over land than ocean, with very few extremely rainy TEWs occurring over land during the cool season. Across the years studied, 2001-2023, TEW times meeting the threshold are observed in both hemispheres in every month.

Some of the extremely rainy oceanic TEWs may be near coastlines or islands. Due to the assignment of surface using the TEW's CV center, these nuances are not accounted for, which may result in slightly more land impacts from rainy TEWs than the results here imply.

Further considering when the driest TEWs occur, Fig. 4.4 suggests that the timing of both the driest and rainiest waves generally mirrors the typical seasonal pattern of TEWs, with more TEWs typically occurring during the warmer half of the year. At the monthly scale, however, more differences appear. In the NH over land, the extremely rainy TEWs most frequently occur in August, with an approximately symmetric distribution surrounding it. For the driest TEWs, however, the distribution is bimodal, with peaks in July and September/October. This may indicate that while general conditions for TEW generation are present throughout the summer, conditions are most optimal in August, leading to not only enhanced activity but enhanced precipitation. Over ocean in the NH, extremely dry TEW activity also peaks in July, while a second peak

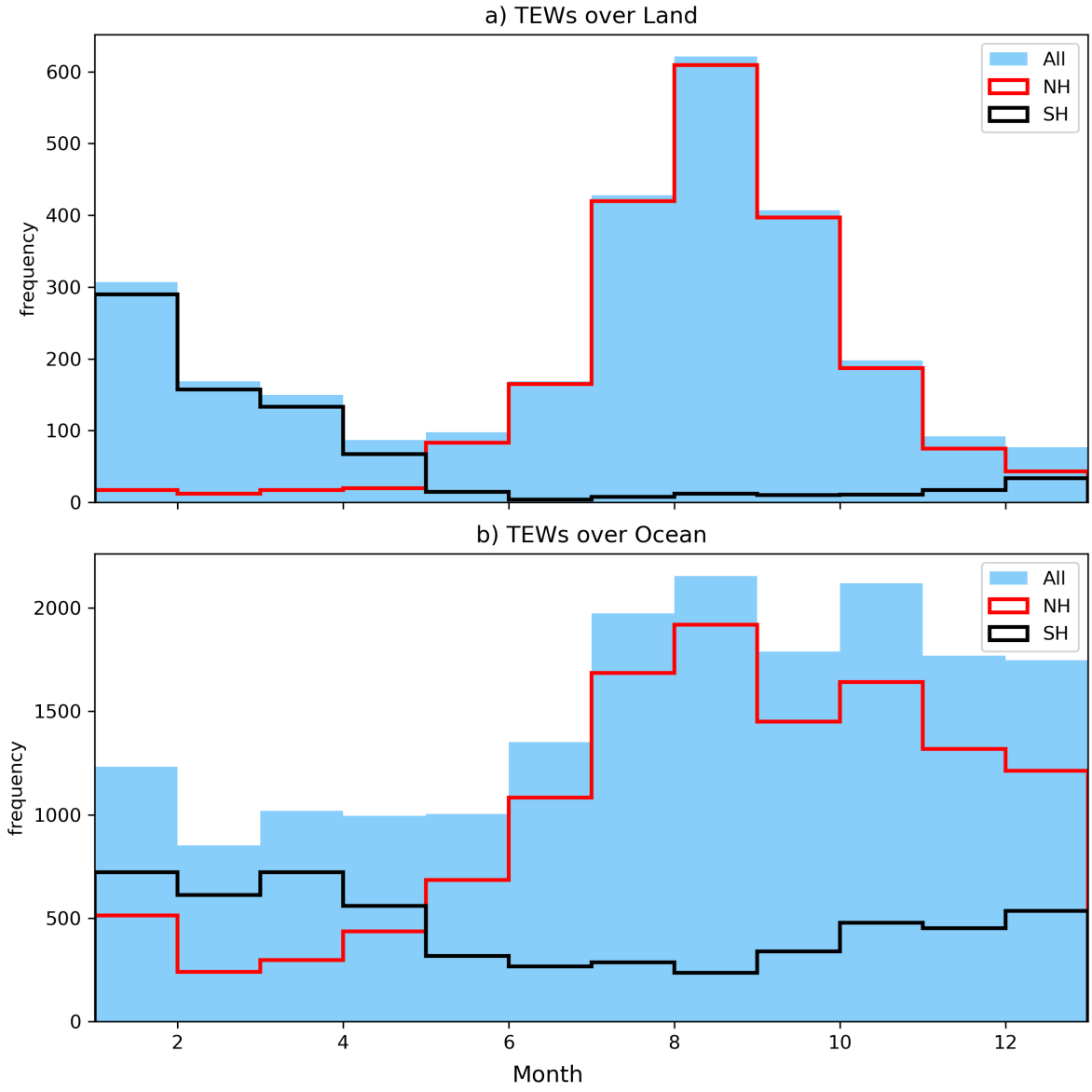


Figure 4.3: Bar/line plots showing the total number of extremely rainy TEWs per month globally and in each hemisphere that occur a) over land and b) over oceans. In each panel, the global counts are shaded in light blue, while the NH is shown with a red line and the SH with a black line.

in September/October is not observed. Regional examination of when these extremes in TEW-associated precipitation would also help untangle whether these distributions are present across the tropics, or are a result of superimposing the activity in different regions.

In the SH, there are comparatively few TEWs over land in either the rainiest or driest categories. However, the rainiest TEWs are most frequent from January-March, while the driest are slightly more frequent in September, rather than in the months straddling the peak in rainiest TEW activity. Over ocean in the SH, while there is significant overlap in the timing of the rainiest and driest TEWs, the frequency of extremely dry TEWs increases ahead of the rainiest TEWs, with a steady monthly increase through the second half of the year leading to a peak in December/January. This supports the hypothesis that for some regions TEW activity climatologically increases before the time when the rainiest TEWs are most likely.

In addition to examining the rainiest individual times represented in the TEW database, we can accumulate the rainfall along entire TEW tracks and normalize by the track's temporal length as a measure of which TEWs are consistently the rainiest. Because TEWs translate across surface types and longitudes, a globally set threshold is necessary, but can still give interesting insights. The patterns in the locations of the rainiest tracks, shown in Fig. 4.5, are similar to the rainiest times, with some key exceptions. The consistently rainiest AEWs, for example, start west of approximately 15°E, while individually rainy times exist across Africa along approximately 10°N. In the southern hemisphere, there are fewer consistently rainy TEWs that reach southern Africa from the South Indian Ocean, while northwestern Australia still receives numerous consistently rainy TEWs.

Considering Fig. 4.1 and Fig. 4.5 together, it appears likely that many of the consistently rainiest TEW tracks also have some of the rainiest individual times along

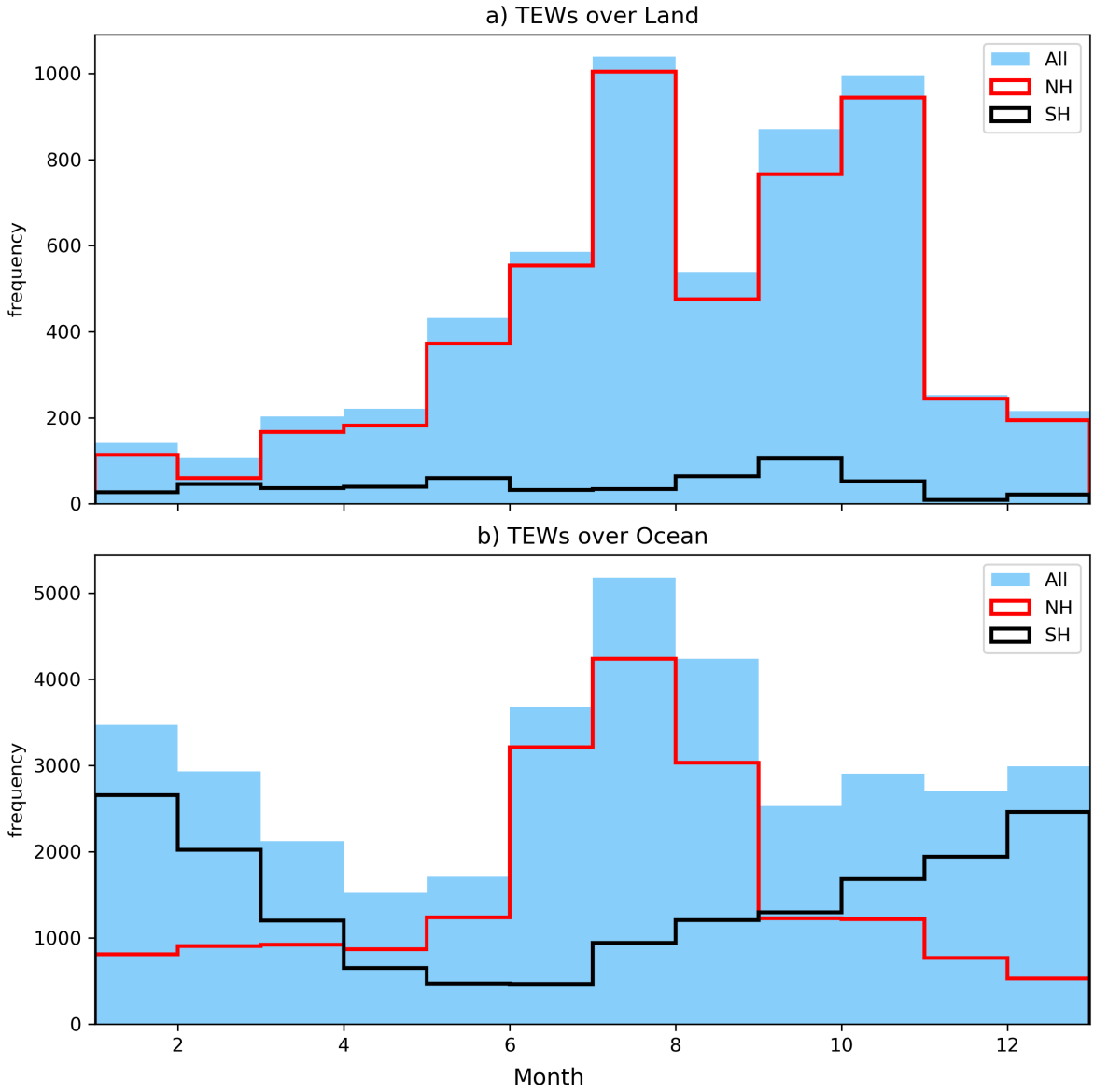


Figure 4.4: As Fig. 4.3 but for the globally driest TEWs.

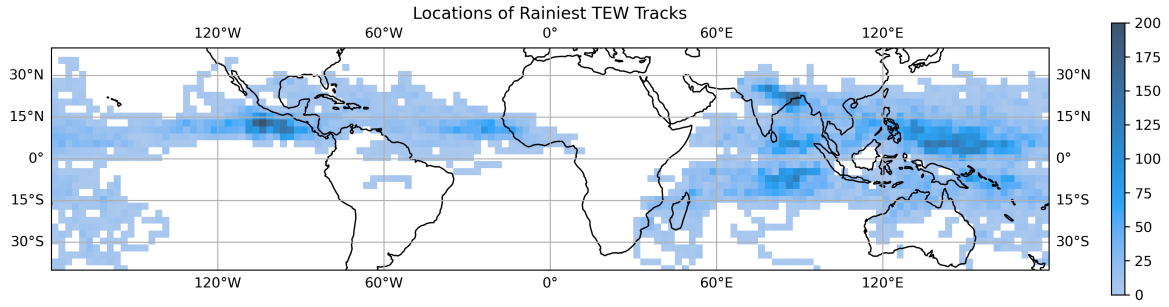


Figure 4.5: Map of the TEW tracks with the highest track duration-normalized accumulated precipitation.

their lengths. This appears especially likely for rainy TEWs around the Bay of Bengal, crossing the West African coast, and in oceanic TEW activity hotspots. It is less clear whether the rainiest times and tracks near northwestern Australia overlap, since there are relatively fewer TEWs here, but such an overlap may be possible.

Additional factors beyond the globally set thresholds may contribute to the discrepancies between the rainiest times and the rainiest tracks. Firstly, we do not consider the TC portion of the life of TEWs that develop into TCs. Secondly, differences in both mean daily and diurnal range in rain rate may favor the inclusion of TEWs with significant portions of their life over ocean.

4.3.2 Locally Rainiest TEWs

If we instead use thresholds relative to the TEW's longitude band in addition to surface type, we gain additional insights into what constitutes a highly-precipitating TEW. Setting these thresholds by surface type and longitude bin is a simple way to account for the differing climatological precipitation across various places. Fig. 4.6 gives the threshold for each hemisphere, surface type, and longitude bin combination. The thresholds vary by multiple orders of magnitude, and are more dependent on hemisphere and longitude bin rather than surface type. Hemisphere/surface/longitude combinations with

less than 100 total points (10 points exceeding the 90th percentile threshold) have been excluded, which mainly affects groups where all of the land points for TEWs are small islands, such as those in the Central Pacific (longitudes 165-240°).

Unlike the results in Chapter 2, which found consistent differences between TEWs over land and ocean, the thresholds for the rainiest 10% of TEWs are not universally higher for one surface type or the other. Some patterns do emerge, with thresholds for area-total precipitation exceeding 15000 mm found largely in the area extending from the Indian Ocean, across the Maritime Continent, and, in the SH, towards the SPCZ. Low thresholds in southeastern Pacific (Fig. 4.6b, longitude bins 180-285°), below 5000 mm, are unsurprising, as the region both climatologically receives less rainfall and has fewer TEWs.

Fig. 4.7 shows the locations of the rainiest TEWs using these locally-defined thresholds, decomposed by each hemisphere's warm season. As with the globally defined threshold, the areas with the most rainy TEW times approximately mirror the overall climatology of TEWs.

Decomposing these waves by season provides additional spatial insights into when TEWs are rainiest. The rainiest AEWs, over both land and ocean, are heavily concentrated in the boreal summer, and are more tightly clustered along 10°N. While some rainy AEWs occur during boreal winter, these occurrences are much fewer, and are closer to the equator than during boreal summer.

Rainy TEWs occur in both the northern and southern Indian Ocean year-round, but their spatial coverage shifts seasonally, generally following monsoon activity. In both hemispheres, more extremely rainy TEWs occur poleward of 10° in summer, while rainy TEW activity remains more confined to the area equatorward of 10° during winter. Furthermore, for nearby land areas, especially adjacent to the Bay of Bengal, there is a strong preference for the rainiest TEWs to occur in the warm season.

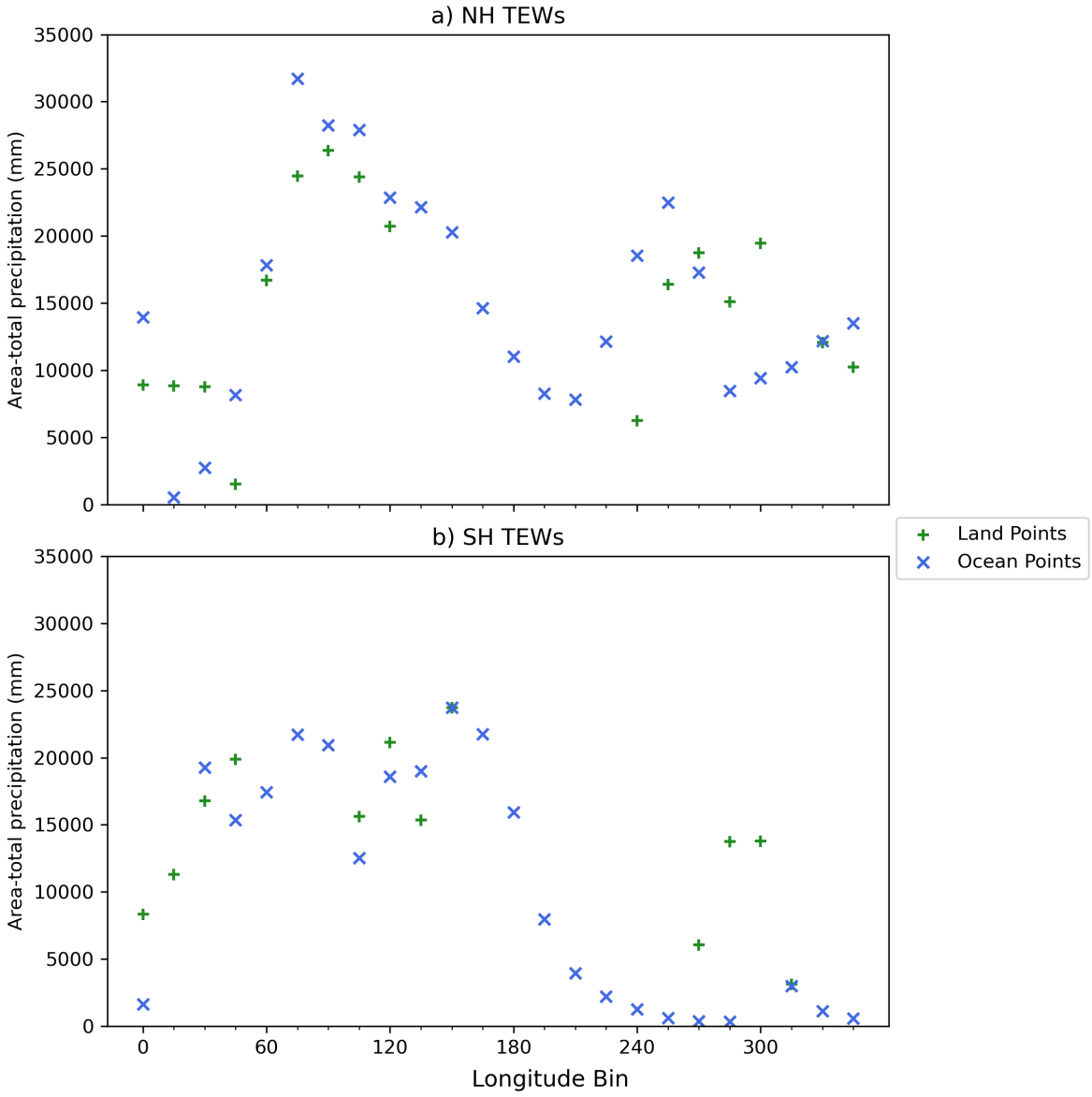


Figure 4.6: Scatter plots of the thresholds used for the locally-defined determination of rainiest TEWs for TEWs in the a) NH and b) SH. Longitude/surface groupings with less than 100 total points have been excluded.

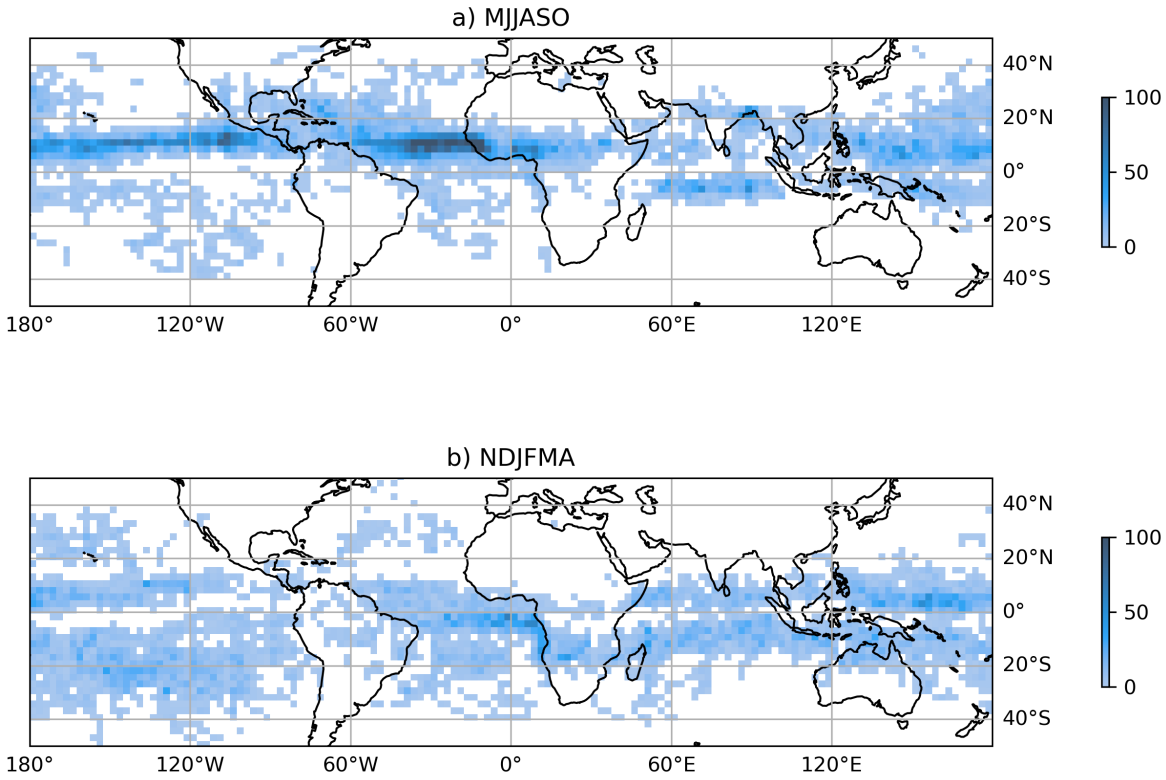


Figure 4.7: Maps showing the rainiest TEW track points using locally-defined rainy thresholds for TEWs during a) MJJASO and b) NDJFMA.

During austral winter, no TEWs over northwestern Australia meet the extremely rainy 90th percentile, and very few extremely rainy TEWs occur over southern Africa. While the lack of activity over northern Australia is likely additionally influenced by the reduced frequency of rainy TEWs in the SPCZ, it appears that any rainy TEWs in the southern Indian ocean weaken or dissipate before reaching the eastern coast of southern Africa during austral winter.

Using a locally-set threshold also results in the inclusion of TEWs in the South Atlantic in the set of rainiest TEWs. While Fig. 4.1a showed some TEWs over southern Africa met a globally-defined threshold, Fig. 4.1b showed almost no rainy TEWs in the South Atlantic. In contrast, Fig. 4.7 has rainy TEWs in the South Atlantic, more commonly in austral summer. These TEWs are most frequent along the western coastline of southern Africa from 20°S towards the equator and in an oceanic band extending west from Africa along approximately 5°S, but also occur across the basin.

Near South America, rainy TEWs are slightly more numerous during austral summer, but also occur year-round. For the easternmost points of South America, this contrasts with the climatological rainy season and TEW activity reported in Gomes et al. (2019), where the peak in both precipitation and TEW activity for locations south of the equator occur between April and August. More investigation into this region may be needed to determine the relationship between general TEW frequency, the rainy season, and the rainiest TEWs.

The locations and seasonality of the locally driest TEWs gives additional insight into the relationship between TEW activity and associated precipitation. For some regions, like North Africa and the North Atlantic, the driest waves more frequently occur during boreal summer (Fig. 4.8a), coinciding with the peak in NH TEW activity and rainy TEW activity. In contrast, for South and Southeast Asia, the locally driest TEWs occur more frequently during boreal winter (Fig. 4.8b). These differences

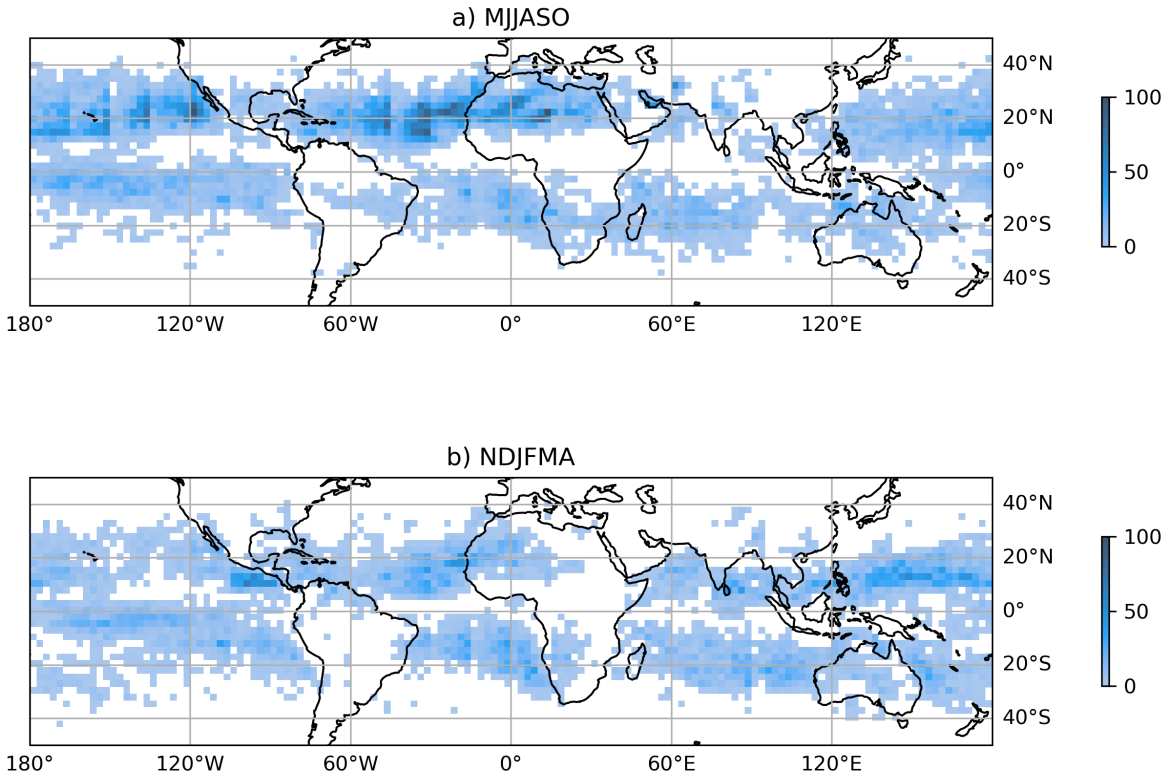


Figure 4.8: As Fig. 4.7 but for the locally driest TEWs.

illustrate that while dry TEW activity largely mirrors the general pattern of TEW activity, local patterns also play a role.

4.3.3 Evolution of Rainiest TEWs

While Chapter 3 examined the potential for a diurnal relationship between near-TEW precipitation and the TEW's strength measured by its CV center, that analysis did not find a strong diurnal cycle in TEW CV. Over the full life of a TEW, however, CV is variable, and the removal of the TC portion of developing TEWs lowers the average TEW CV (Hollis et al., 2024a). Therefore, while CV and precipitation are not diurnally related, both Hollis et al. (2024a) and the definition of curvature vorticity,

where decreases in the radius of curvature and/or increases in wind speed increase CV, imply that CV increases as TEWs develop into tropical cyclones. Based on this and Chapter 2, it also seems reasonable to hypothesize that rainier TEWs have greater CV.

Fig. 4.9 shows the evolution of CV for various groupings of TEW, with an x-axis intended to be read from right to left, mirroring the average motion of TEWs. As we are comparing the lifetime evolution of pre-TC TEWs against other groups, we chose to use the track duration-normalized rainiest and driest TEWs for this analysis. For all TEWs, some change in their CV strength is normal, though the degree of change is strongly enhanced when TEWs are either consistently highly precipitating or develop into tropical cyclones. In both of these hemispheres, both potentially impactful categories of TEW on average have higher CV at track initiation, near 2 s^{-1}, compared to the average CV for all TEWs, less than 1.5 s^{-1}, and especially the non-developing subgroup, which has slightly lower CV than the average of all TEWs. The consistently rainiest and pre-TC TEWs also exhibit larger increases in CV in the first halves of their lives, especially among TEWs in the SH, which on average attain CV strengths of 5 s^{-1}.

Notably, consistently rainy non-developing TEWs have greater CV than the average pre-TC TEW through the first two thirds of their lives, a pattern seen in both hemispheres but more pronounced in the SH. However, the 95% confidence intervals for each group's average evolution overlap, especially in the first quarter of the wave's life for NH TEWs. Nonetheless, these results suggest that TEWs with higher than average CV or whose CV rapidly increases may be areas of interest for increased precipitation, TC genesis, or both.

While non-developing consistently rainy TEWs will eventually see their CV decrease in the latter third to half of their lives, as seen in the darker greens in Fig. 4.9, pre-TC TEWs must have their CV increase up to the point of cyclogenesis, a difference we

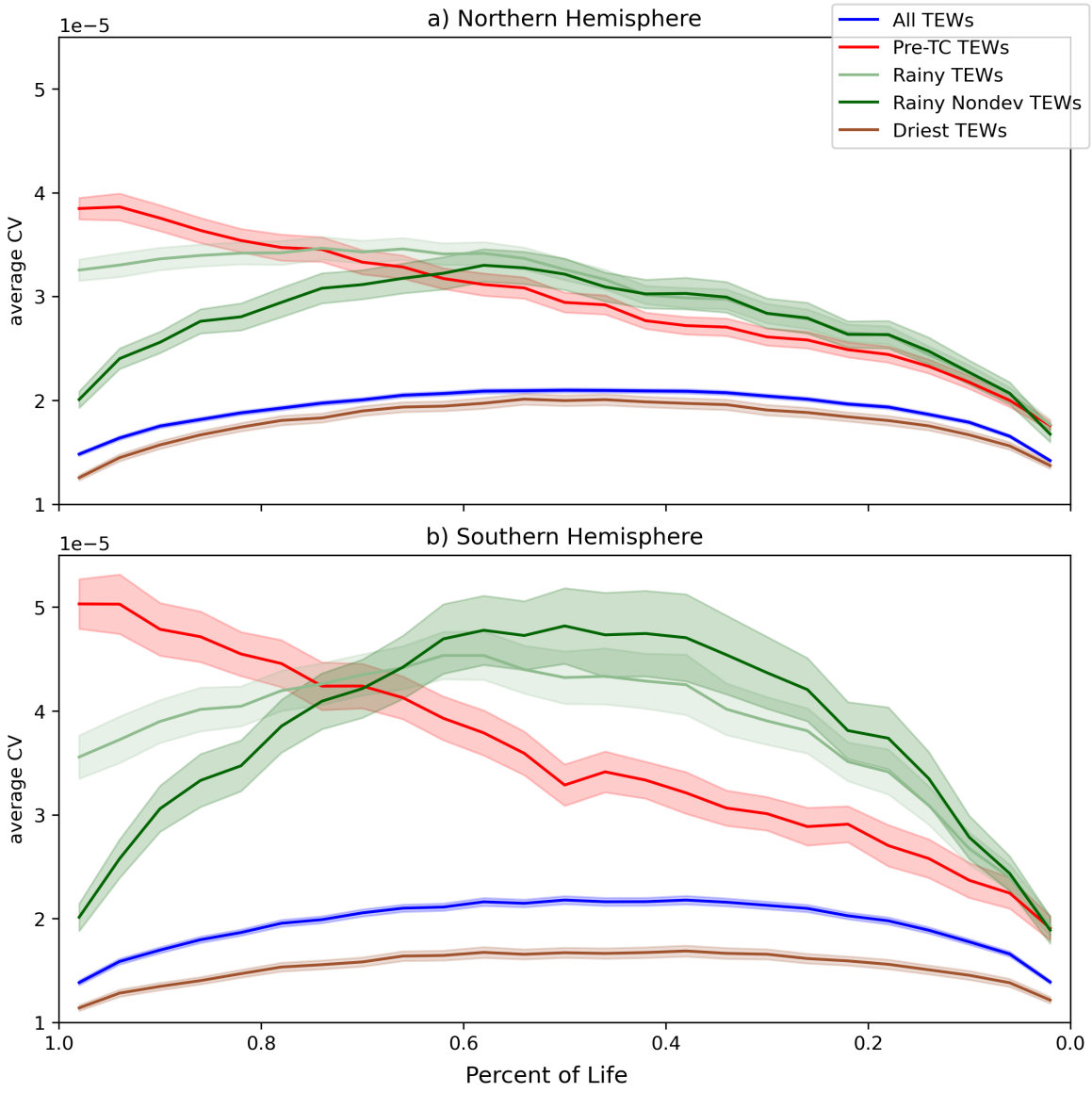


Figure 4.9: Line plots showing the average evolution of CV over the life of various categories of TEWs in the a) NH and b) SH, with CV shown as a function of the percent of the TEW's life elapsed. The mean CV is in solid color, while the 95% confidence interval for each group is shaded in the same color. Note that the x-axis is intended to be read right to left.

see reflected at the leftmost edge of each panel, where pre-TC TEWs attain CV values near 4 s^{-1} in the NH and 5 s^{-1} in the SH. The overlap between consistently rainy and pre-TC TEWs results in the average ending CV for the consistently rainiest TEWs being much higher than the average TEW, between 3-4 s^{-1}, a value that is also higher than the tracking thresholds. When removing the pre-TC TEWs from the consistently rainy category, however, we see that end of life decreases in CV bring these TEWs closer to average TEWs, though still stronger than average, with CV strength still near 2 s^{-1} for consistently rainy TEWs in both hemispheres.

In addition to enhanced CV near rainy and pre-TC TEWs, the driest TEWs typically have lower CV than the average TEW. This lower average CV indicates that these waves not only have less associated convection and precipitation, but are also dynamically weaker. The general pattern exists in both hemispheres, though the driest TEWs in the SH are weaker than those in the NH (average CV remains less than 1.5 s^{-1} for the whole wave life in the SH compared to a maximum of approximately 1.75 s^{-1} in the NH).

While Fig. 4.9 provides evidence for a broad relationship between precipitation and CV in TEWs, this relationship is highly variable among individual TEW points, as shown in Fig. 4.10, with a large spread in area-accumulated precipitation and and curvature vorticity evident in panels a and f, which show all TEWs in the NH and SH, respectively. For Fig. 4.10, while the CV-precipitation relationship at individual times are plotted, the rainiest TEWs in this figure are the consistently rainiest TEWs, those whose accumulated track length-normalized precipitation exceeds the 90th percentile, and the driest are those below the 10th percentile.

The vast majority of TEW points have CV less than 5×10^{-5} (Hollis et al., 2024a), and Fig. 4.10 shows that even among the rainiest TEWs the area-accumulated precipitation does not frequently exceed 50000 mm. Linear regression for the CV-precipitation

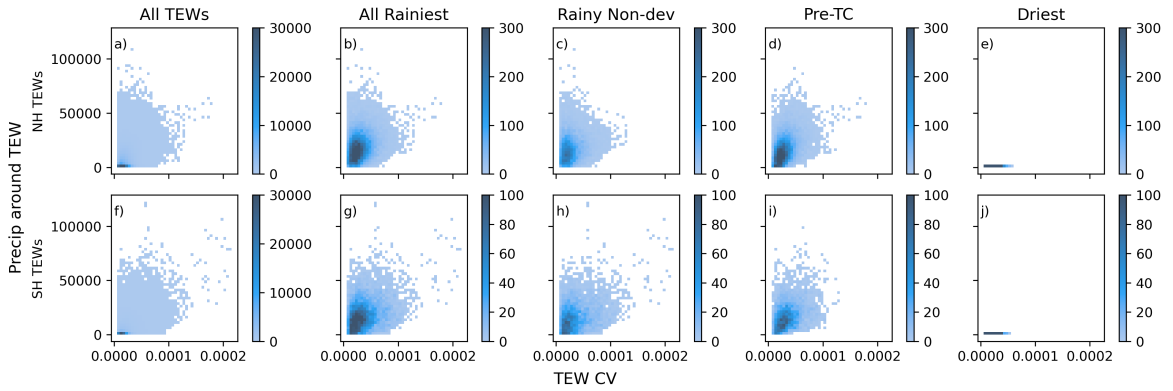


Figure 4.10: Heatmaps of TEW CV against area-accumulated precipitation for a) all NH TEWs, b) all NH rainy TEWs, c) NH rainy non-developing TEWs, d) NH pre-TC TEWs, e) driest NH TEWs, f) all SH TEWs, g) all SH rainy TEWs, h) SH rainy non-developing TEWs, i) SH pre-TC TEWs, and j) driest SH TEWs.

	All TEWs	All Rainiest	Rainy Non-dev	Pre-TC	Driest
NH r-value	0.38	0.26	0.17	0.39	-0.02
SH r-value	0.51	0.31	0.33	0.33	-0.06

Table 4.1: Correlation values for the CV-precipitation linear regression.

relationship suggests a weak linear relationship between the two variables, with r-values typically near 0.3, as shown in Table 4.1, both for potentially impactful TEWs and the general population of TEWs. The p-values for all relationships are much less than 0.05 and therefore significant.

Rainy non-developing TEWs (Fig. 4.10c and h) and pre-TC TEWs (Fig. 4.10d and i) have similar distributions of CV and area-accumulated precipitation, which points to the challenges in determining which TEWs are most likely to develop into TCs. Considered together with the lifetime evolution in Fig. 4.9, it appears that CV or precipitation alone may not be enough to predict the likelihood of TC genesis, but that additional factors like the rate of change of wave strength may be important, as the rainiest non-developing TEWs on average have their CV increase more rapidly in the first quarter of their lives, significantly so for SH TEWs.

Among the driest TEWs (Fig. 4.10e and j), there is considerably less variation in

CV attained, with none of the driest TEWs in either hemisphere attaining CV above 6×10^{-5}. Thus, while CV is not necessarily predictive of precipitation or TC genesis, the driest waves are of average to weaker-than-average intensity compared to all other TEWs, and it appears less likely that weak TEWs will be highly precipitating.

4.4 Discussion and Conclusions

TEWs are important contributors to precipitation across the tropics. In addition to enhancing rainfall across the tropics, they also contribute to extreme rainfall events, primarily in the warm/wet season.

The globally rainiest TEWs typically occur in the areas of peak TEW activity, especially in the NH, which are also typically climatologically rainier locations. However, extremely rainy TEWs also occur in less climatologically rainy locations with more modest TEW activity, such as northwestern Australia and southern Africa. While less studied, exceptionally rainy TEWs in these regions may be particular contributors to their regions' hydroclimates. Further study of these TEWs is needed to better quantify their contribution to precipitation in these places.

We also observed that while the frequency of both the rainiest and driest TEWs peak during the warm/wet months, in line with overall TEW activity, the frequency of the driest TEWs typically increases earlier in the warm season and stays elevated longer, suggesting that the conditions conducive to TEW activity and enhanced precipitation evolve over the course of the warm season. Especially as many TEWs occur in monsoon regions, one possible explanation is that the evolution of wind patterns and available moisture over the course of the monsoon season plays a role in the development of TEWs and the likelihood of extreme rainfall. With a more focused peak in the rainiest TEWs than the driest TEWs, our results suggest that the occurrence

of extreme rainfall may be more sensitive to these conditions than TEW development. A monthly examination of the spatial patterns of both extremes in TEW-associated precipitation, potentially also examining the associated regional wind and moisture patterns, would be helpful in further exploration of this topic.

When considering TEW tracks that are consistently rainy over their whole lives, most occur over ocean, though some originate over or traverse land. Notably, even though some individual time steps over southern Africa meet the globally-defined rainy threshold, no consistently rainy tracks propagate far into southern Africa from the South Indian Ocean, and there are no consistently rainy TEWs in the South Atlantic.

Even though there are no consistently rainy TEWs in the South Atlantic, when using the locally-aware rainy TEW thresholds for individual times along the TEW tracks, ensuring rainy TEWs in every basin, we find that the extremes in TEW-associated precipitation vary seasonally in both location and frequency. For most basins, the locally rainiest TEWs occur during the warm/wet season in regions of peak TEW activity, while the driest ones occur during the cool/dry season and are displaced further poleward. Locally-defined thresholds also provide further support for TEW-monsoon interactions, especially across the Indian Ocean basin and Maritime Continent, where the thresholds for rainy TEWs are higher than many other parts of the tropics.

In addition to examining when and where the rainiest TEWs occur, we also considered the relationship between near-TEW precipitation and TEW strength, measured by CV, both at individual times and over the life of TEWs. We found evidence of a positive correlation between precipitation and CV for most TEWs, with only the driest TEWs exhibiting negative correlations. We also showed that while most TEWs undergo some degree of strength change over their lives, both the rainiest and pre-TC TEWs tend to have higher CV than the average TEW throughout their entire lives, while the driest TEWs are on average weaker than other TEWs. This CV-precipitation rela-

tionship may be useful in forecasting TEW-related impacts, especially extreme rainfall associated with TEWs and which waves undergo TC genesis.

Chapter 5

Summary and Conclusions

Throughout, we have demonstrated a complex relationship between moisture, TEWs, and precipitation. While many aspects of this relationship can be generalized across the tropics, such as the association of TEWs with enhanced moisture and precipitation, there are also notable variations among regions, seasons, and the surface the TEW is over.

While moisture is important to all TEWs, surface-based differences are evident across the characteristics we have examined. In agreement with Mayta and Adames Corraliza (2024) and Núñez Ocasio and Rios-Berrios (2023), moisture is generally important for TEWs over oceans, while temperature variations are also important to TEWs over land. Resultingly, we reinforce the perspective from Adames et al. (2019) that overall considers TEWs as mixed-type systems governed by both moisture and temperature variations, with variations among the population where some TEWs are more moisture mode-like than others. Furthermore, the evidence presented here supports our hypothesis that some land-based TEWs are moisture mode-like (e.g., those in Southeast Asia), while not all oceanic TEWs should be treated as moisture modes (e.g., those in the South Atlantic and Southeast Pacific).

These differences in the importance of moisture translate to differences in the amount of precipitation associated with TEWs. Many of the overall rainiest TEWs occur over oceanic regions whose TEWs are more moisture mode-like, especially tropical oceans in the NH. Among the rainiest TEWs over land, many of these also occur in areas

where moisture is more important to TEWs, such as the Caribbean, South/Southeast Asia, and the Maritime Continent. Similarly, many of the driest TEWs occur in places where temperature variations play a larger role in governing TEWs, which are also often drier regions, including deserts (e.g., the Sahara, interior Australia) and regions of oceans with cooler SSTs or sharper gradients (SE Atlantic, SE Pacific).

The seasonal patterns of the rainiest and driest TEWs indicate that further work is needed when examining the importance of moisture to TEWs. We found that while the overall pattern in these extremes in TEW-associated precipitation follow the general pattern of TEW activity, with peak activity during the warm/wet months, the frequency of dry TEWs increases a month earlier than exceptionally rainy TEWs, and stays elevated longer. This seasonal pattern suggests that the dry dynamics that promote TEW activity become more favorable earlier in the season, while moisture coupling is strongest in a narrower window of time, modulating how closely TEWs resemble moisture modes throughout the year.

Additionally, the degree to which TEWs modulate the diurnal range in precipitation rates varies seasonally. While diurnal ranges are typically greater during the warm/wet season even when TEWs are not present, TEWs still double to triple the diurnal range in many parts of the tropics. These enhancements were not necessarily centered exactly where TEWs occur, however, with enhancements near oceanic TEWs occurring south of the main TEW tracks for the North Atlantic and North Pacific. This is in line with precipitation generally being enhanced on the equatorward side of these waves, and also suggests TEW interactions with the ITCZ. This points to a need for more examination of TEWs in relation to other aspects of tropical circulation.

Both the seasonal patterns in when the rainiest TEWs occur and how strongly TEWs enhance the diurnal range indicate that TEWs more strongly enhance precipitation during the warm/wet season. This may also indicate that how moisture mode-like

TEWs are varies seasonally, with moisture becoming more important to TEWs during the peak in TEW activity at the peak of the warm season. Such seasonal variations would also help explain the differences in our results, using year-round TEW tracks, from those of studies like Mayta et al. (2025a) and Mayta and Adames Corraliza (2024), which focused on summertime TEW activity.

Regardless of whether TEWs are governed by moisture variations, temperature gradients, or a combination thereof, most TEWs are convectively coupled to some degree. Therefore, we also examined the relationship between their strength and precipitation, and the diurnal cycles of these two key metrics. While diurnal cycles in CV were weak, especially over ocean, we found that TEW-associated precipitation typically follows the usual diurnal cycle observed in the tropics, where precipitation over land peaks in the late afternoon while oceanic precipitation peaks in the early morning. Despite the weak diurnal cycle in TEW strength, our results also suggest an out-of-phase diurnal relationship between CV and precipitation. Additional related work examining changes in TEW CV is presented in Appendix A and suggests the existence of cyclic variation in TEW strength, even if these variations are not purely diurnal.

While we did not find a definitive diurnal relationship between TEW strength and precipitation, our other results support a relationship between the two. We found a generally positive relationship between CV and near-TEW precipitation, and that the driest TEWs have lower CV than the average TEW and especially the rainiest TEWs. On average, throughout the life of a TEW, the rainiest TEWs have higher CV, and many of these rainiest TEWs develop into tropical cyclones. This overlap is indicative of a relationship between dynamical strength and convective organization, represented by CV intensity and precipitation, respectively.

The out-of-phase diurnal relationship between CV and precipitation, positive correlation between CV and precipitation, and differences in strength between rainy, dry,

and average TEWs all indicate that more work is needed to understand the CV-precipitation relationship. While our results do not definitively indicate which aspect is the causal element, the fact that the rainiest TEWs have higher CV at track initiation suggests that the wave's dynamical strength leads to enhanced convection. Physically, a stronger wave trough can serve as a favorable location for convection to occur, as the convergence associated with the low-level circulation will typically help support convection. Further work examining how wave-associated precipitation changes over a TEW's life would aid in understanding this relationship.

We are not the first to suggest potential relationships between near-TEW moisture, precipitation, and TEW strength, particularly possible relationships with TC genesis. Núñez Ocasio and Rios-Berrios (2023) suggested that pre-TC AEWs become more moisture mode-like as they approach TC genesis, proposing that a moisture mode-like AEW that is better coupled with an MCS has enhanced low-level moisture flux towards the wave's center, leading to better vertical structuring of the wave and increased likelihood of TC genesis. Our finding that many pre-TC TEWs are also rainier than average, supports the idea of better phasing between TEWs and precipitation in pre-TC TEWs. Further work to test this theory could use the vertical matching between 850 and 700 hPa TEW tracks, described in Hollis et al. (2024a) and Hollis et al. (2024b), the latter of which has already shown that precipitation is strongly enhanced when 850 and 700 hPa TEW CV centers are located within 500 km of each other, which aligns well with the physical pathway laid out in Núñez Ocasio and Rios-Berrios (2023). The combination of enhanced precipitation, increased dynamical strength, and vertical development of the circulation may be helpful features for identifying TEWs that are more likely to develop into TCs.

Overall, these results further our understanding of the relationship between TEWs, moisture, and precipitation, giving additional insight into the convective coupling of

these waves and how they vary across the tropics and throughout the year. Especially given that most analyses of TEWs focus on one region, our global analysis allows for regional differences to be better contextualized. Some possible future steps beyond the work presented here include further investigations of the role of moisture in TEWs, from sub-daily changes to the wave-life scale to seasonal variations, are outlined below.

At the sub-daily to wave-life scales, moisture-vortex instability (MVI) (Adames and Ming, 2018) would be an interesting additional framework to examine the importance of moisture to TEWs. This framework helps to relate the import of moisture towards the TEW and the subsequent convection, vortex stretching, and strengthening and propagation of systems like TEWs. MVI has not been applied to TEWs in all parts of the tropics, so while some studies have shown it explains the behavior of some TEWs well (e.g., Núñez Ocasio and Rios-Berrios, 2023), it is unknown if it is applicable to all TEWs or only a certain subset. The availability of 850 and 700 hPa TEW tracks in the database we used could be of particular use here, as it would allow the comparison of vertically deeper TEWs where circulations are present at both levels against TEWs where a sufficiently strong circulation is only present at one level or the other. Including analysis of TEWs at both levels would also address a key limitation of the work we have done here, which has largely focused on TEWs tracked at 700 hPa, and would enhance our understanding of the role of the vertical development of a TEW's cyclonic circulation in its evolution and potential impactfulness.

The seasonal variations we found in TEW-associated precipitation, namely when the rainiest TEWs occur and how strongly TEWs enhance the diurnal range in each season, suggest that the importance of moisture to TEW also varies seasonally. We did not, however, examine how moisture mode-like these rainiest TEWs may be, or how the importance of moisture to TEWs varies throughout the year. If rainier TEWs are more moisture mode-like, then it would also be likely that warm/wet season TEWs are

on average more moisture mode-like.

We also did not explore how closely individual TEWs behave as moisture modes. Quantifying how many TEWs in a given region behave in this way or whether the relative importance of moisture and temperature gradients varies over the wave's life may be interesting directions to build on our regionally aggregated results. This could be especially relevant to testing the physical pathway proposed in Núñez Ocasio and Rios-Berrios (2023) and described above where AEWs become more moisture mode-like as they strengthen and undergo TC genesis.

Considering periodic variations in near-TEW characteristics, we did not explore the potential for non-diurnal cycles in TEW strength, which Zhang et al. (2022) has found some evidence of in TC precursor disturbances, or possible diurnal cycles in other TEW characteristics, such as their propagation speed. Our analysis of the diurnal cycle of precipitation also only considered area-accumulated precipitation, and did not consider how the distribution of precipitation types (convective vs stratiform) varies diurnally, especially for TEWs coupled to MCSs.

Matching TEWs tropical convective features using databases like TOOCAN (Fiolleau and Roca, 2024) or tracked MCSs via the TAMS algorithm (Núñez Ocasio and Moon, 2024) may also be an interesting way to approach the question of the importance of moisture, wherein there may be a difference in the importance of moisture to TEWs coupled with MCSs compared to those that are not coupled. Furthermore, other ways to assess the strength of near-TEW convection, such as cloud top heights, may yield interesting insights.

Key relationships between TEWs and moisture are summarized in Fig. 5.1. In general, rainier TEWs over ocean are more governed by moisture than dry TEWs over land (Fig. 5.1a), though variations in the importance of moisture exist, especially in coastal regions or relatively cooler and drier oceans. TEWs generally enhance the diurnal

range in their near environments, but these enhancements are especially pronounced when TEWs exist near other convective features, such as the ITCZ (Fig. 5.1b).

These new insights into the relationships between moisture, TEWs, and precipitation help us understand the convective coupling of TEWs from the diurnal to wave-life scale and how the most impactful TEWs evolve. Relating TEW strength and precipitation in particular may have implications for forecasting TEW-related impacts, both from exceptionally rainy TEWs and helping identify those that may develop into TCs. Furthermore, while the behavior of TEWs in a future warming climate is still poorly understood (e.g., Brannan and Martin, 2019), by showing that the rainiest TEWs are typically stronger than average, while the driest TEWs are weaker, as our understanding of future TEW behavior evolves, the behavior of current TEWs may be a valuable point of comparison for simulated future TEWs.

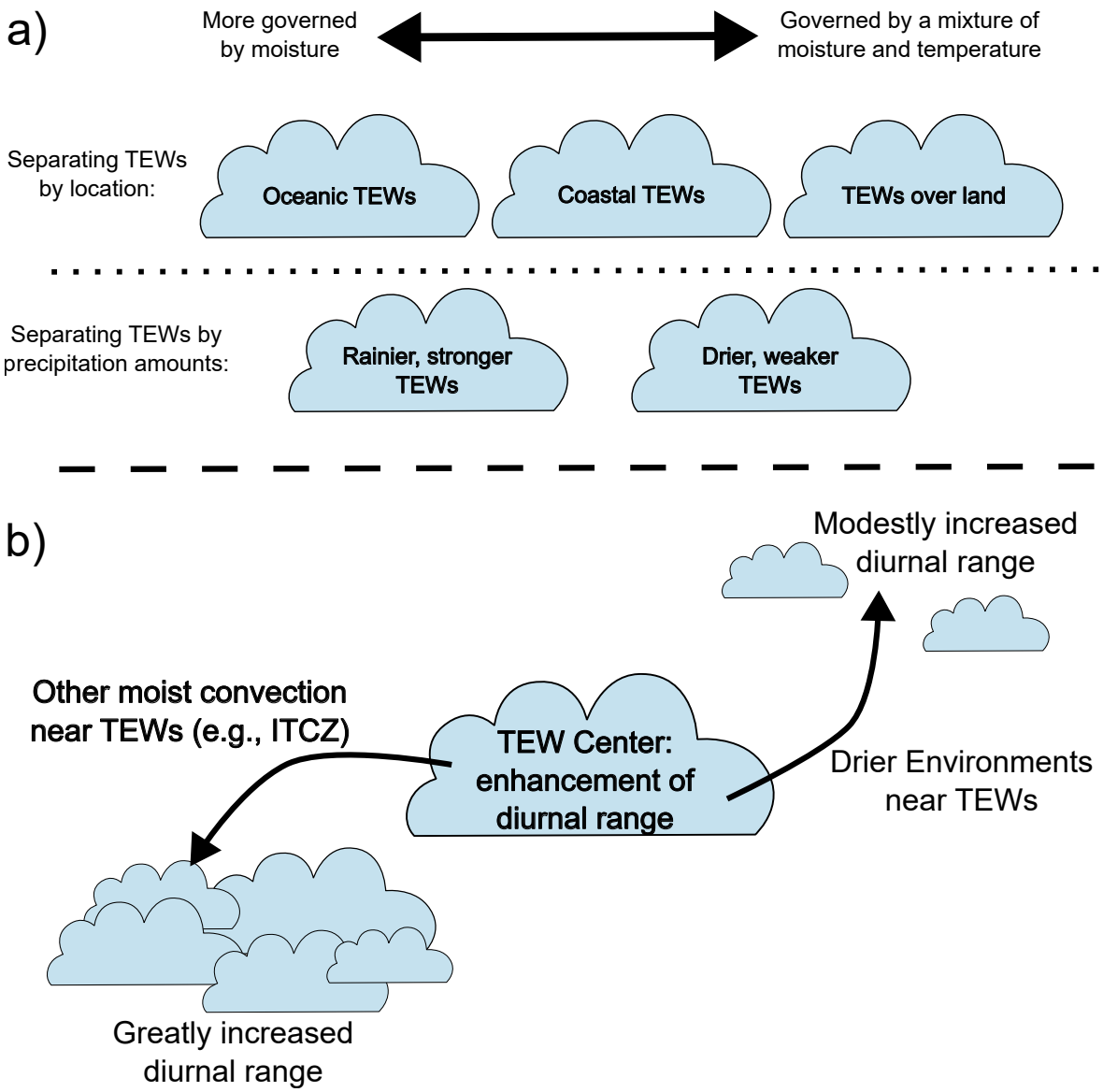


Figure 5.1: A schematic summarizing the results of this dissertation. Part a) summarizes the spectrum of moisture importance for TEWs when separated by the surface they are over and how rainy the TEW is. Part b) summarizes the relationship between TEWs, the diurnal range, and the moisture in the near-TEW environment.

Appendix A

TEW-Following Wave Phases

A.1 Introduction

Across literature, various approaches have been used to study the evolution of convectively coupled waves in the tropics. This dissertation has focused on objective tracking of TEWs and compositing the environments surrounding them.

Examining the evolution of the Madden-Julian oscillation (MJO), Riley et al. (2011) introduced a phase-based framework to quantify the evolution of outgoing longwave radiation (OLR), a common proxy for convective activity. In their framework, the authors defined a "pinwheel" phase space using the standardized OLR and its derivative, and dividing the space into eight phases, characterized by whether convection is active or suppressed on one axis and whether it is growing or decaying on the other.

A similar approach was used by Schlueter et al. (2019) to quantify the convectively active and suppressed phases of AEWs along 0°E in sub-Saharan West Africa. After defining whether an AEW was convectively active in this location, Schlueter et al. (2019) used the local AEW phase to composite precipitation anomalies by both AEW phase and the presence of other convectively coupled waves (CCWs), allowing for a thorough comparison of the contributions of various wave types to rainfall over sub-Saharan West Africa. They showed that, in addition to individually enhancing precipitation during their active phases, CCWs can superimpose on each other, fur-

ther enhancing rainfall, for example when both an AEW and MJO are in their active phases over the region.

Both of these approaches to examining convective activity focus on the evolution of convection over a point or region. In this appendix, we will describe work that attempted to adapt this phase framework to a wave-following approach. When following the convection in dynamically-tracked TEWs, we first assume that a TEW's CV is approximately in-phase with its convection, which Hollis et al. (2024b) and Chapter 2 showed is a reasonable assumption. Because we will always be focused on the convectively active portion of the wave, a wave-following phase framework will contain information about whether the wave is strong or weak, and whether is is strengthening or weakening, rather than whether the wave is active or suppressed.

A.2 Methods

Adapting the methods described in Schlueter et al. (2019) and Riley et al. (2011), our TEW phase space consists of CV and its time derivative, $\frac{d(CV)}{dt}$, both at the tracked point from the TEW database. CV is provided in the TEW tracks, and its calculation is described in Hollis et al. (2024a). The time derivative of CV was calculated using a centered approximation for all points along each track except the first and last points, where forwards and backwards approximations are used instead.

In testing different approaches to putting TEW strength into a phase space, we tried multiple approaches to ensure that waves could be compared fairly. Thus, we separately calculated standardized anomalies of along-track CV using tropics-wide averages, the CV climatology at the nearest grid point, and the CV mean and standard deviation for TEWs. We also used the raw CV as a point of comparison, though Hollis et al. (2024a) showed that the upper bound of CV attained by TEWs is more than an order

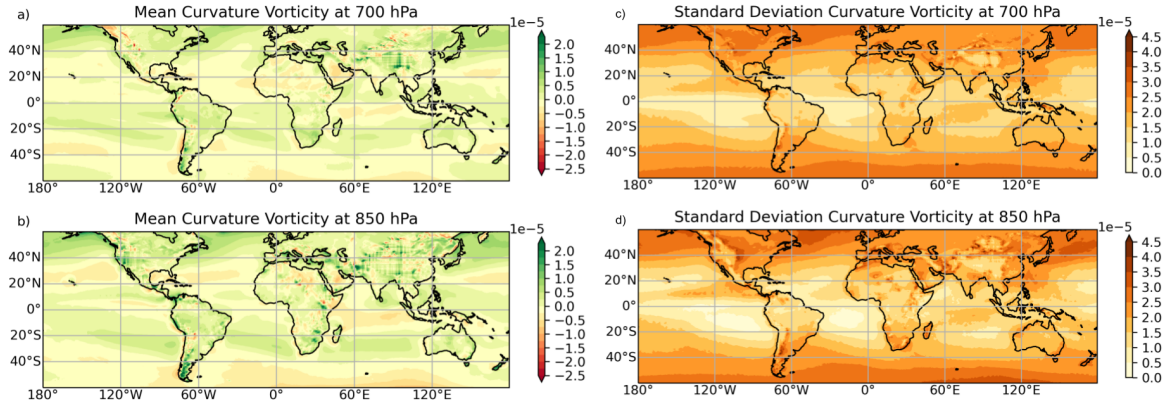


Figure A.1: Means (left panels) and standard deviations (right panels) of CV at 700 (top panels) and 850 hPa (bottom panels).

	850 hPa	700 hPa
NH	1.903×10^{-8}	-3.944×10^{-8}
SH	3.823×10^{-7}	4.129×10^{-7}

Table A.1: Mean CV averaged across 0-40° latitude for each level/hemisphere combination.

of magnitude greater than the mean. The CV climatology is shown in Fig. A.1, and the tropics-averaged values are in Tables A.1 and A.2.

A.3 Results

For individual TEWs, the CV phase space shows some potentially interesting results. The phase space for four TEW tracks from 2014, each from different basins, are shown in Fig. A.2. The phases space in these figures used CV standardized by the local climatology, though results using the other approaches was similar. These four examples

	850 hPa	700 hPa
NH	1.573×10^{-5}	1.627×10^{-5}
SH	1.410×10^{-5}	1.534×10^{-5}

Table A.2: Standard deviation of CV averaged across 0-40° latitude for each level/hemisphere combination.

show that CV evolves in a cyclical pattern, with the example TEWs going through periods of strengthening (positive d(CV')/dt) and weakening (negative d(CV')/dt). This cycle is approximately diurnal for some parts of each phase space. However, there are both shorter and longer oscillations present in each wave's phase space. Additionally, considering that the westward propagation of TEWs would result in solar days longer than 24 hours, while some CV cycles are less than 24 hours, this suggests that additional factors are involved in the evolution of CV in TEWs.

While the phase space for individual TEWs suggests that the diurnal cycle is important to TEW evolution, these example phase diagrams also highlight some of the differences in TEWs that will result in complications for bulk comparisons, which will be discussed below.

While standardizing CV is intended to place all TEWs on comparable axes, when we compare the axes of the panels in the left column of Fig. A.2, we still find that standardized CV can still cover a very large range. This large range is exemplified in Fig. A.2g, with a range of over 2500 standard deviations, compared to the range of up to 20 standard deviations in the other phase space panels.

In addition to the variable axis ranges between each TEW shown in A.2, an additional difference between these wave-following TEWs and the phases shown in Riley et al. (2011) and Schlueter et al. (2019) is that the wave-following phase space is not centered around (0,0). Instead, for each wave, for three of the four TEWs, the TEW's entire life is spent in the negative x-axis (Fig. A.2a,c,e), or the range weaker CV than climatology. This means that the phase space cannot be divided using simple angles. While most TEWs can still be defined by whether they are strengthening or weakening, some waves (not shown), spend their entire lives strengthening or weakening. We believe that the majority of the waves that strengthen over their entire lives are pre-TC TEWs, as this is in line with the general evolution of CV as a function of percent of

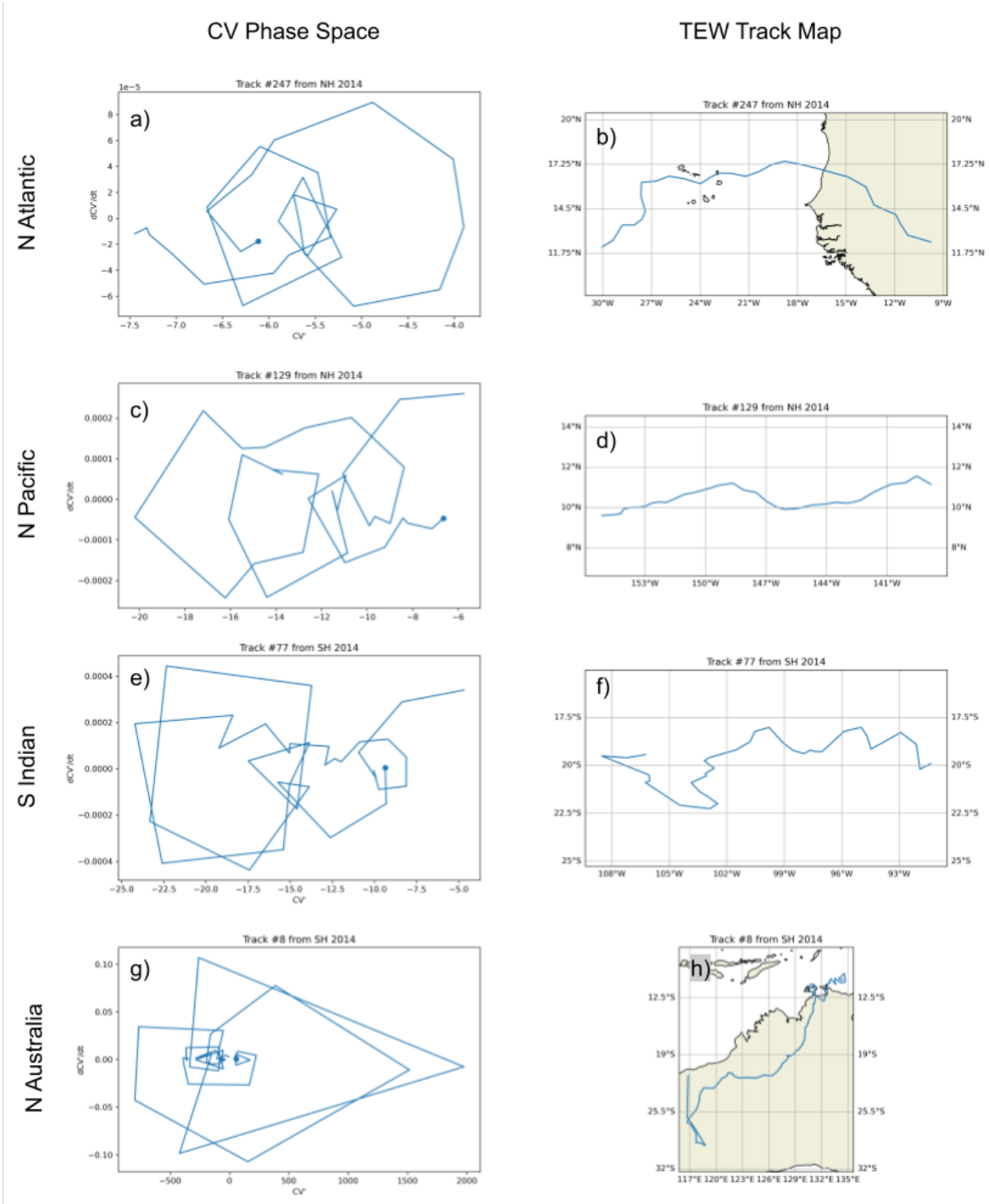


Figure A.2: Phase space (left column) and maps (right column) for four selected TEW tracks from 2014. The first point in the phase space is marked with a dot.

life (See also Chapter 4).

A variety of issues arose when attempting to scale these methods and the phase space to all TEW tracks in the database. Some issues were specific to which standardization approach we used, while others were universal across approaches.

When using raw CV and CV standardized using tropics-wide averages, the scatterplot of CV vs derivative, which should be the phase space, is divided into two main areas, one on each side of the y-axis, as seen in Fig. A.3. This occurs because the sign of cyclonic CV is dependent only on the hemisphere, and standardizing by scalar values only change the magnitude of CV and its derivative. Thus, even if we account for the sign difference and multiply SH values by -1, all points would be clustered on one side of the y-axis.

While standardizing using the climatology for the nearest grid point should address the clustering of points by hemisphere, additional problems arise when using this approach. As shown in Fig. A.4, there are numerous extreme outliers. These extreme outliers are not symmetrically distributed around the phase space, and they appear to preferentially fall along certain angles.

Calculating standardized anomalies using the mean and standard deviation of TEW CV also addresses the hemispheric clustering problem, as shown in Fig. A.5. This method, however, still has some extreme outliers, though they have been excluded from the axes here so that we can examine the region of the phase space occupied by most TEW points.

Unfortunately, this distribution of points is still less than ideal for assigning phases to points along TEW tracks. Due to the relatively small changes in standardized CV anomalies relative to the magnitudes of the standardized anomalies, points are not evenly distributed among theoretical phases like was seen in Riley et al. (2011) and Schlueter et al. (2019).

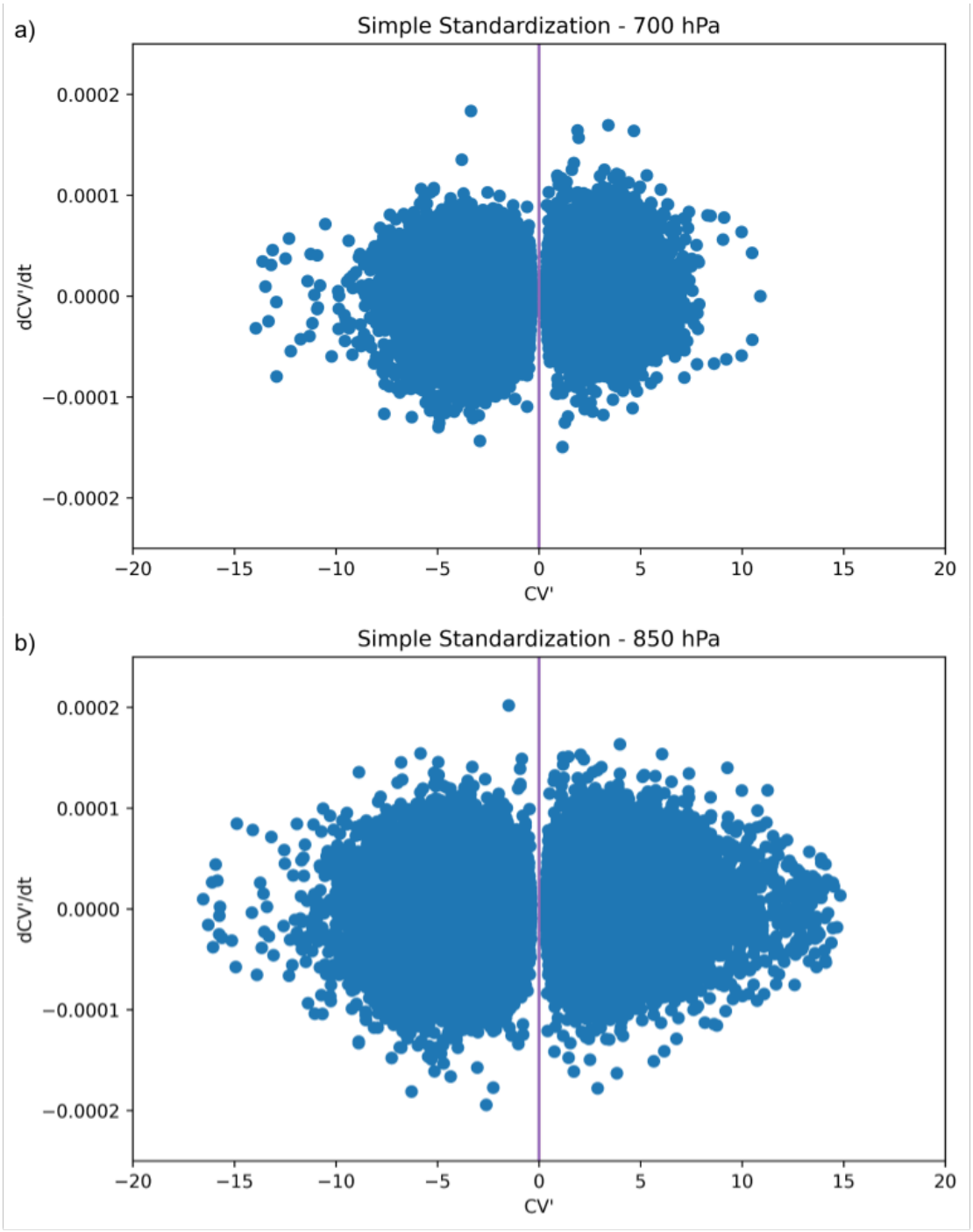


Figure A.3: Scatterplots of TEW-following CV phase space for TEWs at a) 700 hPa and b) 850 hPa, with CV standardized using tropics-wide averages. The y-axis is marked with a purple line.

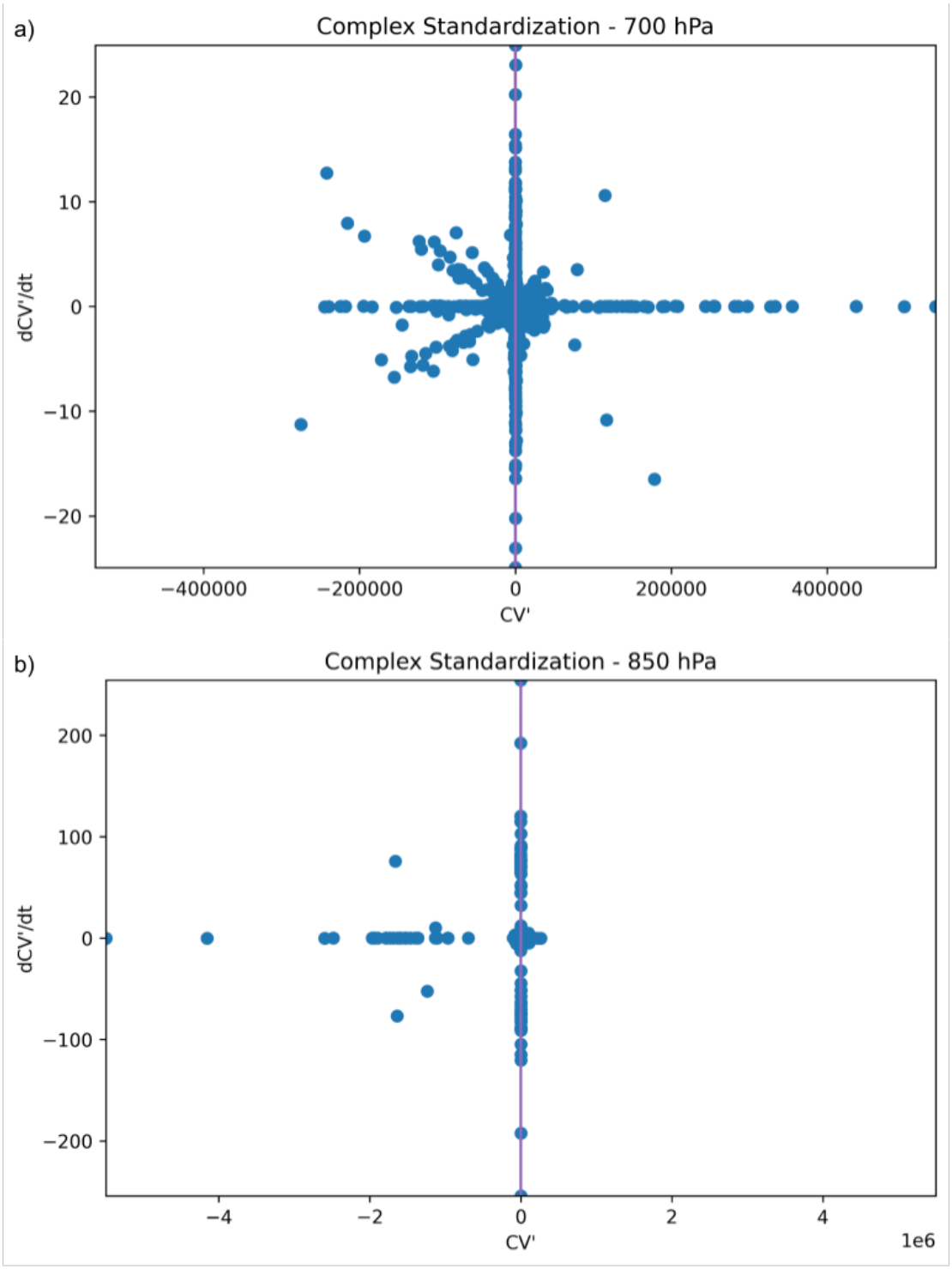


Figure A.4: As Fig. A.3 but with CV standardized using the climatology for the nearest grid point.

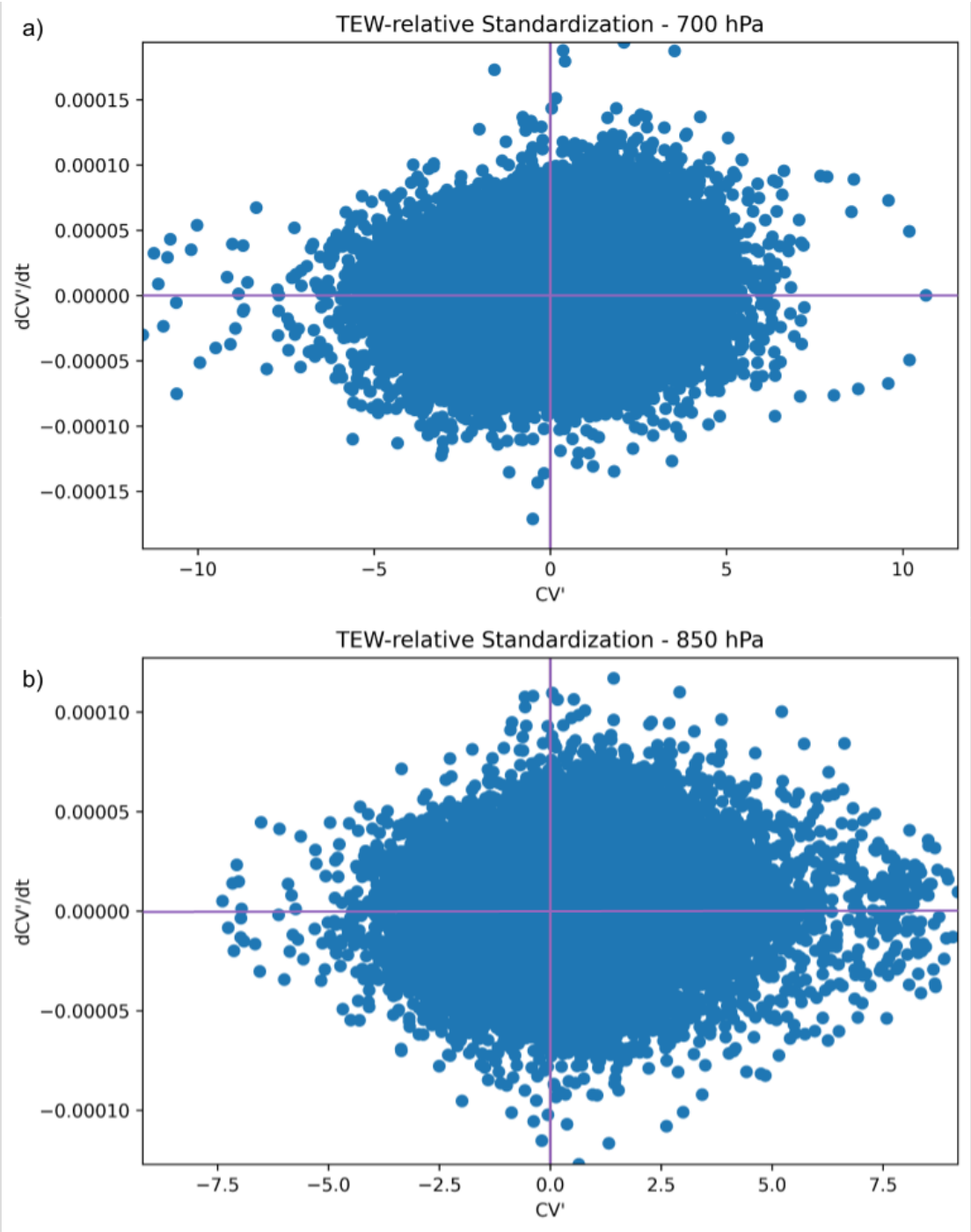


Figure A.5: As Fig. A.3 but with CV standardized using the climatology of TEW CV, and with the addition of an additional purple line on the x-axis.

A.4 Discussion

We have shown here that a phase framework similar to that used in Riley et al. (2011) and Schlueter et al. (2019) is not appropriate for wave-following analysis of TEWs. However, we have still illustrated the climatology of curvature vorticity, and demonstrated evidence for the importance of the diurnal cycle to the evolution of TEWs.

The intention for developing a wave-following phase definition was to apply the definition to both CV and wave-associated precipitation. Our hypothesis was that wave-associated precipitation increased in response to increasing cyclonic CV. While wave-following phases, as used here, were not successful in diagnosing TEW phase and were therefore not applied to precipitation, Chapter 4 visited the topic, finding that the rainiest TEWs often have higher CV.

While this phase framework did not work as intended, recent work has examined the relationship between strengthening/weakening, precipitation, and heating in TEWs. Using a transient strengthening and weakening framework, Lewis-Merritt and Stachnik (2026) has recently shown evidence of differences in MSE for TEWs in each strength tendency category, with strengthening TEWs potentially being more moisture mode-like.

Appendix B

Alternative Heating Calculations

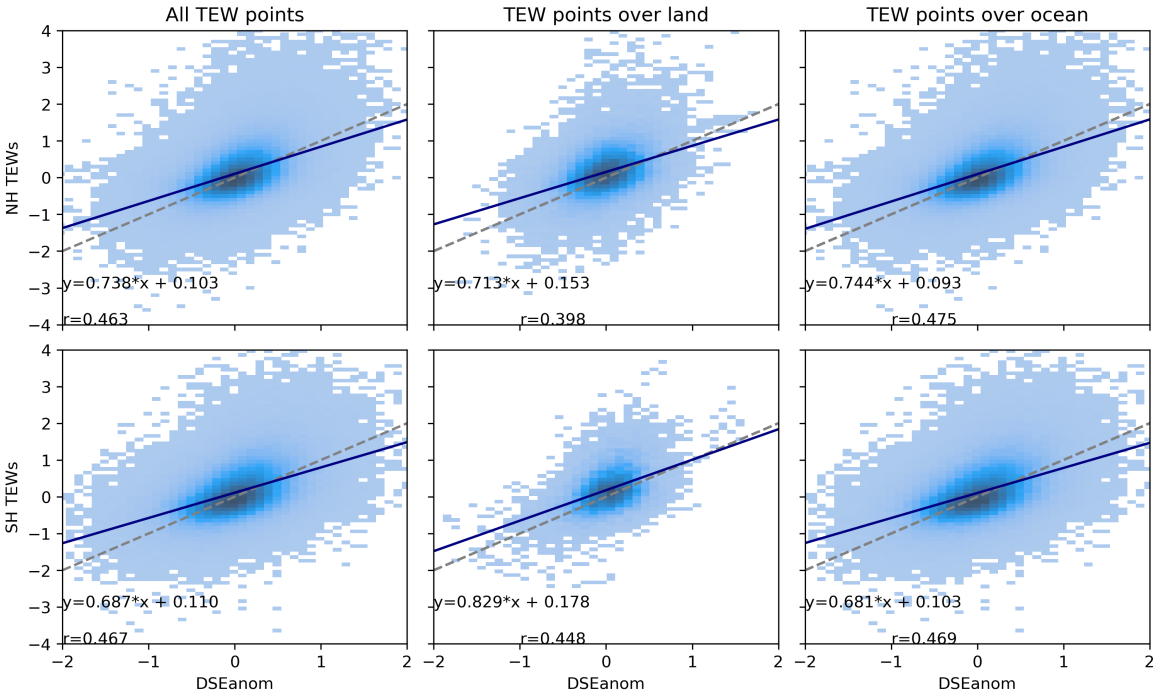


Figure B.1: Heatmaps of area-average standardized anomalies of the column-integrated DSE budget (x-axis) and column-integrated Q1 (y-axis) for TEWs a) all NH b) NH land c) NH ocean d) all SH e) SH land f) SH ocean, using Q1 calculated directly from the DSE tendency. In each panel, the linear fit is shown in solid dark blue while x=y is shown in dashed grey. The correlation is given in teh lower left corner of each panel.

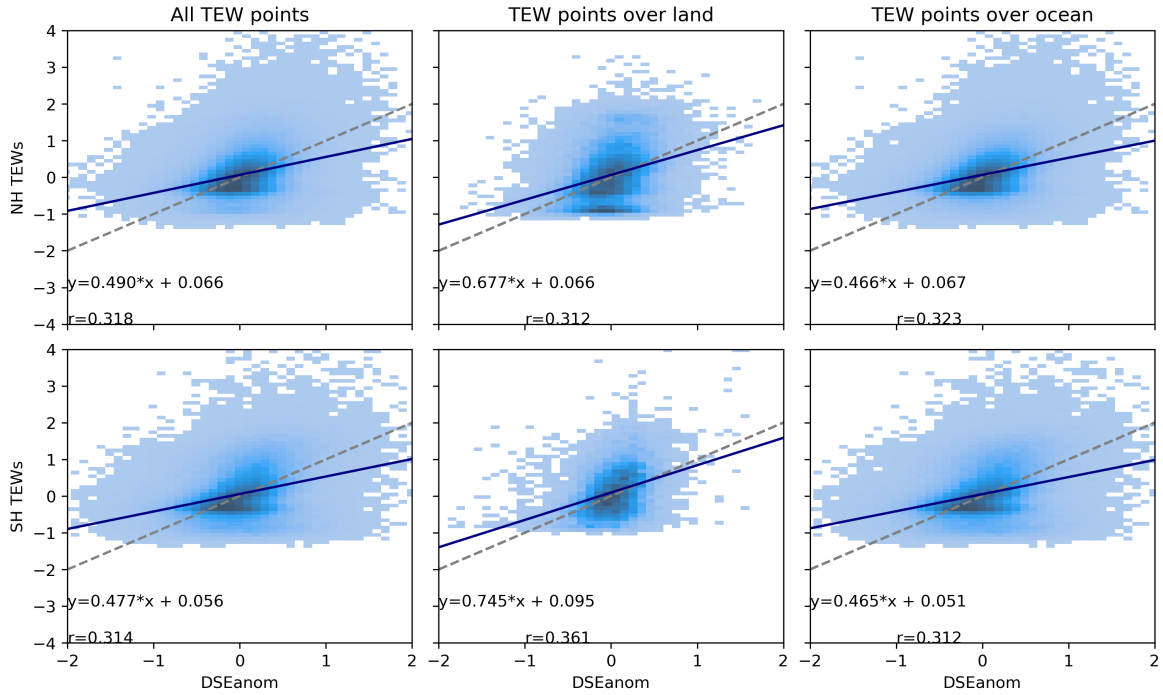


Figure B.2: As Fig. B.1 but using IMERG precipitation to calculate Q1.

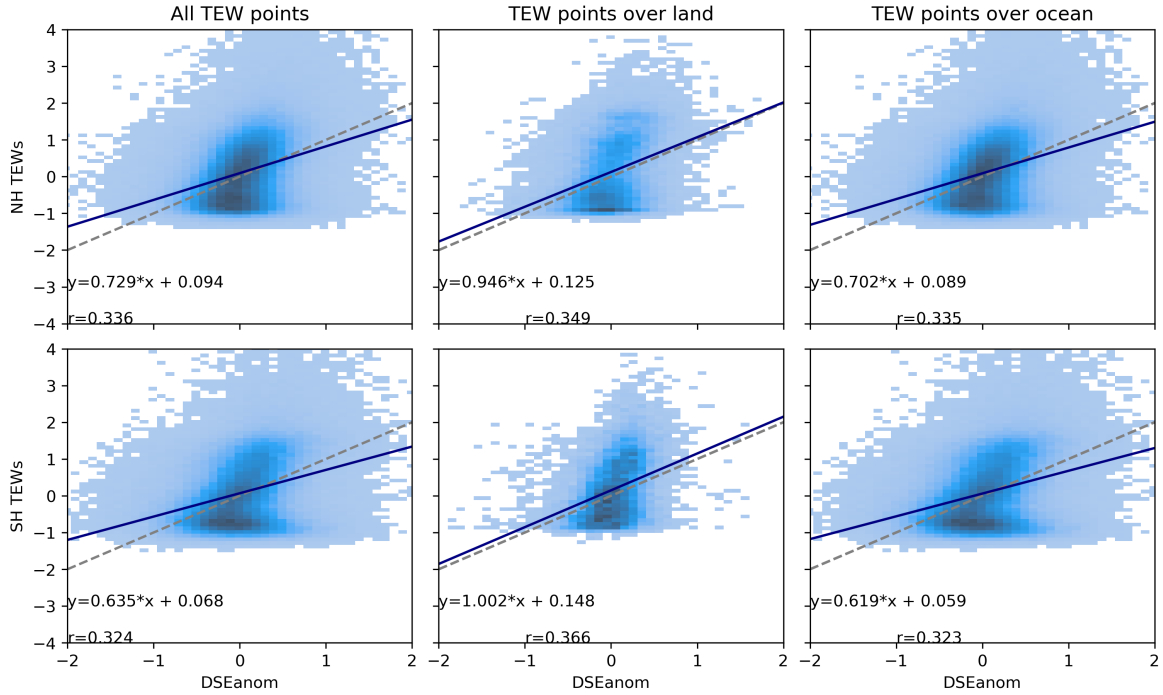


Figure B.3: As Fig. B.1 but using MERRA-2 precipitation to calculate Q1.

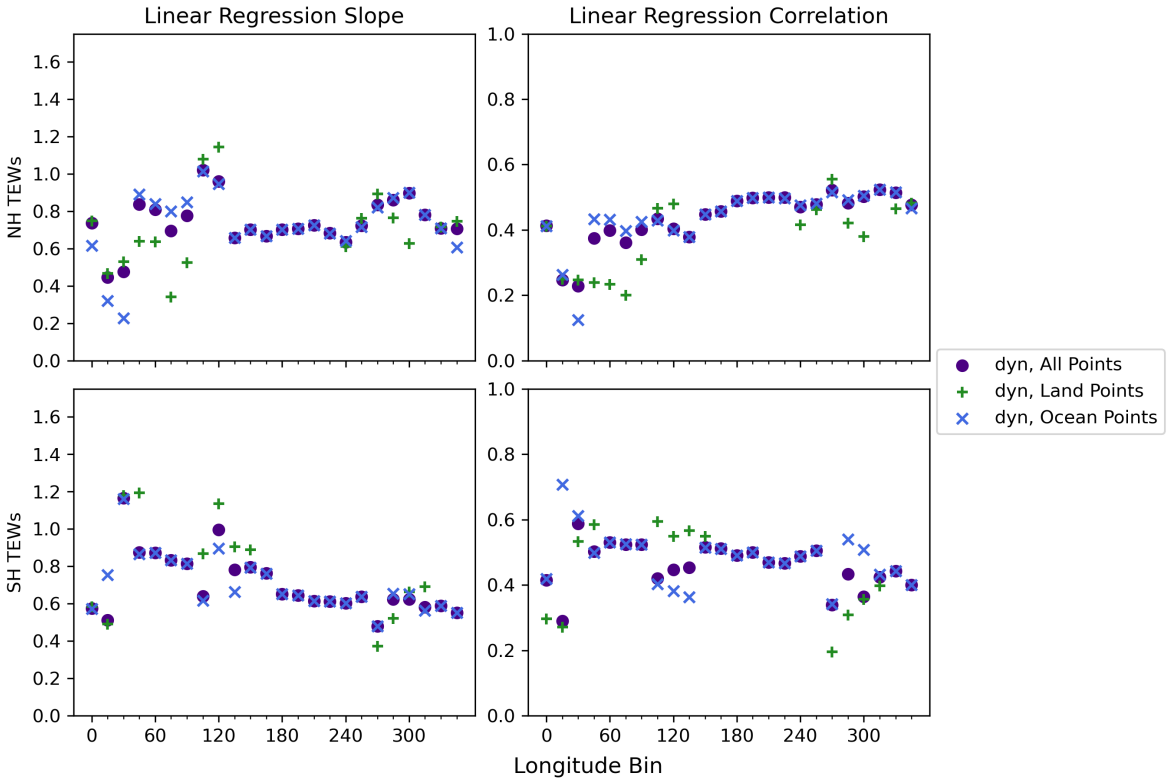


Figure B.4: Scatterplot of the slope (left column) and correlation (right column) for the linear regression between column-integrated DSE budget and column-integrated Q1 for TEWs in the NH (top row) and SH (bottom row), with Q1 calculated directly from the DSE tendency.

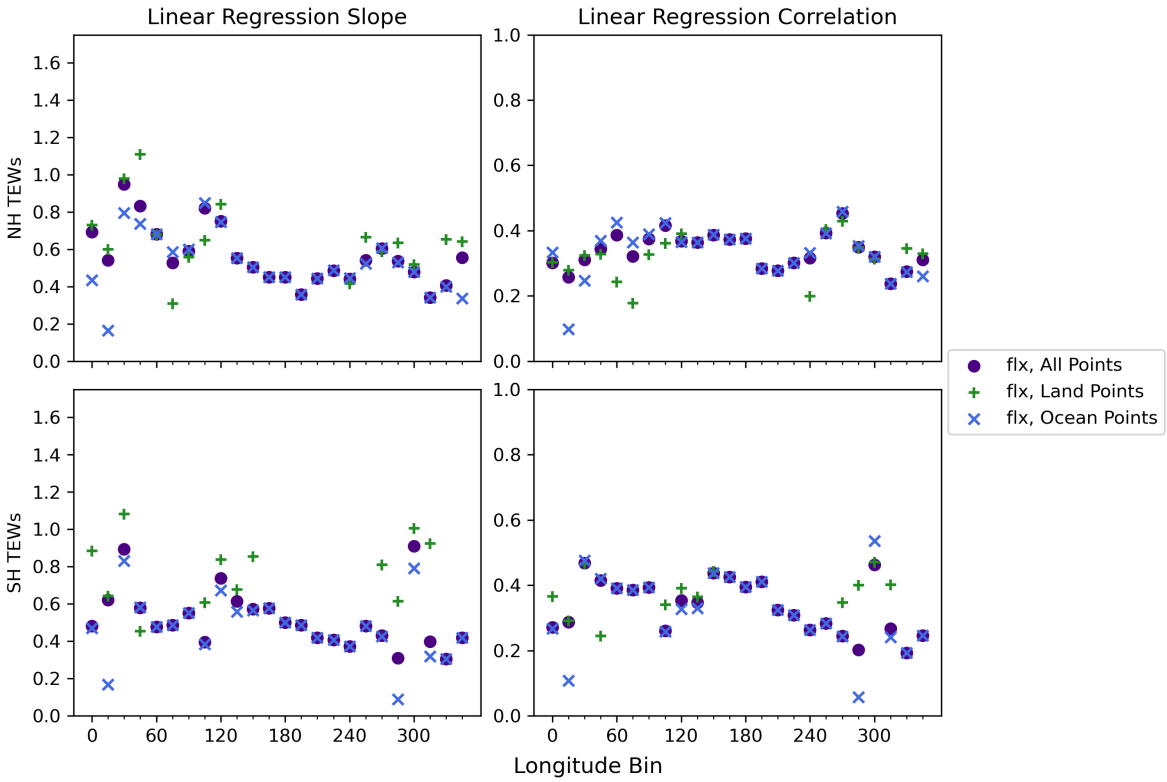


Figure B.5: As Fig. B.4 but using IMERG precipitation to calculate Q1.

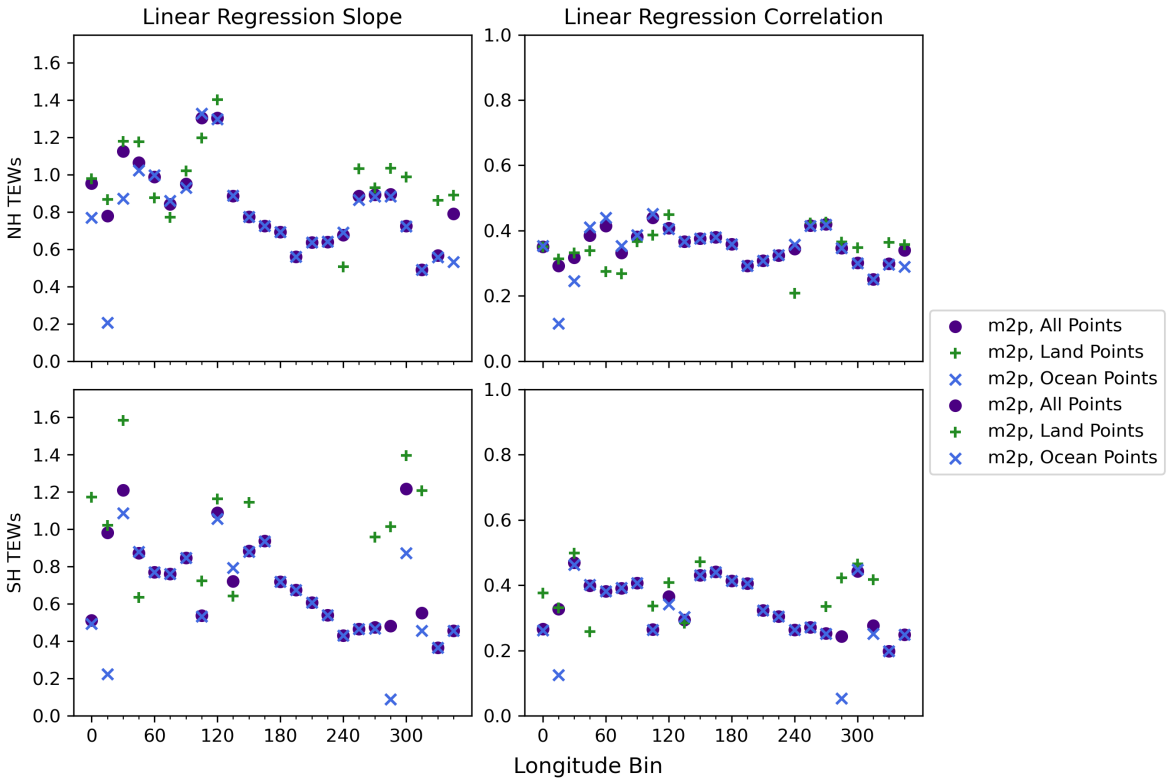


Figure B.6: As Fig. B.4 but using MERRA-2 precipitation to calculate Q1.

Appendix C

Selected Figures for 850 hPa TEWs

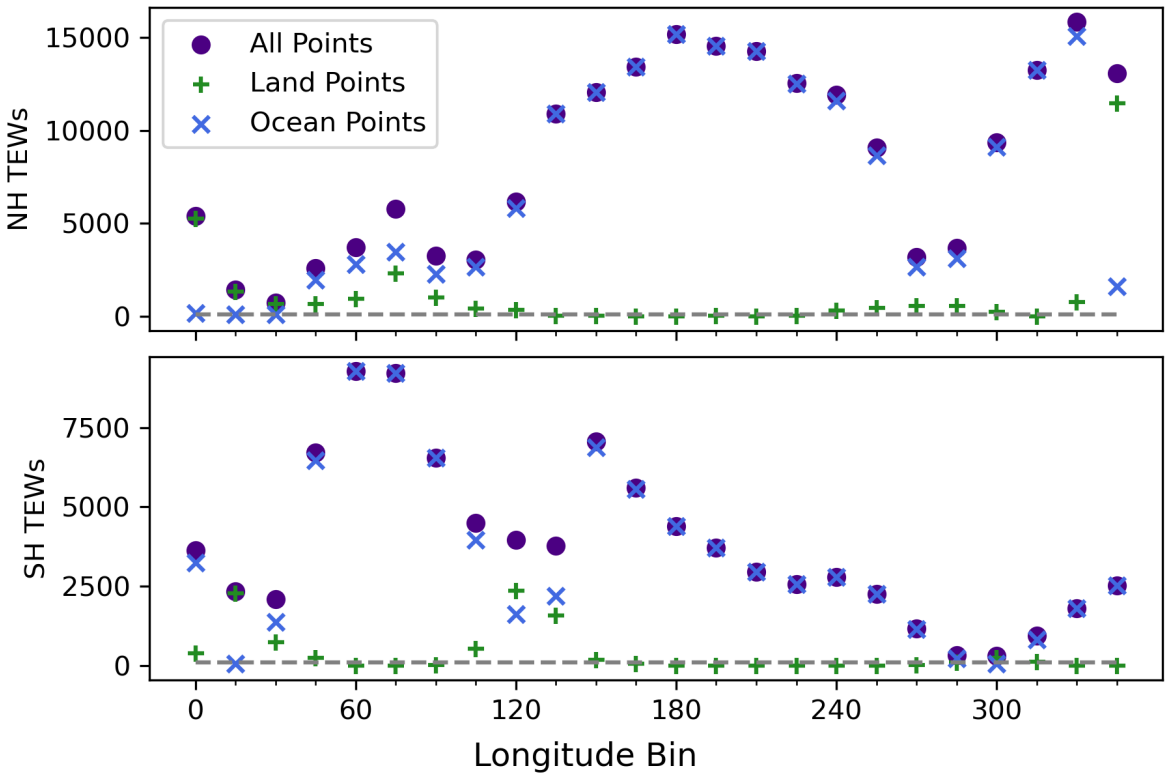


Figure C.1: Scatterplots showing the number of TEW points in each longitude buin over each surface type for TEWs in the NH (top) and SH (bottom). The grey dashed line delineates 100 points.

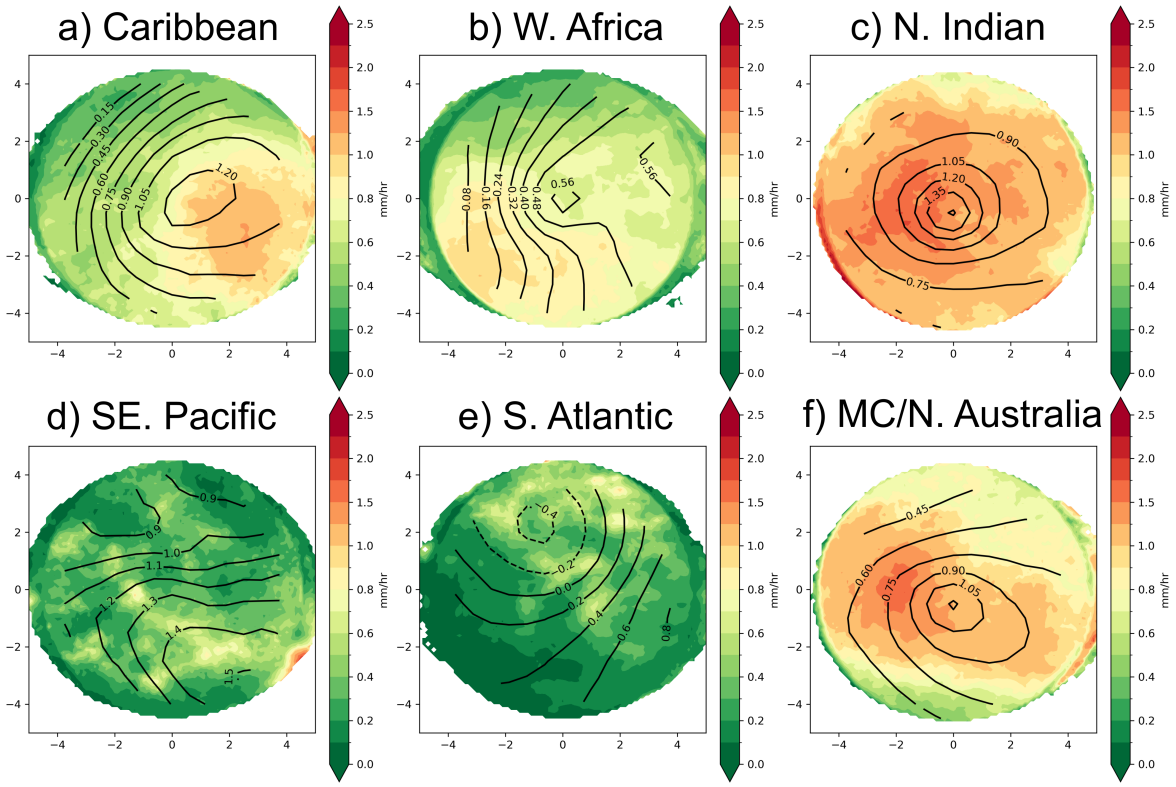


Figure C.2: Contoured plots showing the composite mean precipitation (shaded) and standardized anomalies of q (black solid and dashed lines) for the 500 km radius around 850 hPa TEWs in selected hemisphere/longitude bin combinations.

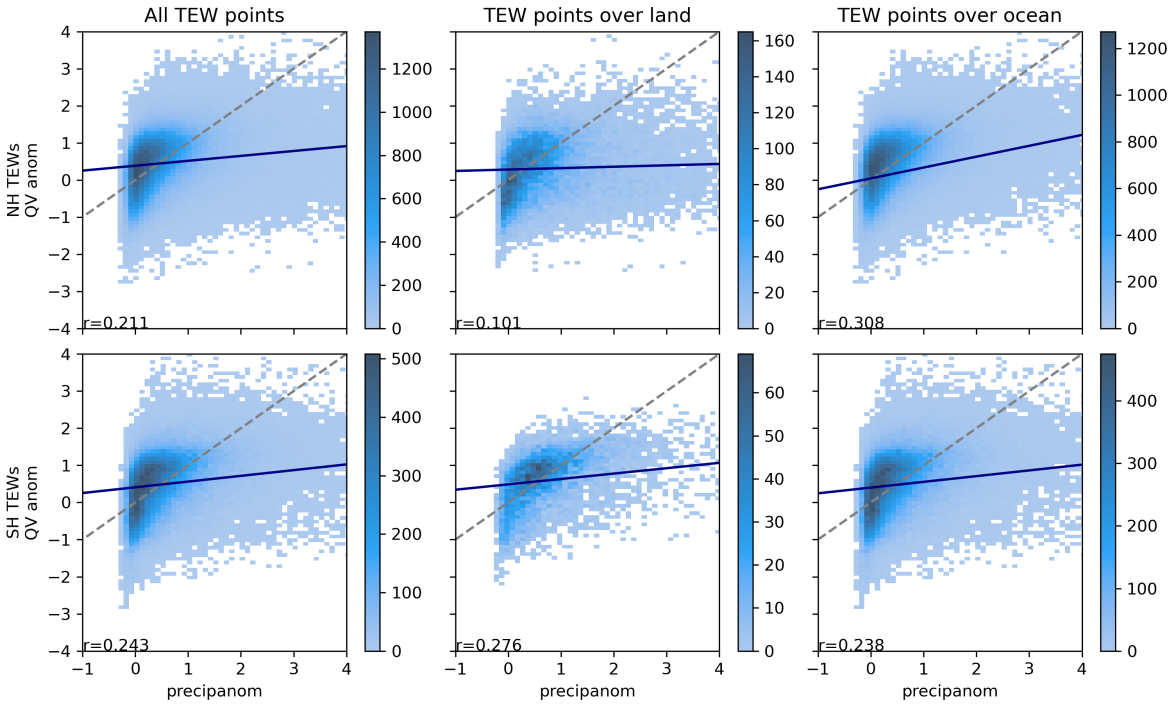


Figure C.3: Heatmaps of area-average standardized anomalies of precipitation (x-axis) and column-integrated specific humidity (y-axis) for TEWs a) all NH b) NH land c) NH ocean d) all SH e) SH land f) SH ocean. In each panel, the linear fit is shown in solid dark blue while x=y is shown in dashed grey. The correlation is given in teh lower left corner of each panel.

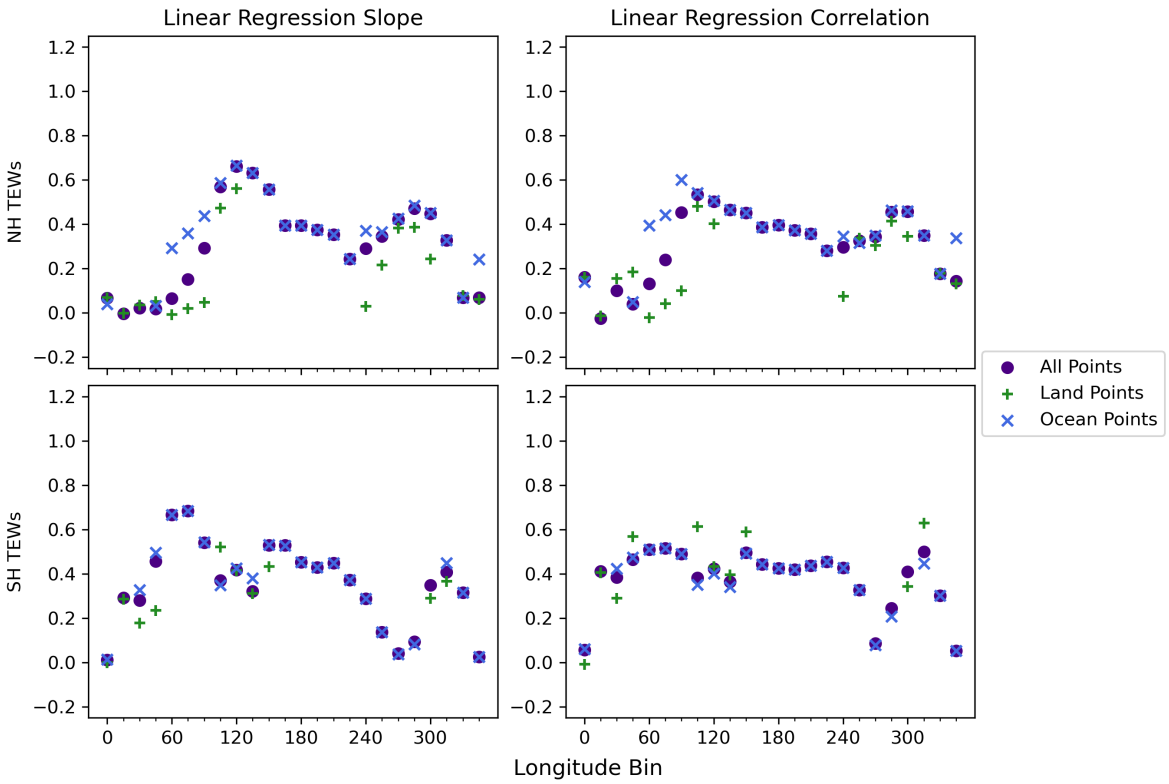


Figure C.4: Scatterplot of the slope (left column) and correlation (right column) for the linear regression between standardized precipitation anomalies and column-integrated specific humidity for 850 hPa TEWs in the NH (top row) and SH (bottom row)

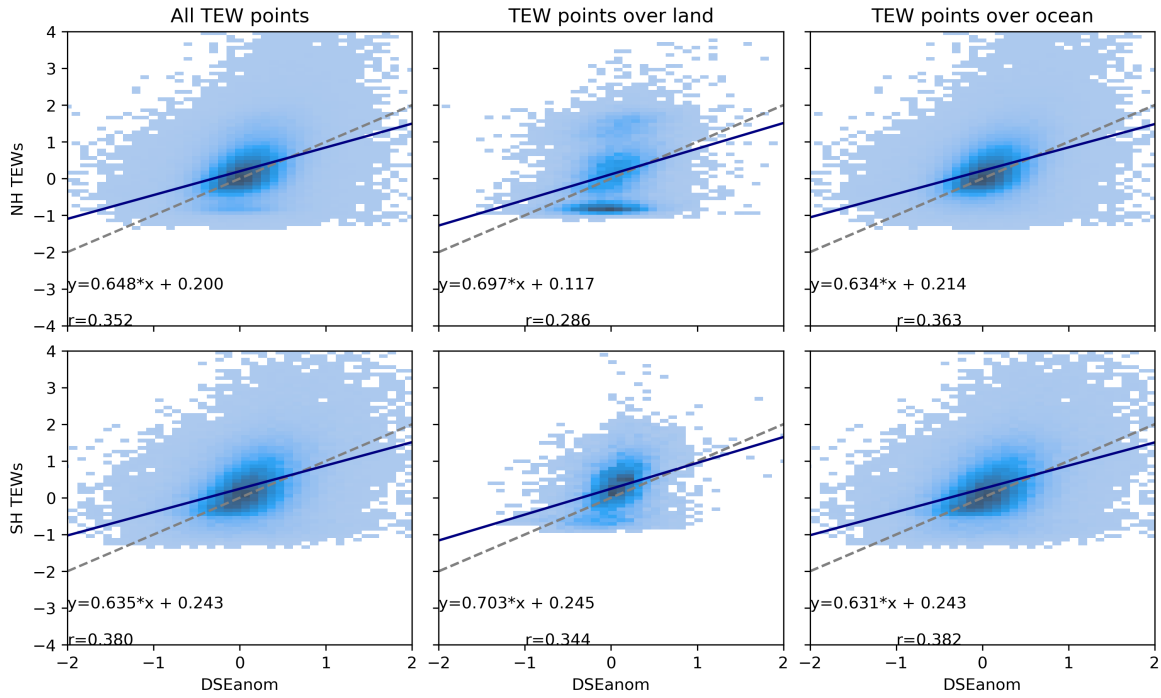


Figure C.5: As Fig. C.3 but for area-average standardized anomalies of the column-integrated DSE budget (x-axis) and column-integrated Q1 (y-axis).

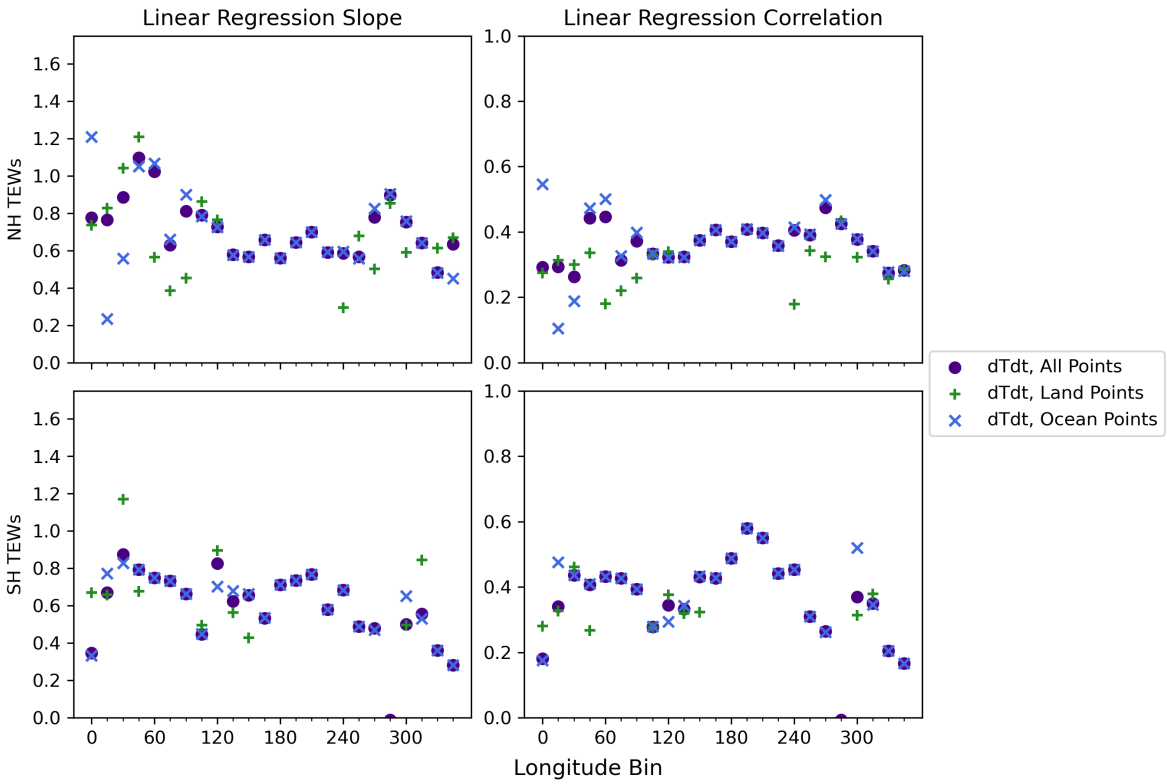


Figure C.6: As Fig. C.4 but for the linear regression between standardized anomalies of the column-integrated DSE budget and column-integrated Q1.

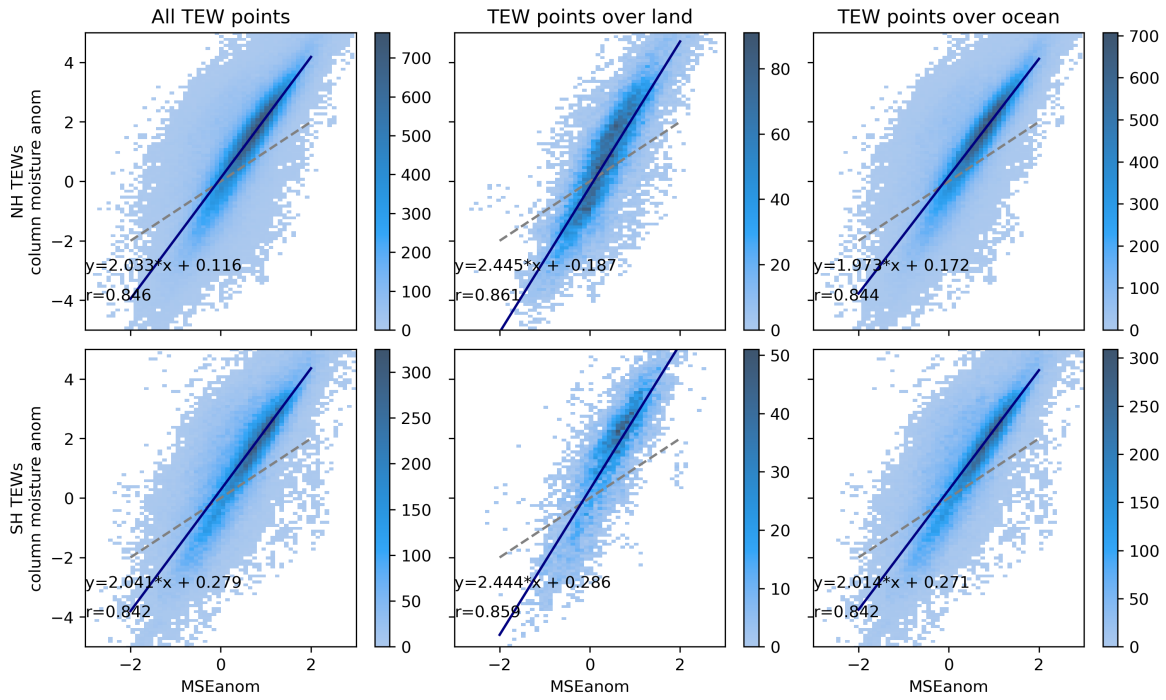


Figure C.7: As Fig. C.3 but for area-average standardized anomalies of MSE (x-axis) and column-integrated moisture (y-axis).

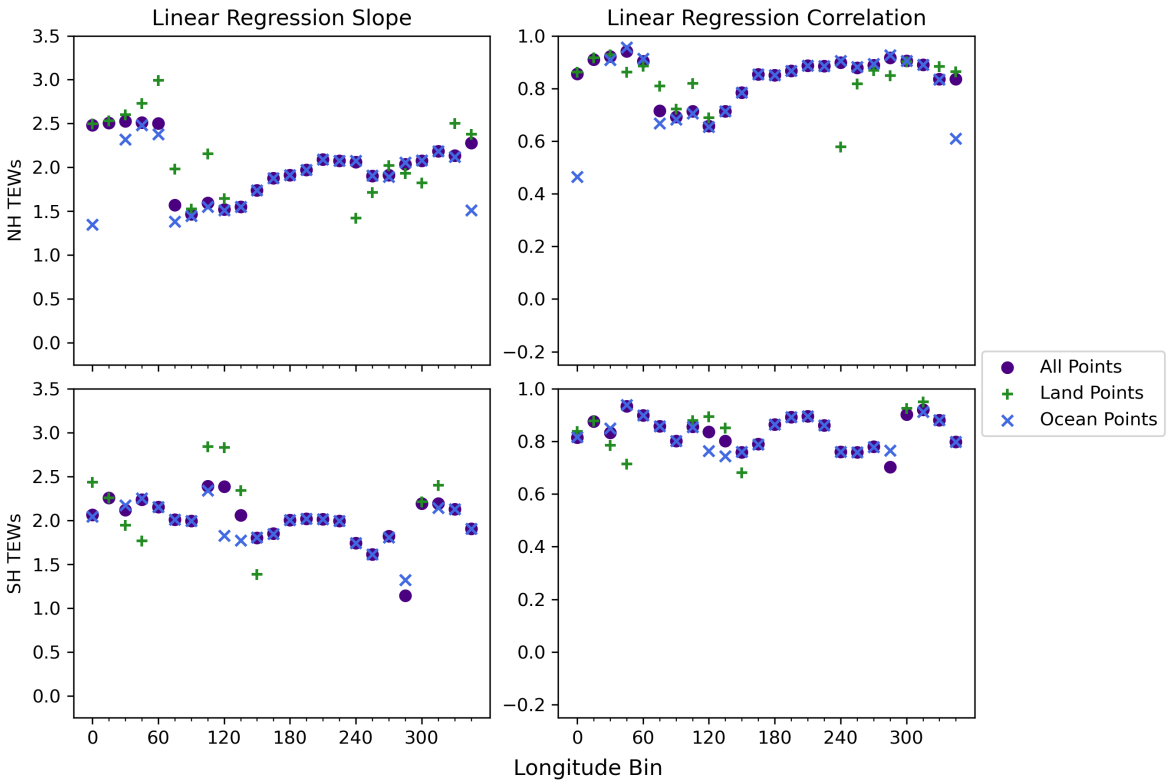


Figure C.8: As Fig. C.4 but for the linear regression between standardized anomalies MSE and column-integrated moisture.

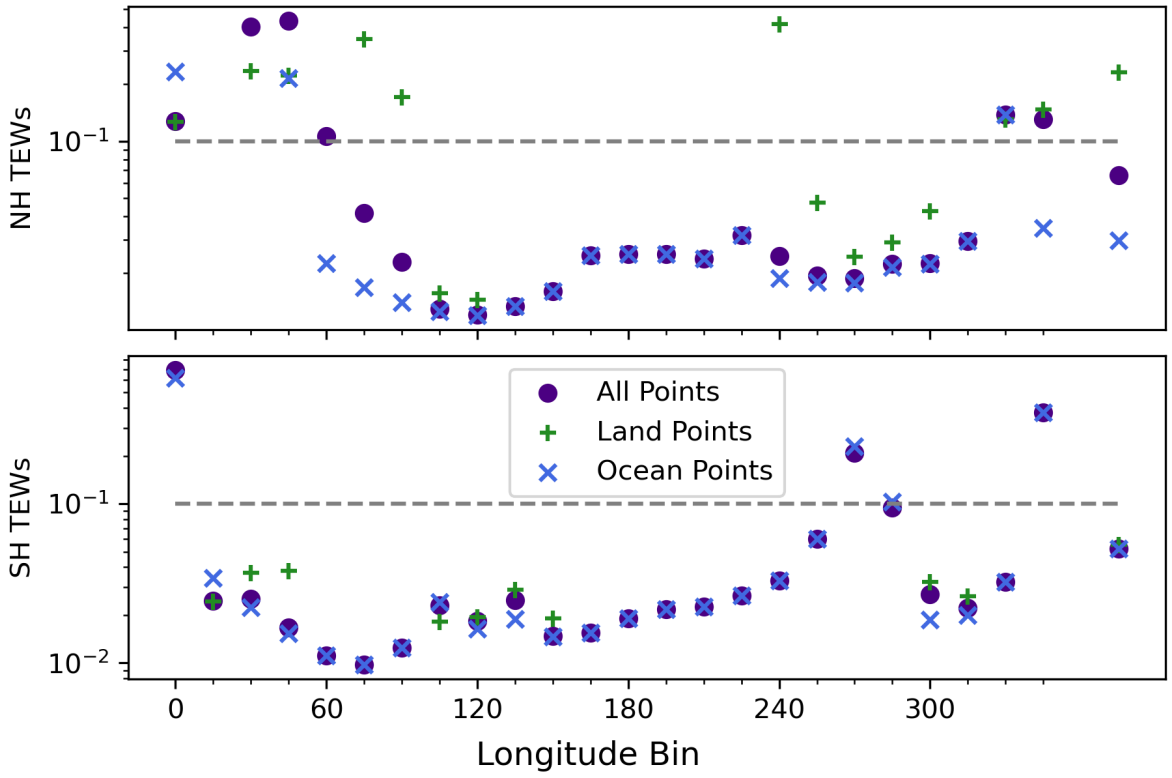


Figure C.9: Scatterplots showing the values of the N-mode parameter for TEWs in the NH (top) and SH (bottom). The horizontal grey dashed line denotes the threshold for small N-mode values, 0.1. Subgroups with fewer than 100 TEW points have been excluded. The rightmost points in each panel, which do not have a tick beneath them, are the global averages.

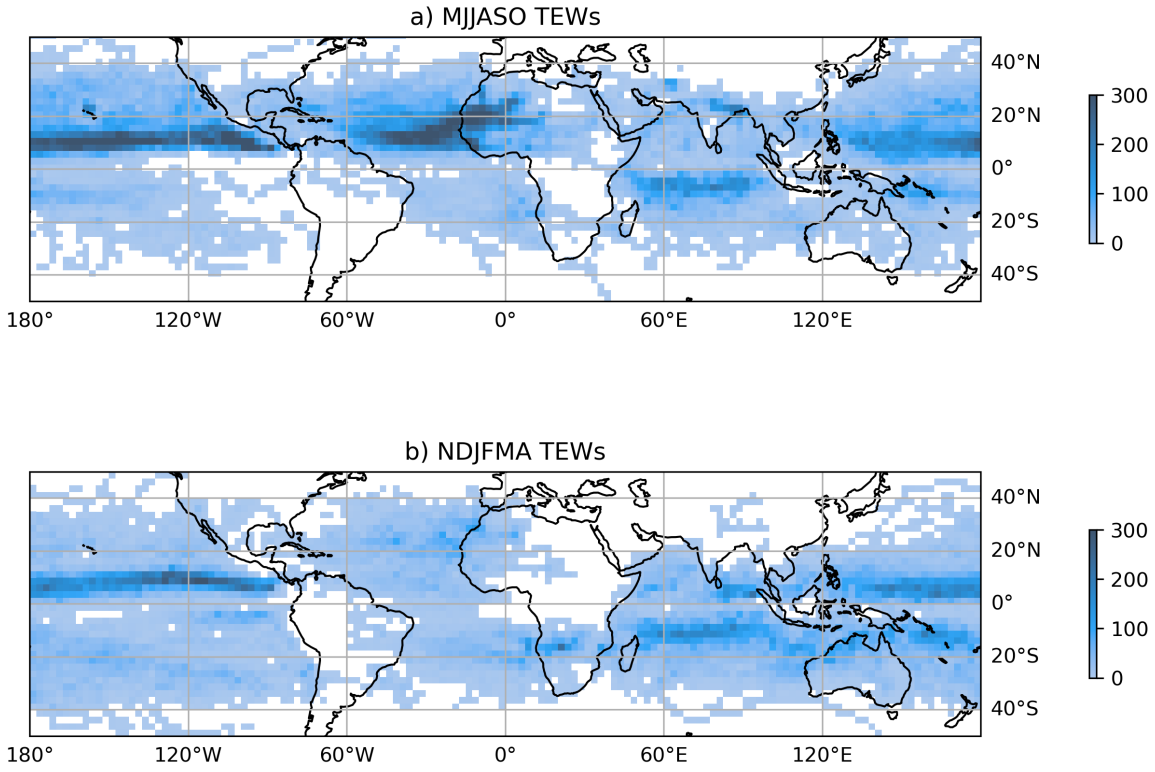


Figure C.10: Maps of TEW track points in 2.5° grid boxes for TEWs tracked at 700 hPa during a) boreal summer (MJJASO) and b) austral summer (NDJFMA).

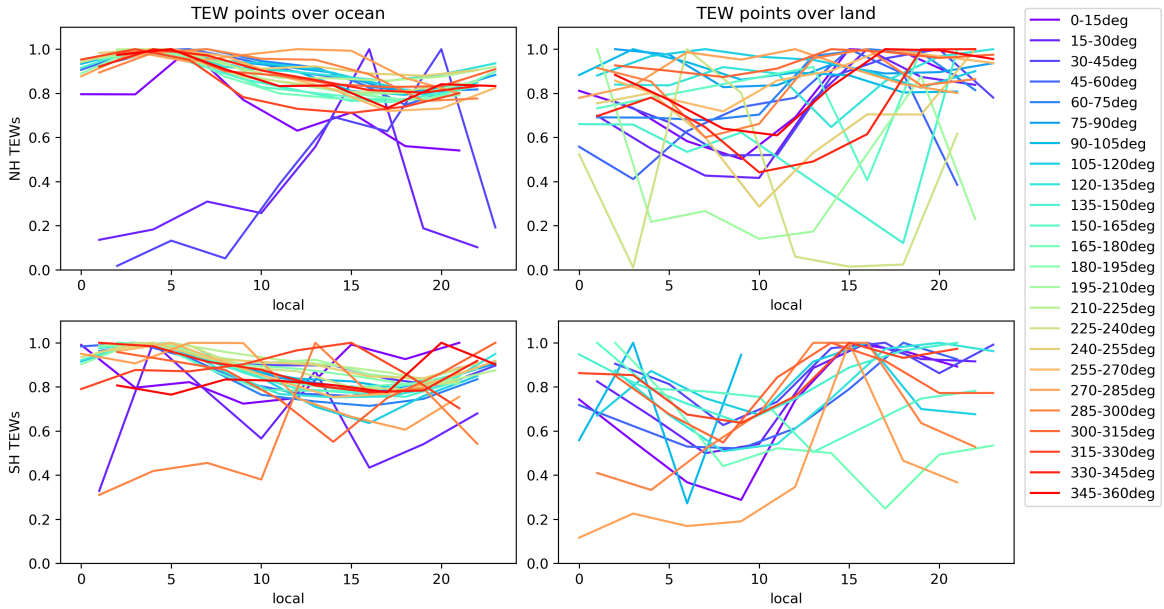


Figure C.11: Line plots showing the diurnal cycle of TEW-associated rainfall, as a percent of the daily maximum, for each longitude bin, for TEWs in the top) NH and bottom) SH, and for TEWs over left) ocean and right) land.

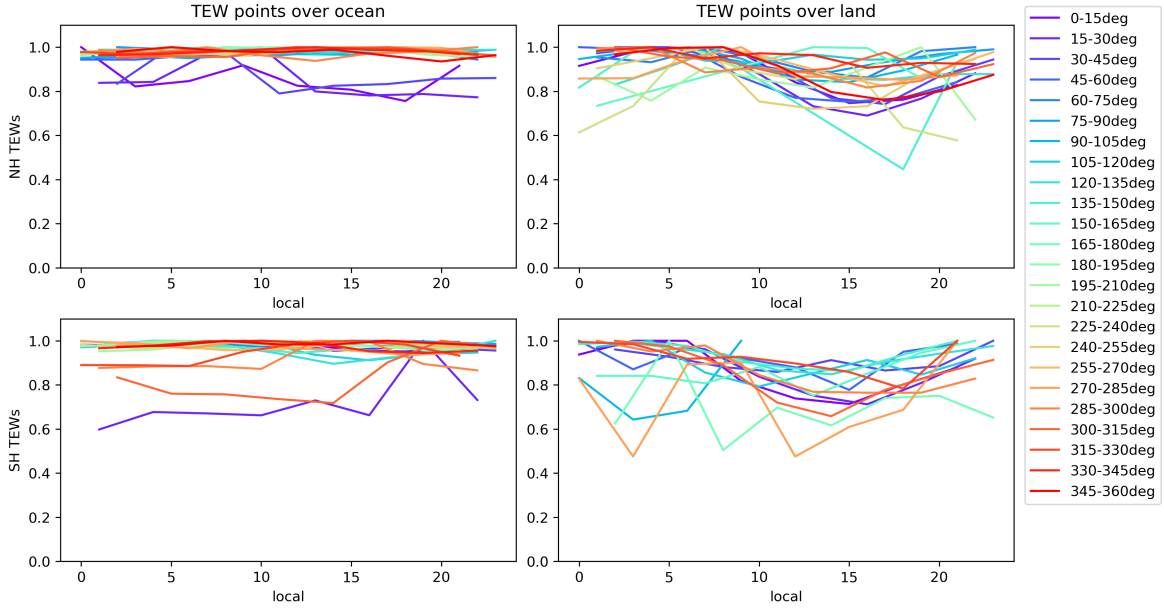


Figure C.12: Line plots showing the mean percent of daily max CV for TEWs in each longitude bin (colors) for TEWs in the top) NH and bottom) SH, and for TEWs over left) ocean and right) land.

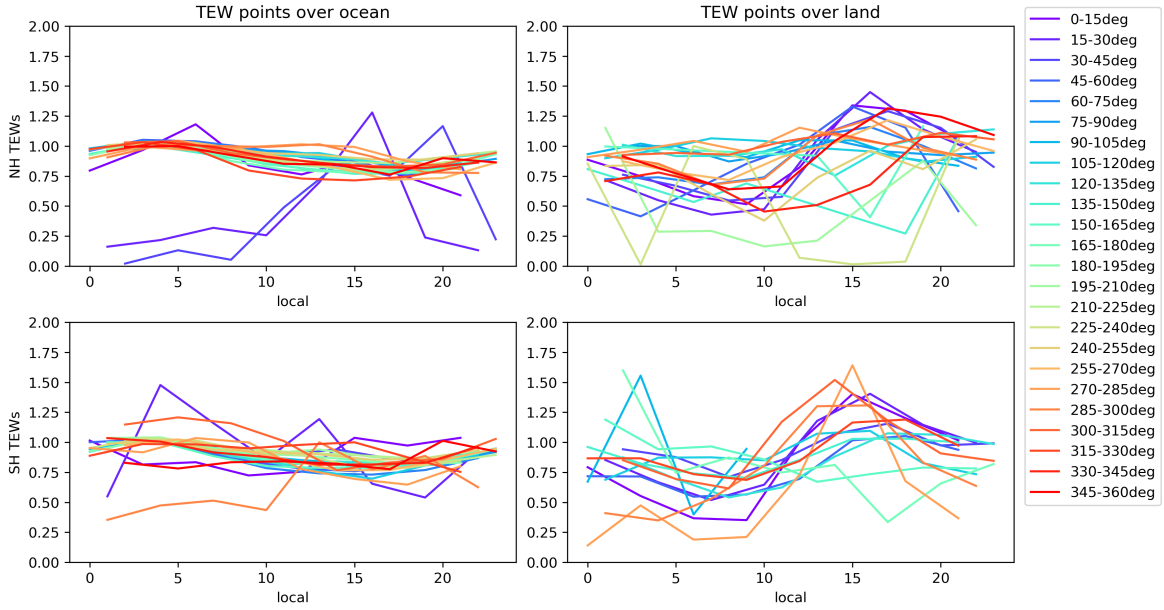


Figure C.13: Line plots showing the ratio of values from Fig. C.11 to Fig. C.12 for TEWs in the top) NH and bottom) SH, and for TEWs over left) ocean and right) land.

Reference List

Adames, À. F., D. Kim, S. K. Clark, Y. Ming, and K. Inoue, 2019: Scale Analysis of Moist Thermodynamics in a Simple Model and the Relationship between Moisture Modes and Gravity Waves. *Journal of the Atmospheric Sciences*, **76 (12)**, 3863–3881, https://doi.org/10.1175/JAS-D-19-0121.1, URL https://journals.ametsoc.org/view/journals/atsc/76/12/jas-d-19-0121.1.xml, publisher: American Meteorological Society Section: Journal of the Atmospheric Sciences.

Adames, À. F., and Y. Ming, 2018: Interactions between Water Vapor and Potential Vorticity in Synoptic-Scale Monsoonal Disturbances: Moisture Vortex Instability. *Journal of the Atmospheric Sciences*, **75 (6)**, 2083–2106, https://doi.org/10.1175/JAS-D-17-0310.1, URL https://journals.ametsoc.org/view/journals/atsc/75/6/jas-d-17-0310.1.xml, publisher: American Meteorological Society Section: Journal of the Atmospheric Sciences.

Adams, J. L., and D. J. Stensrud, 2007: Impact of Tropical Easterly Waves on the North American Monsoon. *Journal of Climate*, **20 (7)**, 1219–1238, https://doi.org/10.1175/JCLI4071.1, URL https://journals.ametsoc.org/jcli/article/20/7/1219/31154/Impact-of-Tropical-Easterly-Waves-on-the-North.

Belanger, J. I., M. T. Jelinek, and J. A. Curry, 2016: A climatology of easterly waves in the tropical Western Hemisphere. *Geoscience Data Journal*, **3 (2)**, 40–49, https://doi.org/10.1002/gdj3.40, URL http://doi.wiley.com/10.1002/gdj3.40.

Berry, G. J., M. J. Reeder, and C. Jakob, 2012: Coherent Synoptic Disturbances in the Australian Monsoon. *Journal of Climate*, **25 (24)**, 8409–8421, https://doi.org/10.1175/JCLI-D-12-00143.1, URL https://journals.ametsoc.org/jcli/article/25/24/8409/33672/Coherent-Synoptic-Disturbances-in-the-Australian.

Brammer, A., and C. D. Thorncroft, 2015: Variability and Evolution of African Easterly Wave Structures and Their Relationship with Tropical Cyclogenesis over the Eastern Atlantic. *Monthly Weather Review*, **143 (12)**, 4975–4995, https://doi.org/10.1175/MWR-D-15-0106.1, URL https://journals.ametsoc.org/mwr/article/143/12/4975/72006/Variability-and-Evolution-of-African-Easterly-Wave.

Brammer, A., and C. D. Thorncroft, 2017: Spatial and Temporal Variability of the Three-Dimensional Flow around African Easterly Waves. *Monthly Weather Review*, **145 (7)**, 2879–2895, https://doi.org/10.1175/MWR-D-16-0454.1, URL http://journals.ametsoc.org/doi/10.1175/MWR-D-16-0454.1.

Brannan, A. L., and E. R. Martin, 2019: Future characteristics of African Easterly Wave tracks. *Climate Dynamics*, **52 (9-10)**, 5567–5584, https://doi.org/10.1007/s00382-018-4465-z, URL http://link.springer.com/10.1007/s00382-018-4465-z.

Burgess, R. W., and M. I. Oyola-Merced, 2024: Saharan dust impact on radiative heating rate errors inherent in reanalysis data in the African easterly wave development region. *Atmospheric Chemistry and Physics*, **24 (21)**, 12 183–12 201, https://doi.org/10.5194/acp-24-12183-2024, URL https://acp.copernicus.org/articles/24/12183/2024/, publisher: Copernicus GmbH.

Burpee, R. W., 1972: The Origin and Structure of Easterly Waves in the Lower Troposphere of North Africa. *Journal of the Atmospheric Sciences*, **29 (1)**, 77–90, URL https://journals.ametsoc.org/view/journals/atsc/29/1/1520-0469_1972_029_0077_toasoe_2_0_co_2.xml, publisher: American Meteorological Society Section: Journal of the Atmospheric Sciences.

Carlson, T. N., 1969: Some Remarks on African Disturbances and Their Progress Over the Tropical Atlantic. *Monthly Weather Review*, **97 (10)**, 716–726, https://doi.org/10.1175/1520-0493(1969)097⟨0716:SROADA⟩2.3.CO;2, URL https://journals.ametsoc.org/view/journals/mwre/97/10/1520-0493_1969_097_0716_sroada_2_3_co_2.xml.

Charney, J. G., and M. E. Stern, 1962: On the Stability of Internal Baroclinic Jets in a Rotating Atmosphere. *Journal of the Atmospheric Sciences*, **19 (2)**, 159–172, https://doi.org/10.1175/1520-0469(1962)019⟨0159:OTSOIB⟩2.0.CO;2, URL https://journals.ametsoc.org/view/journals/atsc/19/2/1520-0469_1962_019_0159_otsoib_2_0_co_2.xml, publisher: American Meteorological Society Section: Journal of the Atmospheric Sciences.

Cifelli, R., T. Lang, S. A. Rutledge, N. Guy, E. J. Zipser, J. Zawislak, and R. Holzworth, 2010: Characteristics of an African Easterly Wave Observed during NAMMA. *Journal of the Atmospheric Sciences*, **67 (1)**, 3–25, https://doi.org/10.1175/2009JAS3141.1, URL https://journals.ametsoc.org/view/journals/atsc/67/1/2009jas3141.1.xml, publisher: American Meteorological Society Section: Journal of the Atmospheric Sciences.

Dai, A., X. Lin, and K.-L. Hsu, 2007: The frequency, intensity, and diurnal cycle of precipitation in surface and satellite observations over low- and mid-latitudes. *Climate Dynamics*, **29 (7)**, 727–744, https://doi.org/10.1007/s00382-007-0260-y, URL https://doi.org/10.1007/s00382-007-0260-y.

Derin, Y., P.-E. Kirstetter, and J. J. Gourley, 2021: Evaluation of IMERG Satellite Precipitation over the Land–Coast–Ocean Continuum. Part I: Detection. *Journal*

of Hydrometeorology, **22 (11)**, 2843–2859, https://doi.org/10.1175/JHM-D-21-0058.1, URL https://journals.ametsoc.org/view/journals/hydr/22/11/JHM-D-21-0058.1.xml, publisher: American Meteorological Society Section: Journal of Hydrometeorology.

Dickinson, M., and J. Molinari, 2000: Climatology of Sign Reversals of the Meridional Potential Vorticity Gradient over Africa and Australia. *Monthly Weather Review*, **128**, 11.

Diedhiou, A., L. A. T. Machado, and H. Laurent, 2010: Mean kinematic characteristics of synoptic easterly disturbances over the Atlantic. *Advances in Atmospheric Sciences*, **27 (3)**, 483–499, https://doi.org/10.1007/s00376-009-9092-5, URL https://doi.org/10.1007/s00376-009-9092-5.

Dominguez, C., J. M. Done, and C. L. Bruyère, 2020: Easterly wave contributions to seasonal rainfall over the tropical Americas in observations and a regional climate model. *Climate Dynamics*, **54 (1)**, 191–209, https://doi.org/10.1007/s00382-019-04996-7, URL https://doi.org/10.1007/s00382-019-04996-7.

Downs, W. B., S. J. Majumdar, and A. D. Mahoney, 2025: Using Deep Learning to Identify Tropical Easterly Waves, the Intertropical Convergence Zone, and the Monsoon Trough. *Monthly Weather Review*, **153 (8)**, 1581–1604, https://doi.org/10.1175/MWR-D-24-0195.1, URL https://journals.ametsoc.org/view/journals/mwre/153/8/MWR-D-24-0195.1.xml, publisher: American Meteorological Society Section: Monthly Weather Review.

Du, X., J.-E. Chu, F.-F. Jin, and H. M. Cheung, 2025: Global coupled dynamics of tropical easterly waves and tropical cyclone genesis. *npj Climate and Atmospheric Science*, **8 (1)**, 125, https://doi.org/10.1038/s41612-025-01014-y, URL https://www.nature.com/articles/s41612-025-01014-y, publisher: Nature Publishing Group.

Engel, T., A. H. Fink, P. Knippertz, G. Pante, and J. Bliefernicht, 2017: Extreme Precipitation in the West African Cities of Dakar and Ouagadougou: Atmospheric Dynamics and Implications for Flood Risk Assessments. *Journal of Hydrometeorology*, **18 (11)**, 2937–2957, https://doi.org/10.1175/JHM-D-16-0218.1, URL https://journals.ametsoc.org/view/journals/hydr/18/11/jhm-d-16-0218_1.xml, publisher: American Meteorological Society Section: Journal of Hydrometeorology.

Fahrin, F., A. O. Gonzalez, B. Chrisler, and J. P. Stachnik, 2024: The Relationship between Convectively Coupled Waves and the East Pacific ITCZ. *Journal of Climate*, **37 (8)**, 2565–2583, https://doi.org/10.1175/JCLI-D-23-0398.1, URL https://journals.ametsoc.org/view/journals/clim/37/8/JCLI-D-23-0398.1.xml, publisher:

American Meteorological Society Section: Journal of Climate.

Fink, A. H., and A. Reiner, 2003: Spatiotemporal variability of the relation between African Easterly Waves and West African Squall Lines in 1998 and 1999. *Journal of Geophysical Research*, **108 (D11)**, 4332, https://doi.org/10.1029/2002JD002816, URL http://doi.wiley.com/10.1029/2002JD002816.

Fiolleau, T., and R. Roca, 2024: A database of deep convective systems derived from the intercalibrated meteorological geostationary satellite fleet and the TOOCAN algorithm (2012–2020). *Earth System Science Data*, **16 (9)**, 4021–4050, https://doi.org/10.5194/essd-16-4021-2024, URL https://essd.copernicus.org/articles/16/4021/2024/, publisher: Copernicus GmbH.

Gelaro, R., and Coauthors, 2017: The Modern-Era Retrospective Analysis for Research and Applications, Version 2 (MERRA-2). *Journal of Climate*, **30 (14)**, 5419–5454, https://doi.org/10.1175/JCLI-D-16-0758.1, URL http://journals.ametsoc.org/doi/10.1175/JCLI-D-16-0758.1.

Gomes, H. B., T. Ambrizzi, D. L. Herdies, K. Hodges, and B. F. Pontes da Silva, 2015: Easterly Wave Disturbances over Northeast Brazil: An Observational Analysis. *Advances in Meteorology*, **2015**, e176 238, https://doi.org/10.1155/2015/176238, URL https://www.hindawi.com/journals/amete/2015/176238/, publisher: Hindawi.

Gomes, H. B., T. Ambrizzi, B. F. Pontes da Silva, K. Hodges, P. L. Silva Dias, D. L. Herdies, M. C. L. Silva, and H. B. Gomes, 2019: Climatology of easterly wave disturbances over the tropical South Atlantic. *Climate Dynamics*, **53 (3)**, 1393–1411, https://doi.org/10.1007/s00382-019-04667-7, URL https://doi.org/10.1007/s00382-019-04667-7.

Hodges, K. I., 1995: Feature Tracking on a Unit Sphere. *Monthly Weather Review*, **123**, 3458–3465.

Hollis, M. A., R. R. McCrary, J. P. Stachnik, C. Lewis-Merritt, and E. R. Martin, 2024a: A global climatology of tropical easterly waves. *Climate Dynamics*, **62 (3)**, 2317–2332, https://doi.org/10.1007/s00382-023-07025-w, URL https://link.springer.com/10.1007/s00382-023-07025-w.

Hollis, M. A., J. P. Stachnik, C. Lewis-Merritt, R. R. McCrary, and E. R. Martin, 2024b: Precipitation Characteristics of Easterly Waves Across the Global Tropics. *Journal of Geophysical Research: Atmospheres*, **129 (7)**, e2023JD039 957, https://doi.org/10.1029/2023JD039957, URL https://onlinelibrary.wiley.com/doi/abs/10.1029/2023JD039957, _eprint: https://onlinelibrary.wiley.com/doi/pdf/10.1029/2023JD039957.

Holton, J. R., 1971: A Diagnostic Model for Equatorial Wave Disturbances: The Role of Vertical Shear of the Mean Zonal Wind. *Journal of the Atmospheric Sciences*, **28 (1)**, 55–64, https://doi.org/10.1175/1520-0469(1971)028⟨0055:ADMFEW⟩2.0.CO;2, URL https://journals.ametsoc.org/view/journals/atsc/28/1/1520-0469_1971_028_0055_admfew_2_0_co_2.xml, publisher: American Meteorological Society Section: Journal of the Atmospheric Sciences.

Hopsch, S. B., C. D. Thorncroft, and K. R. Tyle, 2010: Analysis of African Easterly Wave Structures and Their Role in Influencing Tropical Cyclogenesis. *Monthly Weather Review*, **138 (4)**, 1399–1419, https://doi.org/10.1175/2009MWR2760.1, URL https://journals.ametsoc.org/view/journals/mwre/138/4/2009mwr2760.1.xml, publisher: American Meteorological Society Section: Monthly Weather Review.

Hsieh, J.-S., and K. H. Cook, 2005: Generation of African Easterly Wave Disturbances: Relationship to the African Easterly Jet. *Monthly Weather Review*, **133 (5)**, 1311–1327, https://doi.org/10.1175/MWR2916.1, URL https://journals.ametsoc.org/view/journals/mwre/133/5/mwr2916.1.xml.

Huaman, L., E. D. Maloney, C. Schumacher, and G. N. Kiladis, 2021: Easterly Waves in the East Pacific during the OTREC 2019 Field Campaign. *Journal of the Atmospheric Sciences*, **78 (12)**, 4071–4088, https://doi.org/10.1175/JAS-D-21-0128.1, URL https://journals.ametsoc.org/view/journals/atsc/78/12/JAS-D-21-0128.1.xml, publisher: American Meteorological Society Section: Journal of the Atmospheric Sciences.

Huffman, G. J., E. F. Stocker, D. T. Bolvin, E. J. Nelkin, and J. Tan, 2019: Gpm imerg final precipitation l3 half hourly 0.1 degree× 0.1 degree v06, goddard earth sciences data and information services center (ges disc), greenbelt, md.

Hurley, J. V., and W. R. Boos, 2015: A global climatology of monsoon low-pressure system. *Quarterly Journal of the Royal Meteorological Society*, **141 (689)**, 1049–1064, https://doi.org/10.1002/qj.2447, URL http://doi.wiley.com/10.1002/qj.2447.

Jury, M. R., 2014: Weather–Climate Interactions in the Eastern Antilles and the 2013 Christmas Storm. *Earth Interactions*, **18 (19)**, 1–20, https://doi.org/10.1175/EI-D-14-0011.1, URL https://journals.ametsoc.org/view/journals/eint/18/19/ei-d-14-0011.1.xml, publisher: American Meteorological Society Section: Earth Interactions.

Kiladis, G. N., C. D. Thorncroft, and N. M. J. Hall, 2006: Three-Dimensional Structure and Dynamics of African Easterly Waves. Part I: Observations. *Journal of the Atmospheric Sciences*, **63 (9)**, 2212–2230, https://doi.org/10.1175/JAS3741.1, URL https://journals.ametsoc.org/view/journals/atsc/63/9/jas3741.1.xml, pub-

lisher: American Meteorological Society Section: Journal of the Atmospheric Sciences.

Landsea, C. W., and W. M. Gray, 1992: The Strong Association between Western Sahelian Monsoon Rainfall and Intense Atlantic Hurricanes. *Journal of Climate*, **5 (5)**, 435–453, https://doi.org/https://doi.org/10.1175/1520-0442(1992)005%3C0435:TSABWS%3E2.0.CO;2.

Lewis-Merritt, C., and J. P. Stachnik, 2026: Regional Variability of Moist Thermodynamics and Energy Associated with Transient Changes in Easterly Waves. *Journal of the Atmospheric Sciences*, **83 (4)**, 453–473, https://doi.org/10.1175/JAS-D-25-0117.1, URL https://journals.ametsoc.org/view/journals/atsc/83/4/JAS-D-25-0117.1.xml, publisher: American Meteorological Society Section: Journal of the Atmospheric Sciences.

Lewis-Merritt, C., J. P. Stachnik, M. A. Hollis, E. R. Martin, and R. R. McCrary, 2024: A Global Climatology of Diabatic Heating in Tropical Easterly Waves. *Journal of Climate*, **(aop)**, https://doi.org/10.1175/JCLI-D-23-0196.1, URL https://journals.ametsoc.org/view/journals/clim/aop/JCLI-D-23-0196.1/JCLI-D-23-0196.1.xml, publisher: American Meteorological Society Section: Journal of Climate.

Mamalakis, A., and E. Foufoula-Georgiou, 2018: A Multivariate Probabilistic Framework for Tracking the Intertropical Convergence Zone: Analysis of Recent Climatology and Past Trends. *Geophysical Research Letters*, **45 (23)**, 13,080–13,089, https://doi.org/10.1029/2018GL079865, URL https://onlinelibrary.wiley.com/doi/abs/10.1029/2018GL079865, _eprint: https://onlinelibrary.wiley.com/doi/pdf/10.1029/2018GL079865.

Mayta, V. C., À. F. Adames, and F. Ahmed, 2022: Westward-Propagating Moisture Mode Over the Tropical Western Hemisphere. *Geophysical Research Letters*, **49 (6)**, e2022GL097 799, https://doi.org/10.1029/2022GL097799, URL https://onlinelibrary.wiley.com/doi/abs/10.1029/2022GL097799, _eprint: https://onlinelibrary.wiley.com/doi/pdf/10.1029/2022GL097799.

Mayta, V. C., and À. F. Adames Corraliza, 2024: The Stirring Tropics: The Ubiquity of Moisture Modes and Moisture-Vortex Instability. *Journal of Climate*, **-1 (aop)**, https://doi.org/10.1175/JCLI-D-23-0145.1, URL https://journals.ametsoc.org/view/journals/clim/aop/JCLI-D-23-0145.1/JCLI-D-23-0145.1.xml, publisher: American Meteorological Society Section: Journal of Climate.

Mayta, V. C., À. F. Adames Corraliza, Q.-J. Lin, and R. M. Vargas Martes, 2025a: Caribbean Easterly Waves: Structure, Thermodynamics, and Instability Mecha-

nisms. *Journal of the Atmospheric Sciences*, **82 (7)**, 1451–1465, https://doi.org/10.1175/JAS-D-24-0232.1, URL https://journals-ametsoc-org.ezproxy.lib.ou.edu/view/journals/atsc/82/7/JAS-D-24-0232.1.xml, publisher: American Meteorological Society Section: Journal of the Atmospheric Sciences.

Mayta, V. C., À. F. A. Corraliza, K. Torres Maldonado, H. Luo, and K. M. Núñez Ocasio, 2025b: Thermodynamic Processes Governing the Evolution of Developing and Strong Non-developing African Easterly Waves. *Journal of the Atmospheric Sciences*, **-1 (aop)**, https://doi.org/10.1175/JAS-D-24-0125.1, URL https://journals.ametsoc.org/view/journals/atsc/aop/JAS-D-24-0125.1/JAS-D-24-0125.1.xml, publisher: American Meteorological Society Section: Journal of the Atmospheric Sciences.

Nowottnick, E. P., and Coauthors, 2024: Dust, Convection, Winds, and Waves: The 2022 NASA CPEX-CV Campaign. *Bulletin of the American Meteorological Society*, **105 (11)**, E2097–E2125, https://doi.org/10.1175/BAMS-D-23-0201.1, URL https://journals.ametsoc.org/view/journals/bams/105/11/BAMS-D-23-0201.1.xml, publisher: American Meteorological Society Section: Bulletin of the American Meteorological Society.

Núñez Ocasio, K. M., C. A. Davis, Z. L. Moon, and Q. A. Lawton, 2024: Moisture Dependence of an African Easterly Wave Within the West African Monsoon System. *Journal of Advances in Modeling Earth Systems*, **16 (6)**, e2023MS004 070, https://doi.org/10.1029/2023MS004070, URL https://onlinelibrary.wiley.com/doi/abs/10.1029/2023MS004070, _eprint: https://onlinelibrary.wiley.com/doi/pdf/10.1029/2023MS004070.

Núñez Ocasio, K. M., and Z. L. Moon, 2024: TAMS: a tracking, classifying, and variable-assigning algorithm for mesoscale convective systems in simulated and satellite-derived datasets. *Geoscientific Model Development*, **17 (15)**, 6035–6049, https://doi.org/10.5194/gmd-17-6035-2024, URL https://gmd.copernicus.org/articles/17/6035/2024/, publisher: Copernicus GmbH.

Núñez Ocasio, K. M., and R. Rios-Berrios, 2023: African Easterly Wave Evolution and Tropical Cyclogenesis in a Pre-Helene (2006) Hindcast Using the Model for Prediction Across Scales-Atmosphere (MPAS-A). *Journal of Advances in Modeling Earth Systems*, **15 (2)**, e2022MS003 181, https://doi.org/10.1029/2022MS003181, URL https://onlinelibrary.wiley.com/doi/abs/10.1029/2022MS003181, _eprint: https://onlinelibrary.wiley.com/doi/pdf/10.1029/2022MS003181.

Pasch, R. J., and L. A. Avila, 1994: Atlantic Tropical Systems of 1992. *Monthly Weather Review*, **122 (3)**, 539–548, https://doi.org/https://doi.org/10.1175/1520-0493(1994)122%3C0539:ATSO%3E2.0.CO;2.

Reed, R. J., and E. E. Recker, 1971: Structure and Properties of Synoptic-Scale Wave Disturbances in the Equatorial Western Pacific. *Journal of the Atmospheric Sciences*, **28 (7)**, 1117–1133, https://doi.org/10.1175/1520-0469(1971)028⟨1117:SAPOSS⟩2.0.CO;2, URL https://journals.ametsoc.org/view/journals/atsc/28/7/1520-0469_1971_028_1117_saposs_2_0_co_2.xml, publisher: American Meteorological Society Section: Journal of the Atmospheric Sciences.

Riley, E. M., B. E. Mapes, and S. N. Tulich, 2011: Clouds Associated with the Madden–Julian Oscillation: A New Perspective from CloudSat. *Journal of the Atmospheric Sciences*, **68 (12)**, 3032–3051, https://doi.org/10.1175/JAS-D-11-030.1, URL https://journals.ametsoc.org/view/journals/atsc/68/12/jas-d-11-030.1.xml, publisher: American Meteorological Society Section: Journal of the Atmospheric Sciences.

Russell, J. O. H., A. Aiyyer, and J. Dylan White, 2020: African Easterly Wave Dynamics in Convection-Permitting Simulations: Rotational Stratiform Instability as a Conceptual Model. *Journal of Advances in Modeling Earth Systems*, **12 (1)**, https://doi.org/10.1029/2019MS001706, URL https://onlinelibrary.wiley.com/doi/abs/10.1029/2019MS001706.

Sakaeda, N., and Coauthors, 2025: Synoptic Modulation of the West African Coastal Atmosphere and Mesoscale Convective Systems. *Monthly Weather Review*, **-1 (aop)**, https://doi.org/10.1175/MWR-D-24-0281.1, URL https://journals-ametsoc-org.ezproxy.lib.ou.edu/view/journals/mwre/aop/MWR-D-24-0281.1/MWR-D-24-0281.1.xml, publisher: American Meteorological Society Section: Monthly Weather Review.

Sawaisarje, G. K., P. Khare, H. S. Chaudhari, N. Puviarasan, and M. R. Ranalkar, 2019: Easterly wave activity and associated heavy rainfall during the pre-monsoon season of 2005. *Meteorology and Atmospheric Physics*, **131 (3)**, 313–327, https://doi.org/10.1007/s00703-017-0575-0, URL https://doi.org/10.1007/s00703-017-0575-0.

Schlueter, A., A. H. Fink, P. Knippertz, and P. Vogel, 2019: A Systematic Comparison of Tropical Waves over Northern Africa. Part I: Influence on Rainfall. *Journal of Climate*, **32 (5)**, 1501–1523, https://doi.org/10.1175/JCLI-D-18-0173.1, URL http://journals.ametsoc.org/doi/10.1175/JCLI-D-18-0173.1.

Schreck, C. J., J. Molinari, and K. I. Mohr, 2011: Attributing Tropical Cyclogenesis to Equatorial Waves in the Western North Pacific. *Journal of the Atmospheric Sciences*, **68 (2)**, 195–209, https://doi.org/10.1175/2010JAS3396.1, URL https://journals.ametsoc.org/jas/article/68/2/195/26740/Attributing-Tropical-Cyclogenesis-to-Equatorial.

Seastrand, S., Y. Serra, C. Castro, and E. Ritchie, 2015: The dominant synoptic-scale modes of North American monsoon precipitation. *International Journal of Climatology*, **35 (8)**, 2019–2032, https://doi.org/10.1002/joc.4104, URL https://onlinelibrary.wiley.com/doi/abs/10.1002/joc.4104, _eprint: https://rmets.onlinelibrary.wiley.com/doi/pdf/10.1002/joc.4104.

Serra, Y. L., G. N. Kiladis, and M. F. Cronin, 2008: Horizontal and Vertical Structure of Easterly Waves in the Pacific ITCZ. *Journal of the Atmospheric Sciences*, **65 (4)**, 1266–1284, https://doi.org/10.1175/2007JAS2341.1, URL https://journals.ametsoc.org/view/journals/atsc/65/4/2007jas2341.1.xml, publisher: American Meteorological Society Section: Journal of the Atmospheric Sciences.

Wheeler, M., and G. N. Kiladis, 1999: Convectively Coupled Equatorial Waves: Analysis of Clouds and Temperature in the Wavenumber–Frequency Domain. *Journal of the Atmospheric Sciences*, **56 (3)**, 374–399, https://doi.org/10.1175/1520-0469(1999)056⟨0374:CCEWAO⟩2.0.CO;2, URL https://journals.ametsoc.org/view/journals/atsc/56/3/1520-0469_1999_056_0374_ccewao_2.0.co_2.xml, publisher: American Meteorological Society Section: Journal of the Atmospheric Sciences.

Wiggins, R. M., B. R. Lintner, Y. L. Serra, A. M. Durán-Quesada, M. Garbanzo-Salas, D. Hernández-Deckers, and G. Torri, 2023: Tropical Easterly Waves Over Costa Rica and Their Relationship to the Diurnal Cycle of Rainfall. *Geophysical Research Letters*, **50 (20)**, e2023GL104 159, https://doi.org/10.1029/2023GL104159, URL https://onlinelibrary.wiley.com/doi/abs/10.1029/2023GL104159, _eprint: https://onlinelibrary.wiley.com/doi/pdf/10.1029/2023GL104159.

Wilson, A. V., S. J. Majumdar, J. A. Zawislak, and J. P. Dunion, 2025: Structures of Low-Level Wind and Convection in the Pregenesis Environment of Western Caribbean Tropical Cyclones. *Monthly Weather Review*, **153 (11)**, 2513–2534, https://doi.org/10.1175/MWR-D-24-0266.1, URL https://journals.ametsoc.org/view/journals/mwre/153/11/MWR-D-24-0266.1.xml, publisher: American Meteorological Society Section: Monthly Weather Review.

Yanai, M., and R. H. Johnson, 1993: Impacts of Cumulus Convection on Thermodynamic Fields. *The Representation of Cumulus Convection in Numerical Models*, K. A. Emanuel, and D. J. Raymond, Eds., American Meteorological Society, Boston, MA, 39–62, https://doi.org/10.1007/978-1-935704-13-3_4, URL https://doi.org/10.1007/978-1-935704-13-3_4.

Zhang, X., J. Fang, and Z. Yu, 2022: Characteristics of the Quasi-Periodic Outbreaks of Deep Convection During Tropical Cyclone Genesis. *Journal of Geophysical Research: Atmospheres*, **127 (12)**, e2021JD035 312, https://doi.org/10.1029/2021JD035312, URL https://onlinelibrary.wiley.com/doi/abs/10.1029/2021JD035312, _eprint:

https://agupubs.onlinelibrary.wiley.com/doi/pdf/10.1029/2021JD035312.